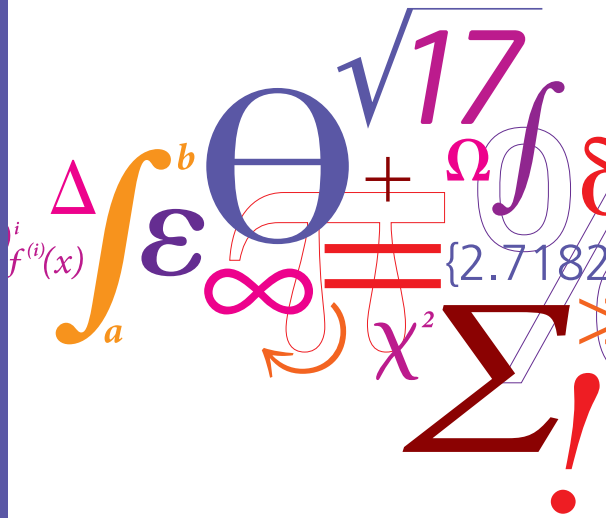


Microbial Enhanced Oil Recovery – Advanced Reservoir Simulation



Sidsel Marie Nielsen

Ph.D. Thesis

July 2010

Microbial Enhanced Oil Recovery – Advanced Reservoir Simulation

Sidsel Marie Nielsen

Center for Energy Resources Engineering
Department of Chemical and Biochemical Engineering
Technical University of Denmark
Kongens Lyngby, Denmark

Technical University of Denmark
Department of Chemical and Biochemical Engineering
Building 229, DK-2800 Kongens Lyngby, Denmark
Phone +45 45252800, Fax +45 45882258
kt@kt.dtu.dk
www.kt.dtu.dk

Copyright © Sidsel Marie Nielsen, 2010
ISBN -13: 978-87-92481-31-3
Printed by Frydenberg A/S, Copenhagen, Denmark

Preface

This thesis is submitted as a partial fulfillment of the requirement for obtaining the PhD degree at the Technical University of Denmark (DTU). The work has mainly taken place at the Center for Energy Resources Engineering and at the Department of Chemical and Biochemical Engineering at DTU. The duration of the PhD study was three years finishing August 2010. The project is partly financed by DONG Energy, Forsker Uddannelsesrådet, and DTU in the MP₂T graduate school. During my PhD study, I have been fortunate to have the opportunity to spend four months in 2009 at the University of Southern California (USC), Los Angeles, USA.

During the course of the study, a number of people have provided their help and support, for which I am very grateful. First of all, I would like to thank my supervisors at DTU, Alexander A. Shapiro, Michael L. Michelsen and Erling H. Stenby, for their guidance, encouragement and many valuable inputs, but most of all for their patience and allowing me to pursue my own ideas and interest. A special thanks to my external supervisor Kristian Jessen and his family for the friendly welcoming during my stay at USC. I am grateful for his guidance and many suggestions.

I would also like to thank my dear colleagues at CERE for providing a fun and stimulating research environment, especially thanks for your encouragement when necessary.

Finally, I would like to thank my husband Kim and our son Esben for their patience and for following me overseas to USC in Los Angeles to experience new things in a time that had already been rich on experiences and challenges, being a newly started family.

Kongens Lyngby, July 2010

Sidsel Marie Nielsen

Summary

In this project, a generic model has been set up to include the two main mechanisms in the microbial enhanced oil recovery (MEOR) process; *reduction of the interfacial tension* (IFT) due to surfactant production, and *microscopic fluid diversion* as a part of the overall fluid diversion mechanism due to formation of biofilm. The construction of a one-dimensional simulator enables us to investigate how the different mechanisms and the combination of these influence the displacement processes, the saturation profiles and thus the oil recovery curves.

The reactive transport model describes convection, bacterial growth, substrate consumption, and surfactant production in one dimension. The system comprises oil, water, bacteria, substrate, and surfactant. There are two flowing phases: Water and oil. We introduce the partition of surfactant between these two phases determined by a partitioning constant. Another effect is attachment of the bacteria to the pore walls and formation of biofilm. It leads to reduction of porosity and, under some assumptions, to increase the fraction of oil in the flow.

Surfactant is our key component in order to reduce IFT. The surfactant concentration in the water phase must reach a certain concentration threshold, before it can reduce the interfacial tension and, thus, the residual oil saturation. The relative permeabilities depend on the water phase concentration, so when surfactant is moved into the oil phase, the effect from the surfactant on the oil production is reduced. Therefore, the transfer part of the surfactant to oil phase is equivalent to its “disappearance”. The oil phase captures the surfactant, but it may as well be adsorbed to the pore walls in the oil phase.

We have looked into three methods how to translate the IFT reduction into changes of the relative permeabilities. Overall, these methods produce similar results. Separate investigations of the surfactant effect have been performed through exemplifying simulation cases, where no biofilm is formed. The water phase saturation profiles are found to contain a waterfront initially following the saturation profile for pure waterflooding. At *the oil mobilization point* – where the surfactant effect starts to take place – a sufficient surfactant concentration has been built up in order to mobilize the residual oil. A second waterfront is produced, and an oil bank is created. The recovery curve consists of several parts. Initially, the recovery curve follows pure waterflooding recovery until breakthrough of the oil bank. The next part of the recovery curve continues until

breakthrough of the second waterfront. The incline is still relatively steep due to a low water cut. In the last part, the curve levels off.

Partitioning of surfactant between the oil and water phase is a novel effect in the context of microbial enhanced oil recovery. The partitioning coefficient determines the time lag before the surfactant effect can be seen. The surfactant partitioning does not change final recovery, but a smaller partitioning coefficient gives a larger time lag before the same maximum recovery is reached. However, if too little surfactant stays in the water phase, we cannot obtain the surfactant effect.

The final recovery depends on the distance from the inlet to the oil mobilization point. Additionally, it depends on, how much the surfactant-induced IFT reduction lowers the residual oil. The surfactant effect position is sensitive to changes in growth rate, and injection concentrations of bacteria and substrate, which then determine the final recovery. Variations in growth rate and injection concentration also affect the time lag until mobilization of residual oil occurs. Additionally, the final recovery depends on, how much the surfactant-induced interfacial tension reduction lowers the residual oil saturation. The effects of the efficiency of surfactants are also investigated.

The bacteria may adhere to the pore walls and form a biofilm phase. The bacteria distribution between the water and biofilm phase is modeled by the Langmuir expression, which depends on the bacteria concentration in the water phase. The surface available for adsorption is scaled by the water saturation, as bacteria only adsorb from the water phase. The biofilm formation implies that the concentration of bacteria near the inlet increases. In combination with surfactant production, the biofilm results in a higher surfactant concentration in the initial part of the reservoir. The oil that is initially bypassed in connection with the surfactant effect, can be recovered as formation of biofilm shortens the distance from the inlet to the point of oil mobilization. The effect of biofilm formation on the displacement profiles and on the recovery is studied in the present work.

Formation of biofilm also leads to porosity reduction, which is coupled to modification of permeability. This promotes the fluid diversion mechanism. A contribution to fluid diversion mechanism is *microscopic fluid diversion*, which is possible to investigate in a one-dimensional system. The relative permeability for water is modified according to our modified version of the Kozeny-Carman equation. Bacteria only influence the water and biofilm phases directly, so the oil phase remains the same. We have assessed the effect from biofilm formation together with microscopic fluid diversion. When sufficient amount of surfactant is produced in the water phase, the effect from surfactant generates a larger contribution to recovery compared to microscopic fluid diversion.

To study the MEOR performance in multiple dimensions, the one-dimensional model with the surfactant effect alone has been implemented into existing simulators; a streamline simulator and a finite difference simulator. In the streamline simulator, the effect of gravity is introduced using an operator splitting technique. The gravity effect stabilizes oil displacement causing markedly improvement of the oil recovery, when the oil density becomes relatively low. The general characteristics found for MEOR in one-dimensional simulations are also demonstrated both in two and three dimensions.

Overall, this MEOR process conducted in a heterogeneous reservoir also produces more oil compared to waterflooding, when the simulations are run in multiple dimensions.

The work presented in this thesis has resulted in two publications so far.

Resumé

Formålet med denne afhandling er at konstruere en generel model, der inkluderer de to primære mekanismer i mikrobiel forbedret olie indvinding (MEOR); *reduktion af olie-vand grænsefladepændingen* (IFT) ved bakteriel produktion af surfaktant samt *mikroskopisk fluid omdirigering* ved dannelse af biofilm. Konstruktionen af en endimensionel simulator gør det muligt at undersøge, hvorledes de forskellige mekanismer påvirker fortrængningsprocessen, mætningsprofilen and herved olieindvindingskurven.

Den reaktive transport model beskriver konvektion, bakterievækst, næringsforbrug og produktion af surfaktant i en dimension. Systemet består af olie, vand, bakterier, næring og surfaktant. Der er to flydende faser: Olie og vand. Vi har introduceret fordeling af surfaktant mellem olie- og vandfasen, hvor fordelingen er bestemt ved en fordelingskoefficient. En anden effekt er bakterieadsorption på porevæggene, hvorved biofilm dannes. Dette fører til reduktion af porøsiteten, og under nogle antagelser øges fraktionen af olie i flowet.

Surfaktant er vores hovedkomponent, der reducerer IFT. Surfaktantkoncentrationen i vandfasen skal nå en vis grænseværdi, før surfaktant kan sænke IFT og hermed også den residuale olie. Idet den relative permeabilitet afhænger af vandfasekoncentrationen af surfaktant, vil effekten af surfaktant på olieproduktionen mindskes, når en fraktion af surfaktant bevæger sig over i oliefasen. Det svarer det til, at surfaktantfraktionen, der er overført til oliefasen, er "forsvundet". Surfaktantfraktionen, der er fanget i oliefasen, kan lige så vel være adsorberet til porevæggen i oliefasen.

Vi har undersøgt tre metoder for at overføre reduktionen af IFT til ændring af den relative permeabilitet. Totalt set, giver de tre metoder lignende resultater. Separate undersøgelser af surfaktant effekten er udført ved simuleringseksempler, hvori der ikke dannes biofilm. Vandmætningsprofilen karakteriseres ved en front, som også opstår ved ren vandinjektion. Ved oliemobiliseringspunktet, hvor effekten af surfaktant indtræder, er tilstrækkeligt med surfaktant dannet til at kunne mobilisere den residuale olie. En anden vandfront dannes, mens en oliebanke opstår. Indvindingskurven består af flere dele. Første del af kurven følger profilen for ren vandinjektion ind til oliebankens gennembrud. Den næste del af indvindingskurven forsætter indtil gennembruddet for den anden vandfront. Indvindingkurven er endnu stejl, idet oliefraktionen af produktionsvæsken er høj. I den sidste del flader kurven ud.

I forbindelse med MEOR er fordeling af surfaktant mellem olie- og vandfasen en ny

tilgang. Fordelingskoefficienten bestemmer tidsforsinkelsen, før effekten fra surfaktant indtræder. Surfaktantfordelingen ændrer ikke ved indvindingsgraden, men en mindre fordelingskoefficient medfører en større tidsforsinkelse, før den maksimale indvinding opnås. Dog kan surfaktanteffekten ikke opnås, hvis andelen af surfaktant, der forbliver i vandfasen, er for lille.

Det vises, at indvindingsgraden afhænger af afstanden fra injektionsbrønden til oliemobiliseringspunktet. Desuden afhænger indvindingen af, hvor meget reduktionen af IFT kan sænke den residuale oliemætning. Positionen for surfaktanteffektens indtrædelse er følsom over for forandringer i den bakterielle væksthastighed samt injektionskoncentrationerne af bakterier og næring, hvorfor dette bestemmer indvindingsgraden. Variationer i bakterievæksthastigheden og injektionskoncentrationerne påvirker også tidsforsinkelsen, før oliemobilisering sker. Indvindingsgraden afhænger desuden af, hvor meget den surfaktant-inducerede IFT sænker den residuale oliemætning. Effektiviteten af surfaktant er også undersøgt i afhandlingen.

Bakterier adsorberer til poreoverfladerne og danner biofilm. Ved at benytte Langmuir udtrykket, der er en funktion af bakteriekoncentrationen i vandfasen, fordeles bakterierne fordeles mellem vand- og biofilmfasen. Overfladen af porerne, der er tilgængelig for adsorption, er skaleret med vandmætningen, idet bakterier kun adsorberer fra vandfasen. Dannelse af biofilm medfører, at koncentrationen af bakterier nær injektionsbrønden stiger. I kombination med surfaktant produktion betyder biofilmdannelse, at der opnås en højere koncentration af surfaktant ved begyndelsen af reservoiret. Olie, som førhen blev forbigået ved surfaktanteffekten alene, indvindes nu, idet dannelsen af biofilm forkorter afstanden fra indgangen til oliemobiliseringspunktet. I denne sammenhæng er effekten af surfaktant på fortrængningsprofilerne samt olieindvindingen undersøgt.

Dannelse af biofilm bidrager også til reduktion af porøsiteten, der påvirker permeabiliteten. Dette fører til fluid omdirigeringsmekanismen. Et bidrag til fluid omdirigeringsmekanismen er mikroskopisk fluid omdirigering, som er muligt at undersøge i vores én-dimensionelle system. Den relative permeabilitet for vand ændres i overensstemmelse med vores modificerede Kozeny-Carman ligning. Bakterier påvirker vand- og biofilmfaserne direkte, mens oliefasen forbliver uændret. Ved hjælp af simuleringseksempler har vi undersøgt den kombinerede effekt af biofilm og mikroskopisk fluid omdirigering. Når surfaktant produceres i tilstrækkelige mængder i vandfasen, bliver effekten fra surfaktant betydeligt større sammenlignet med mikroskopisk fluid omdirigering.

For at undersøge MEOR processen i flere dimensioner, er den én-dimensionelle model blevet implementeret i to eksisterende simulatorer; en strømningsliniesimulator og en *finite difference* simulator. I strømningslinie simulatoren er bidraget fra tyngdekraften inkluderet ved at benytte operator opsplnitning. Tyngdekraften stabiliserer fortrængningen af olie, hvilket medfører forbedringer af olieindvindingsgraden, når densiteten af olien er tilpas lav. De generelle karakteristika for MEOR processen i en dimension, ses også i både to og tre dimensioner. Samlet set giver denne MEOR process, som er udført i et heterogent reservoir og er modelleret i flere dimensioner, en større produktion af olie sammenlignet med ren vandinjektion.

Arbejdet, der er præsenteret i denne afhandling, har indtil videre resulteret i to publikationer.

Contents

Preface	iii
Summary	v
Resumé	ix
1 Background	1
1.1 Introduction	1
1.2 Enhancement of oil production and recovery	3
1.3 Petroleum microbiology	3
1.3.1 Physical factors	4
1.3.2 Chemical factors	5
1.3.3 Microbial growth and nutrients	6
1.3.4 Metabolites	7
1.3.5 Attachment and detachment processes	7
1.3.6 Chemotaxis	8
1.4 MEOR mechanisms	8
1.4.1 Results from laboratory and field trials	9
1.4.2 Reduction of oil-water interfacial tension	10
1.4.3 Fluid diversion	12
1.4.4 Reduction of oil viscosity	13
1.4.5 Compatibility	14
1.5 Objectives	16
1.6 Publications	17
2 The reactive transport model	19
2.1 Review of MEOR model approaches	19
2.2 The general model	21
2.2.1 Fractional flow function	22
2.3 Specific model formulation	23
2.3.1 Assumptions	24
2.3.2 Component mass balances	26
2.3.3 Relative Permeability	27
2.3.4 Reactions	28

2.3.5	Bacteria Partition	30
2.3.6	Surfactant Partition	31
2.3.7	Porosity changes	32
2.4	Implementation	33
2.4.1	General approaches	33
2.4.2	Reduction of oil-water interfacial tension	33
2.4.3	Permeability Modifications	41
2.4.4	Microscopic fluid diversion	46
2.5	Summary of model	46
3	Solution procedure	49
3.1	Dimensionless form	50
3.2	Discretization scheme	51
3.3	Application of Newton-Raphson procedure	52
4	One-dimensional simulations	57
4.1	Selection of parameters	57
4.2	Verification of simulator	61
4.3	Surfactant effect	63
4.3.1	Characteristics due to surfactant effect	63
4.3.2	Effect of surfactant partitioning	65
4.3.3	Effect of growth rate	66
4.3.4	Effect of substrate and bacterial injection concentrations	67
4.3.5	Comparison of interpolation methods	68
4.3.6	Effect of surfactant efficiency	70
4.4	Effect of biofilm formation	72
4.4.1	Parameters revisited	72
4.4.2	Effect of bacteria adsorption	73
4.4.3	Effect of water relative permeability	75
4.4.4	Assumption about constant viscosities	77
4.5	Combination of mechanisms	79
4.5.1	Parameters revisited	79
4.5.2	Biofilm formation with surfactant effect	79
4.5.3	Microscopic fluid diversion with surfactant effect	80
4.6	Summary of 1D results	82
5	Streamline simulations	85
5.1	Introduction	86
5.2	The multi-dimensional model	86
5.2.1	Solution methods	87
5.2.2	Gravity	89
5.3	Parameters	90
5.4	Verification of implementation	93
5.5	Comparison of 2D results	93
5.6	The MEOR characteristics	95
5.7	Simulations in 2D with gravity effect	95
5.8	Simulations in 3D with gravity effect	97

5.9 Summary of multidimensional results	99
6 Conclusion	101
7 Future work	105
A Parameters in Langmuir expression	107
B Multivariable Newton iteration	109
C Analytical solution of Buckley-Leverett equation	111
Nomenclature	113
Bibliography	117

Background

The purpose of this chapter is to set the basis for the modeling work presented in the following chapters. The chapter introduces the microbiology of a petroleum reservoir and the microbial enhanced oil recovery (MEOR) explaining the mechanisms that are responsible for the enhancement of oil recovery. Results from laboratory experiments and field trials are also presented to highlight the potential of the MEOR. The chapter is rounded off with presenting the objectives for this PhD project.

1.1 Introduction

The principle source of fluid fuels is the hydrocarbon resources. The finite nature of our hydrocarbon reserves has been discussed as discoveries of new oil reservoirs decrease. For the present techniques of oil recovery, a large amount of oil remains in the reservoir after secondary flooding, where the oil reservoirs must be abandoned as the production is no longer economically feasible. Methods of enhanced oil recovery (EOR) have been developed, but they are often considered economically unattractive (Green and Willhite, 1998; Lazar et al., 2007; Maudgalya et al., 2007; Sen, 2008). In several cases, MEOR has shown its potential as a tertiary oil recovery method. The microorganisms require only cheaper substrates to perform MEOR, so from an economical point of view, the process itself is affordable compared to other EOR processes (Maudgalya et al., 2007; Lazar et al., 2007).

A long-term goal is to be able to design a robust MEOR process. This task can seem cumbersome, since microorganisms are involved in multiple mechanisms at the same

time and they can change physiology in response to fluctuations in their surroundings (Van Hamme et al., 2003; Sen, 2008). Together with experimental procedures such as core floodings and field trials, a step on the way is the development of simulation tools in order to understand and reveal the full potential of MEOR.

ZoBell (1947) was one of the pioneers in MEOR, where residual oil was recovered by application of microorganisms. Since then many researchers has performed MEOR laboratory experiments and field tests with different degrees of success (Lazar et al., 2007; Maudgalya et al., 2007). The most active applications of the MEOR process are as listed below (Bryant and Burchfield, 1989; Brown, 1992; Maudgalya et al., 2007; Amro, 2008; Rafique and Ali, 2008).

- Use of microbial systems for permeability modification to improve water flooding sweep efficiency.
- Use of microorganisms to produce gas, surfactant, acids and alcohols improving recovery in the course of flooding throughout the reservoir
- Single-well stimulation: treatment of a wellbore zone for removal of near-wellbore paraffin deposits or other constituents leading to formation damage, or for oil mobilization in the region around the wellbore.

Our focus is chosen within the two first applications, where MEOR flooding is looked into. The field trials have generally shown improvement of oil production or oil recovery, but there have been very fluctuating improvements of oil recovery, and the technical performance in many field trials has been inconsistent (Youssef et al., 2007; Maudgalya et al., 2007). Major improvements of recovery have been found in laboratory experiments, while smaller improvements have been found in the field trials (Maudgalya et al., 2007).

Bryant and Lockhart (2002) and Gray et al. (2008) present in their work a critical analysis of MEOR. They have performed an assessment analysis based on estimates for each MEOR mechanism using general reactor analysis and mass balance calculations. They conclude that only a small part of the mechanisms taking place during MEOR, have any prospect for enhancing oil recovery. More likely combination of the mechanisms can lead to a significant enhancement of oil recovery. Generally, further studies are required in order to perform a more complete assessment of the MEOR process (Gray et al., 2008).

1.2 Enhancement of oil production and recovery

The goal of the EOR methods is to recover more oil from the underground oil fields. In the literature, the oil recovery and the enhancement of the oil production are measured in several ways. For instance, the enhancement is 'extra oil recovered in relation to residual oil after waterflooding', 'extra oil recovered in relation to the original oil in place', 'reduction of watercut', or 'increased oil production'.

In this work, we choose to use oil recovery as the oil that has been recovered over the original oil in place (OOIP):

$$\frac{\text{oil produced}}{\text{original oil in place}} \cdot 100 = \% \text{ OOIP} \quad (1.1)$$

We attempt to present oil recoveries as % OOIP *or* the increment in oil recovery over that of waterflooding, still using increment in OOIP.

1.3 Petroleum microbiology

Many kinds of microorganisms are found within the reservoir. Regarding indigenous microorganisms, Magot et al. (2000) emphasize that anaerobic microorganisms are considered true inhabitants. Anaerobes ferment and cannot use oxygen as O₂ for respiration, and for strict anaerobes, the presence of oxygen is toxic. Both aerobic and facultatively aerobic microorganisms have also been found. The aerobes can respire, while the facultative aerobes are able to grow either as aerobes or anaerobes determined by the nutrient availability and environmental conditions (Madigan et al., 2003). Regarding the presence of aerobes and facultative aerobes, the role as true inhabitants is uncertain and thus considered contaminants. Contaminant microorganisms are transferred to the reservoir through fluid injection or during drilling devices (Magot et al., 2000).

Concerning the anaerobic condition in the reservoir and the difficulty in supplying oxygen, it is regarded more feasible to inject anaerobic species such as *Clostridium* instead of aerobic species such as e.g. *Pseudomonas* (Jang et al., 1984; Aslam, 2009a). The applicability of *Pseudomonas* in a MEOR process is questionable, even though it is a hydrocarbon-degrading bacteria, able to survive with oil as the primary carbon source (Blanchet et al., 2001; Aslam, 2009a).

Commonly used bacterial species are *Bacillus* and *Clostridium*. The *Bacillus* species produce surfactants, acids and some gases, and *Clostridium* produce surfactants, gases, alcohols and solvents. Few *Bacillus* species also produce polymers. Microorganisms that have been used for MEOR, are listed in table 1.1 (Bryant and Burchfield, 1989).

Bacillus and *Clostridium* are often able to bear extreme conditions existing in the oil

Table 1.1: Bacteria that are used in MEOR and their products (Bryant and Burchfield, 1989). Facultative means that the organism can grow with or without the presence of oxygen.

Family	Respiration type	Products
<i>Clostridium</i>	Anaerobic	Gases, acids, alcohols and surfactants
<i>Bacillus</i>	Facultative	Acids and surfactants
<i>Pseudomonas</i>	Aerobic	Surfactants and polymers, can degrade hydrocarbons
<i>Xanthomonas</i>	Aerobic	Polymers
<i>Leuconostoc</i>	Facultative	Polymers
<i>Desulfovibrio</i>	Anaerobic	Gases and acids, sulfate-reducing
<i>Arthrobacter</i>	Facultative	Surfactants and alcohols
<i>Corynebacterium</i>	Aerobic	Surfactants
<i>Enterobacter</i>	Facultative	Gases and acids

reservoirs. The survival originates from the ability to form spores. The spores are dormant, resistant forms of the cells (Bryant and Burchfield, 1989), which can survive in stressful environments exposing them to high temperature, drying, and acid. The duration of the dormancy can be extremely long and yet the survival rate is large (Madigan et al., 2003).

Microorganisms are complex in their way of responding to the surrounding environment. The cells change physiological state in order to have optimal chances for survival meaning that substrate consumption, growth and metabolite production may change significantly (Van Hamme et al., 2003).

Microorganisms present in an oil reservoir or other porous media are subjected to many physical (temperature, pressure, pore size/geometry), chemical (acidity, oxidation potential, salinity) and biological factors (cell processes) (Marshall, 2008). The most important cellular processes are growth, cell decay, chemotaxis, and cell attachment and detachment to pore walls (Ginn et al., 2002). Often, the microorganisms are considered as a black box, where only the important substrates and metabolites are taken into account (Nielsen et al., 2003).

1.3.1 Physical factors

The oil reservoirs are harsh environments for microorganisms. The reservoir temperature can be up to 150 °C. Data suggest that microorganisms may grow at temperatures

below 82 °C as microorganisms were only isolated from reservoirs below this temperature (Magot et al., 2000). The microorganisms depend on their enzyme function. High temperatures can disrupt the enzyme function due to denaturation or disruption around the catalyzing sites (Marshall, 2008; Madigan et al., 2003). The effect obtained from the high pressure is more indirect as changes in gene expression and protein synthesis occur (Marshall, 2008) and thus influence the physiological and metabolic state (Magot et al., 2000).

The pore size is a physical constraint for microorganisms to penetrate the reservoir. Bacteria are mainly applied because of their small size around 2 μm (Madigan et al., 2003). For instance, the size of a specific *Bacillus* strain rod is $4 \times 1.5 \mu\text{m}$ (Sharma and Georgiou, 1993). For tight reservoirs, bacteria might be in the same order of magnitude as the pores. Penetration of bacteria is regarded possible in reservoirs with minimum pore diameters of at least 2 μm (Marshall, 2008) and preferably from 6–10 μm (Sharma and Georgiou, 1993, estimated from filtration theory).

1.3.2 Chemical factors

The pH in the reservoir is often as low as 3–7 as the high pressure lets gases dissolve in the fluids (Magot et al., 2000). The acidity determines the microbial surface charge affecting the bacteria transport through the reservoir. The bacterial growth rate is reduced by acidity, where the ionization of membrane transport proteins can alter the transport efficiency (Marshall, 2008).

The transport of the bacteria depends on physiology. If the bacterial surface is solely hydrophobic, the bacteria tend to stick together and will be transported in flocs. On the other hand, the hydrophilic bacteria will more often flow as single bacteria (Crescente et al., 2006).

The water existing in the reservoir is fresh to salt-saturated water being a combination of connate reservoir water and injected saline sea water. The salinity influences the growth, where the microorganisms have to sustain the optimal salinity of cellular fluids to maintain enzymatic action (Madigan et al., 2003).

A thermodynamically favorable oxidation potential are crucial for microbial survival. For bacterial growth to take place, electron donors and acceptors must be present, where they become oxidized and reduced in the biochemical processes, respectively. In aerobic respiration, oxygen as O_2 is the terminal electron acceptor, where large amounts of energy are obtained used in growth and maintenance processes. When oxygen is not present, only anaerobic processes occur. Specific for the petroleum reservoir, the redox potential is very low and electron acceptors such as ferric ion, nitrate and sulfate are

utilized. The water contains sulphate and carbonate at various concentrations, which have led to assume that the major metabolic processes occurring naturally are sulfate reduction, methanogenesis, acetogenesis and fermentation (Magot et al., 2000; Marshall, 2008).

1.3.3 Microbial growth and nutrients

The microbial growth is determined by the presence of different nutrients. Cell nutrient requirements are wide, but some nutrients are required in larger amounts than others. The primary nutrients consumed is carbon and nitrogen, which are the main constituent parts of the cell and enter many cell processes (Madigan et al., 2003). The substrates for growth of hydrocarbon-degrading bacteria include different crude oil components such as n-alkanes, homocyclic aromatic compounds, polycyclic aromatic compounds, nitrogen and sulfur heterocyclics (Van Hamme et al., 2003).

The large requirements for carbon and nitrogen cause these compounds to be limiting nutrients, and thereby determine the growth rate. However, if the substrate concentration is too high, then substrate inhibition may occur (Nielsen et al., 2003). Other essential nutrients are phosphorus, sulfur, potassium and magnesium, and they are required in a much smaller amount (Madigan et al., 2003).

Trace elements such as e.g. iron, zinc and manganese are critical to cell function even though the amount required is small. The trace elements play a structural role in various enzymes and catalysts. However, as only tiny amounts are required, the natural occurrence is abundant. Other essential compounds for some organisms are vitamins and amino acids, which are required only in small amounts as they are important for enzymatic function (Madigan et al., 2003).

If microbial transport happens over a large distance in the reservoir then the injection of nutrients should be performed, so the nutrient supply is kept at a reasonable concentration. It should be taken into account that the transport differs for nutrients and microorganisms (Bryant and Burchfield, 1989). Especially, the effect from dilution should be considered, when the nutrient mix with the reservoir water.

Inside the bacteria, many processes take place, catalyzed by different complexes. Proper function of these complexes in order for the bacterium to survive, requires energy for maintenance. Often, maintenance is negligible compared to the energy spent for growth and metabolite production, but occasionally a significant part of the energy goes to maintenance. As an example, some bacteria in a highly acidic environment spends large amounts of energy to sustain the optimal pH within the cell (Nielsen et al., 2003).

1.3.4 Metabolites

Some conditions will promote one kind of metabolites while other conditions promote a whole different set of metabolites. Maintaining a certain physiological state of microorganisms in oil reservoirs could be difficult as many uncertainty factors exist (Van Hamme et al., 2003). For microorganisms producing a certain metabolite, the possibility for the metabolite inhibiting growth and its own metabolite production occurs (Nielsen et al., 2003), so a necessary metabolite concentration can not be reached.

The metabolites include biosurfactants, biopolymers, solvents, acids and gases as listed in table 1.1 (Van Hamme et al., 2003). As an example, a commonly produced acid is acetate, but benzoate, butyrate, formate and propionate are also found (Magot et al., 2000).

1.3.5 Attachment and detachment processes

The porous media has a large surface area to volume. This leads to much contact with the surface during transport of components. Nutrients usually do not adsorb markedly, but a metabolite such as surfactant exists in smaller amounts and has a greater tendency to adsorb. Nutrients and metabolites will to a lesser extent also attach to pore wall, compared to bacteria (Kim, 2006).

1.3.5.1 Formation of biofilm

Bacteria generally stick to all kind of surfaces forming biofilms (Characklis and Wilderer, 1989; Shafai and Vafai, 2009). Biofilm consists of a number of immobile cells, sticky polysaccharides, dissolved components, particular material and water. The water constitutes a large part of the biofilm. The biofilm acts as a micro-environment, where the biofilm matrix water exchanges solutes such as nutrients and waste products with the surroundings. There may be limitation of transport to and from the biofilm. This is mainly determined by the thickness of the biofilm and the internal biofilm porosity (Thullner, 2009).

Bacteria such as *Pseudomonas* form biofilm with only one layer of cell, where other species form multilayered biofilms (Characklis and Wilderer, 1989). The multilayered biofilms can form large mushroom shapes valving from the surface, in order to increase the surface area for solute transport to and from the biofilm (Characklis and Wilderer, 1989; Thullner, 2009). The bacterial growth in the adsorbed phase is occasionally lower, which is considered a consequence of the limitations in transport of nutrient (Murphy and Ginn, 2000).

In the context of porous media, the bacteria size may not be much smaller than the pore size. Thus, the pore size may also constrain how many layers of cell a biofilm can be composed of. If pore sizes are small, biofilm accumulation can be enhanced by the process of filtration (Characklis and Wilderer, 1989), but otherwise the retention of bacteria is primarily determined by the adsorption process (Stevik et al., 2004).

Kim (2006) suggests that attachment to the pore walls is a process that primarily depend on the properties of media, rock surface and cell surface. Some studies suggest that microorganisms perform active adhesion/detachment processes as a response to the local nutrient availability and as a survival mechanism (Ginn et al., 2002; Rockhold et al., 2004). Detachment from the biofilm is also caused by erosion, which is the removal of small particles from the surface of the biofilm caused by shear stresses (Characklis and Wilderer, 1989).

1.3.6 Chemotaxis

Chemotaxis is a part of the cell response to a chemical gradient for motile bacteria. Bacteria move toward an increasing concentration of beneficial substances such as nutrients and away from detrimental substances such as toxins (Sen et al., 2005; Kim, 2006). The movement requires energy as the bacteria use their flagellar motor in order to tumble towards direction of e.g. the nutrient (Valdés-Parada et al., 2009). Therefore chemotaxis is strongly coupled to the bacterial growth rate (Ginn et al., 2002). In the context of oil reservoirs, chemotaxis may take place by motile bacteria, but the effect from chemotaxis is regarded minimal.

1.4 MEOR mechanisms

The MEOR process applies microorganisms that are already present in the reservoir or microorganisms that are adapted to the harsh environment. Injection of microorganisms is performed in order ensure growth and production of specific metabolites.

Indigenous microorganisms are mostly activated by injection of substrates, whereas exogenous microorganisms are injected with their substrates or in between slugs of substrates. Regarding continuous injection, the plugging of the reservoir injection well becomes an issue if the microbial injection concentration is too high (Aslam, 2009a). To keep the cost low, the selected media is generally molasses, corn syrup or other industrial waste products (Bryant and Burchfield, 1989; Lazar et al., 2007; Aslam, 2009a). However, the application of cheaper substrates would require quality control (Bryant and Burchfield, 1989).

The microorganisms penetrate the reservoir, while they consume substrates, grow and produce different important metabolites. A combination of different mechanisms rely on the microbes or their metabolites to mobilize residual oil or improve the areal sweep. The most important MEOR mechanisms are listed below.

- Reduction of interfacial tension and alteration of wettability due to in situ surfactant production
- Fluid diversion due to microbial growth and polymer production (bacterial plugging)
- Viscosity reduction of oil by degradation of oil components or gas production

The latter mechanism is mainly regarded as a beneficial side effect, but can partly contribute to increase the oil production (Jenneman et al., 1984; Banat, 1995; Bryant and Burchfield, 1989; Bryant et al., 1989; Chisholm et al., 1990; Sarkar et al., 1994; Desouky et al., 1996; Vadie et al., 1996; Delshad et al., 2002; Feng et al., 2002; Maudgalya et al., 2007; Gray et al., 2008; Sen, 2008; UTCHEM, 2000).

During experimental work multiple processes take place at the same time, so the mechanisms can be difficult to separate from each other (Maudgalya et al., 2007). Some studies are set-up mainly to investigate one MEOR mechanism, but it is still not possible to ascribe the enhancement of oil recovery entirely to one mechanism.

The energy-rich nutrients such as sugars are easy to consume, which is why these nutrients are the first to be consumed by the microorganisms. Therefore, viscosity reduction of oil mainly occurs, when oil is the carbon source for bacterial growth. Generally, when nutrients are injected, reduction of interfacial tension and fluid diversion are the main mechanisms to take place, while viscosity reduction becomes more important during MEOR with oil as the sole carbon source.

1.4.1 Results from laboratory and field trials

MEOR floodings conducted in the laboratory are generally more successful than the field trials. The flooding experiments are restricted in size and performed under controlled conditions in a limited time range. As an advantage, the laboratory experiments have the possibility for fine tuning the process. MEOR floodings in the laboratory obtain extra oil recoveries up to 20% OOIP over that of waterflooding (Jang et al., 1984; Bryant and Douglas, 1988; Bryant et al., 1989; Chisholm et al., 1990; Deng et al., 1999; Sugihardjo and Pratomo, 1999; Feng et al., 2002; Mei et al., 2003; Ibrahim et al., 2004; Feng et al., 2006; Crescente et al., 2006; Amro, 2008; Zhaowei et al., 2008; Samir et al., 2010).

Field trials run for a longer time, but often the MEOR process has not run long enough to utilize the full potential. Therefore, success is measured as an increase in the oil production and a decrease in water cut instead of showing what final recovery achievements, when the maximum MEOR recovery is reached (Maudgalya et al., 2007). The good performance should also show that the effect from MEOR extends for a sufficient period of time confirming the stability of the MEOR implementation (Segovia et al., 2009). As an example, Gullapalli et al. (2000) conducted a field trial for 8 months and the biofilm formed within the reservoir was still stable after these months indicating that the biofilm could remain stable, but no long term effect was investigated.

Conclusions on stability and the MEOR performance should be based on results that also include the long term effect (Portwood, 1995; Maudgalya et al., 2007; Brown, 2010).

Field trials have been performed with different degrees of success (Bryant and Douglas, 1988; Grula et al., 1989; Jenneman, 1989; Streeb and Brown, 1992; Buciak et al., 1995; Dietrich et al., 1996; Deng et al., 1999; Gullapalli et al., 2000; Maure et al., 2001; Brown and Vadie, 2002; Nagase et al., 2002; Feng et al., 2002; Hitzman et al., 2004; Maure et al., 2005; Feng et al., 2006; Maudgalya et al., 2007; Zhaowei et al., 2008; Bao et al., 2009). Portwood (1995) presents the evaluation of 322 field trials conducted in USA. The MEOR process is found successful in 78 % of the trials demonstrating that a decrease in the oil production decline rate. The oil production has increased with an average of 36 %. During the unsuccessful field trials, there was no apparant effect from MEOR.

Other field trials showed around up to 25 % increase in oil production (Vadie et al., 1996; Hitzman et al., 2004). Brown and Vadie (2002) present their field results, where 8 out of 15 wells show a positive response to MEOR. No effect from MEOR is seen on the remaning wells. Two of these wells are considered uneconomical and thus closed. Based on estimations of the pre-MEOR and MEOR decline curves, the increment in oil recovery is expected to be 3–4 % OOIP.

1.4.2 Reduction of oil-water interfacial tension

Microorganisms produce surfactants as secondary metabolites. The surfactants are involved in different cell processes: Transport of water-insoluble compounds into the cell, biofilm formation and adhesion of cell on different surfaces. Specifically, hydrocarbon-oxidizing bacteria always produce surfactants in order to promote hydrocarbon penetration into the cells (Nazina et al., 2003).

Surfactants are biphilic molecules consisting of a hydrophilic and a hydrophobic part. Surfactants interact with; each other, surfaces with different polarity, adsorb at water-air and water-oil boundaries and cause wetting of hydrophobic surfaces. They may

also form structures that resemble lipid films or membranes and reduces the surface and interfacial tensions (IFT) of solutions (Nazina et al., 2003). Surfactant lowers IFT and mobilizes oil that cannot be displaced by water alone (Chisholm et al., 1990; Zekri and Almehaideb, 1999; Sen, 2008). The formed oil-in-water emulsion flows having a improvement of the effective mobility ratio until unfavorably conditions occurs, where the surfactant is diluted or lost due to adsorption to the pore wall (Sen, 2008).

Generally, oil-water systems have IFT around 30 mN/m (Bryant and Burchfield, 1989; McInerney et al., 2005; Gray et al., 2008; Crescente et al., 2008). Experimental work has shown that surfactants can lower the oil-water IFT to around 10^{-3} mN/m (Bryant and Burchfield, 1989; Sharma and Georgiou, 1993; Crescente et al., 2008). Ghojavand et al. (2008) find an IFT at 0.1 mN/m, which corresponds to a two orders of magnitude reduction, but this tends to be the typical reduction (Gray et al., 2008). It should be mentioned the existence of cases with only a 5–30 % reduction of IFT, but this is also achieved using oil as the sole carbon source (Sugihardjo and Pratomo, 1999; Halim et al., 2009). Green and Willhite (1998) recommend that IFT for chemical surfactant flood should be from 10^{-2} to 10^{-3} mN/m, while Gray et al. (2008) propose that the oil recovery will be improved, when IFT is reduced to 0.4 mN/m and lower.

During surfactant flooding, a major problem is adsorption of surfactant to the rock surface. Thus, the efficient concentration of surfactant decreases resulting in a concentration possibly lower than required. This problem exists during the MEOR process, but it is regarded limited, when the surfactant is produced *in situ*. With the thorough penetration of microorganisms into the reservoir, a locally high surfactant concentration can be achieved (Jenneman et al., 1984; Chisholm et al., 1990; Sunde et al., 1992; Zekri and Almehaideb, 1999).

Researchers present different results from their experimental work, where some studies only have minor IFT reductions (McInerney et al., 2005; Kowalewski et al., 2006) and only a little or no improvement of recovery, while others have presented major IFT reductions together with good incremental recoveries from 2 to 20 % OOIP (Bryant and Douglas, 1988; Deng et al., 1999; Feng et al., 2002; Bordoloi and Konwar, 2008). In the experiments, the effect from the surfactant can only be partly ascribed to surfactant production as other mechanisms interfere. Still, the surfactant effect is investigated in both the laboratory and in the fields, where the latter is expected to result in only moderate performances.

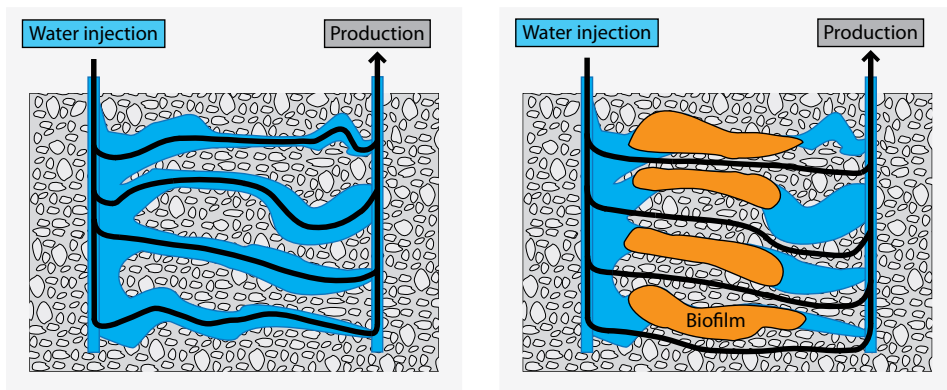
The effect from the surfactant can be obtained, when a certain threshold concentration is achieved (critical micelle concentration), but some researchers questions whether is possible actually to achieve the required amounts of surfactant (Bryant and Lockhart, 2002; Gray et al., 2008). To mobilize oil, the general engineering criteria is that the surfactant concentration should be 10-20 mg/l (Youssef et al., 2007). Field tests show

surfactant concentrations in the production fluids to be around 90 mg/l (Youssef et al., 2007) and 210–350 mg/l (McInerney et al., 2005). Fortunately, these results reveal that surfactant actually can be produced in the oil fields at much higher concentrations than are needed. Thus, it shows that the effect from surfactant has the potential to be an efficient MEOR mechanism (McInerney et al., 2005).

1.4.3 Fluid diversion

The theory of *fluid diversion* or selective plugging is applicable in an oil reservoir with a heterogeneous permeability distribution. Figure 1.1 illustrates the principle of macroscopic fluid diversion. During waterflooding in a heterogeneous reservoir, channeling takes place, where a larger fraction of the water flows through the high permeable regions, also called thief zones (figure 1.1(a)). The areal sweep is poor as only little water flows into the low permeable regions, bypassing large amounts of oil. The idea behind this mechanisms is to plug these channels with biofilm in order to divert fluids to the unswept regions, shown in figure 1.1(b).

In MEOR, either bacteria are injected together with nutrients or indigenous bacteria are activated by injection of nutrients only. The nutrient-rich water flows through the channels promoting good conditions for bacterial growth. In the channels, biofilm is formed, when bacteria attach to the pore walls. Attachment of more bacteria, multiplication of the biofilm bacteria, and production of sticky polysaccharides increase the volume of biofilm. The porosity and thus the permeability decreases in these channels due to biofilm formation, reducing the ease of flow. The reduced permeability ideally causes the flow to be diverted to the previously bypassed oil-rich regions. The areal



(a) Channeling in thief zones.

(b) Diversion of fluid to unswept areas due to biofilm formation.

Figure 1.1: Illustration of macroscopic fluid diversion.

sweep efficiency has increased and, hence, the oil recovery is improved (Updegraff, 1983; Jenneman et al., 1984; MacLeod et al., 1988; Bryant and Burchfield, 1989; Kowalewski et al., 2006; Sen, 2008; Aslam, 2009a,b).

In order to apply fluid diversion successfully, several criteria should be fulfilled (Jenneman et al., 1984). It depends on:

1. Controlled penetration of microorganisms throughout the reservoir
2. Controlled transport of nutrients for microbial growth and metabolism
3. Reduction of the apparent permeability of the reservoir rock as a result of microbial growth and metabolism

The risk of bacterial plugging is occurrence of undesirable plugging especially in the well bore region (Jack et al., 1989; Gray et al., 2008; Aslam, 2009a), which can generally lead to damages to the reservoir, reducing the oil production (Lazar et al., 2007).

The mechanisms of fluid diversion are investigated both in the laboratory and in the field trials, where extra oil is recovered. Tracer tests confirm that fluid diversion does occur (Nagase et al., 2002; Aslam, 2009b). Laboratory experiments find that the average permeability is reduced by 20–70 % (Gandler et al., 2006; Aslam, 2009b). Raiders et al. (1985, 1986) found a significant reduction of permeability together with an incremental oil recovery over that of water flooding at 5–20 % OOIP.

For practical application of fluid diversion, nutrients with bacteria or nutrients solely for the indigenous bacteria are injected into the reservoir. Then the reservoir is shut down for a period of time in order to let the bacteria grow and plug the selected thief zones. Post-flush is waterflooding or nutrient flooding to recover the previously bypassed oil (Sugihardjo and Pratomo, 1999; Gullapalli et al., 2000).

1.4.4 Reduction of oil viscosity

The reduction of oil viscosity occurs due to effects such as bacterial degradation of oil or dissolution of components such as surfactants or solvents into the oil phase. The oil mobility is improved by a reduction of oil viscosity (Brown, 1992; Deng et al., 1999).

Peihui et al. (2001) conduct flooding experiments injecting bacteria into cores, where sole carbon source (substrate) is oil components. Concurrently, growth happens on behalf of digestion of the oil components. The viscosity of crude oil is reduced from 28 mPa·s to 18 mPa·s together with a reduction of IFT from 36 mN/m to 8 mN/m. A chromatographic analysis shows that the ratio between light and heavy oil components, $\sum C_{21}^- / \sum C_{21}^+$, increases 54 % due to bacterial degradation of oil components.

The corefloodings reveal an incremental oil recovery of 10 % OOIP over that of waterflooding, even though a part of the oil is lost due to bacterial digestion (Peihui et al., 2001).

Similar results are obtained by Deng et al. (1999) during laboratory experiments and field tests. The chromatographic analysis is shown in figure 1.2 showing that the heavier hydrocarbons are consumed, while more lighter hydrocarbons are produced. Generally, the amount of problematic paraffin is reduced by 40 %. In the laboratory, the recovery improvement was 8–10 % OOIP over that of the waterflooding. During the field trials, the oil production increased 18 %. The main mechanisms contributing to the improvement are degradation of oil components also being the sole carbon and energy source, due to the low bacterial count (Brown, 1992; Deng et al., 1999).

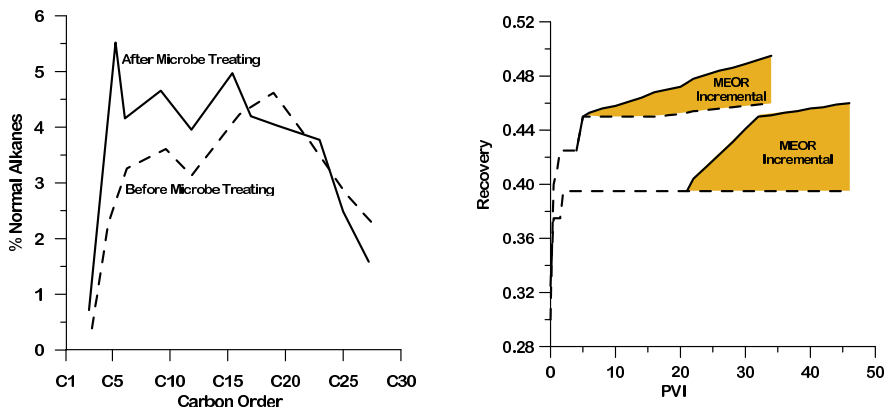


Figure 1.2: (Left) Change of oil composition due to bacterial action. (Right) Improved oil recovery from laboratory corefloodings. Adapted from Deng et al. (1999).

In some cases, bacterial metabolism produces gases such as carbon dioxide or methane. A free gas phase has been found to induce reductions of the residual oil saturation. Chisholm et al. (1990) experience that the presence of gas phase decrease the residual oil saturation of 6–10 % of pore volume. The gas phase saturation should be kept high (> 0.15), if gas should recover more oil. The effect from *in situ* gas production is regarded limited as it is unlikely that the required amount of gas can be produced (Bryant and Lockhart, 2002; Marshall, 2008; Gray et al., 2008). Therefore, the viscosity reduction by gas production is considered a minor, but beneficial side effect.

1.4.5 Compatibility

MEOR is a process benefiting from injected and/or indigenous microorganisms. It should be expected that reservoirs contain some habitant microorganisms and, consequently, knowledge about the indigenous microorganisms is necessary to secure a successful recovery. Strategies for injection of microorganisms should be ascertain that

injected and indigenous microorganisms are compatible in the sense that their collaboration is beneficial. Otherwise, this could have an adverse effect, where the indigenous microorganisms could overgrow and outcompete the microorganisms of interest. This will most probably provide a less successful recovery (Bryant and Burchfield, 1989; Sharma and Georgiou, 1993; Maudgalya et al., 2007; Marshall, 2008).

A typical example of the indigenous bacteria found in the reservoir is sulfate-reducing bacteria (SRB). Besides the risk of outcompeting the MEOR microorganisms, other problems arise. Care must be taken, because the seawater used for flooding contains sulfate, stimulating growth of SRB (Bryant and Burchfield, 1989). SRB produce the toxic and corrosive gas, hydrogen sulfide, which lead to problems such as reservoir souring, contamination of gas and oil, corrosion of metal surfaces and plugging of reservoirs due to the precipitation of metal sulfides and subsequently a reduction of the oil recovery (Davidova et al., 2001; Van Hamme et al., 2003).

The growth of SRB depends of reduction of sulfate to sulfide coupled to the oxidation of hydrogen and a wide variety of organic electron donors. Normally, electron donors in oil reservoirs are in slight excess entailing that the activity of SRB is limited to the availability of sulfate being the terminal electron acceptor (Davidova et al., 2001). Based on the different problems caused by SRB, a counter-strategy is developed. Nitrate-reducing bacteria (NRB) are added with nitrate to outcompete SRB. Nitrate and sulfate are terminal electron acceptors for NRB and SRB, respectively. The bacteria compete for the available electron donors based on the thermodynamics, kinetics and redox potential. An advantage for NRB is that reduction of nitrate to nitrogen or ammonia provides more Gibbs free energy than the sulfate reduction. Another advantage is that growth of SRB is inhibited, when the redox potential of the environment is raised. In addition, some nitrate-reducing bacteria are able to oxidize the sulfides removing the toxic sulfide by reaction with nitrite (Davidova et al., 2001; Eckford and Fedorak, 2002).

The hydrogen sulfide in production fluids and gases is a major problem, but there are examples of reducing the hydrogen sulfide production during the MEOR process. Hitzman et al. (2004) present results from the field trials, where the oil production is increased by 24 % in combination with reductions of the hydrogen sulfide production. The concentration in the produced gas goes from 80 ppm to 5 ppm, and the concentration in the production water drops from 20 ppm to less than 1 ppm. In this case, the bacteria in the MEOR process have a positive influence, reducing the hydrogen sulfide production (Hitzman et al., 2004), but it remains unclear which mechanisms are responsible (Davidova et al., 2001).

Overall, it is important to consider, which microorganisms are already present in reservoir and their compatibility with injected microorganisms in order to obtain a robust MEOR process.

1.5 Objectives

The main concern of this project is to investigate how each mechanism and the combination of mechanisms influence both the saturation profiles and the oil recovery. This should be done by setting up a generic mathematical model (chapter 2) in order to construct a one-dimensional simulator (chapter 3). The model should comprise the relevant components and phases, so the necessary reactions and partitions can take place. The model is generic in the sense that the parameters are selected to obtain reasonable accordance with the experimental work, but still the type of microorganism and reservoir remains unspecific. Especially, the influence on the saturation profiles and recovery curves becomes important as the characteristics for the MEOR process should be determined (chapter 4).

Surfactant is the key component for reducing IFT. We shall have to look into the production of surfactants with different efficiencies, where the surfactants are characterized by critical micelle concentrations and minimum attainable IFTs. Different methods should be applied in order to translate the IFT reduction into the changes of the relative permeabilities (chapter 2). The efficient surfactant concentration is the important issue for mobilizing residual oil. However, surfactant does adsorb to pore walls, which reduces the actual effect of surfactant. The reduced effect of surfactant should also be considered. The influence of the surfactant effect together with the importance of selected process parameters are to be investigated (chapter 4).

Bacteria are transported through the porous media and generally they tend to stick to surfaces such as pore walls. The formation of bacterial biofilm influence the bacteria transport. The mathematical model should be able to handle that bacteria adsorb to form biofilm and thus changes the porosity. The permeability is generally modified due to porosity changes. The biofilm formation should be investigated resolving the effect on both the absolute and relative permeabilities (chapter 3). The influence on the saturation profiles should be investigated determining their contribution to the enhanced oil recovery (chapter 4).

Working with simulators in one dimension gives some indications of the MEOR process behavior in multiple dimensions. To study the MEOR performance in multiple dimensions, the 1D model should be implemented in existing simulators; a streamline simulator and a finite difference simulator (chapter 5). The mechanism for surfactant only is to be investigated, as the model that includes formation of biofilm and the resulting porosity reductions, is not well suited for streamline simulators.

1.6 Publications

The work performed during my PhD have so far lead to two publications. Parts of the work in chapter 2 about the model set-up and section 4.3 about the effect from surfactant has resulted in the following article:

Nielsen, S. M., A. A. Shapiro, M. L. Michelsen, and E. H. Stenby (2010). 1D simulations for microbial enhanced oil recovery with metabolite partitioning. *Transport Porous Med* 85, 785–802.

Parts of the work performed in chapter 5 about MEOR in the streamline simulator, which is based on the model presented in chapter 2, has lead to publication of a conference paper:

Nielsen, S. M., K. Jessen, A. A. Shapiro, M. L. Michelsen, and E. H. Stenby (2010). Microbial enhanced oil recovery: 3D simulation with gravity effects. *SPE-131048 presented at the EUROPEC/EAGE Conference and Exhibition, Barcelona, Spain, 14–17 June.*

The reactive transport model

A simulator is constructed to investigate how the important MEOR mechanisms influence the saturation profiles and the oil recovery. *Reduction of oil-water interfacial tension* due to surfactant production and *fluid diversion* due to the formation of biofilm, are regarded the major mechanisms (cf. section 1.4). The one-dimensional simulator is used to investigate the characteristics for MEOR.

This chapter introduces the model for MEOR where the primary mechanisms are included. Section 2.1 is a review of different MEOR models describing how the modeling is approached. Section 2.2 presents the general reactive transport equations. Then the model approach taken in this project and its assumptions are presented in section 2.3. The implementation of the mechanisms is introduced in section 2.4.

2.1 Review of MEOR model approaches

Modeling of MEOR includes several approaches. There are both one-dimensional models (Zhang et al., 1992; Sarkar et al., 1994; Sharma and Georgiou, 1993; Desouky et al., 1996) and models extendable to two and three dimensions (Islam, 1990; Islam and Gianetto, 1993; Chilingarian and Islam, 1995; Chang et al., 1991; Wo, 1997; Delshad et al., 2002; UTCHEM, 2000; Sugai et al., 2007; Behesht et al., 2008). All models are based on the mass balance which will later be presented as the combination of equations (2.2) and (2.3). Researchers use either two or three phases presenting either an oil-water or oil-water-gas system. Only Islam (1990) models how the gas phase influences the flooding system. The UTCHEM simulator is developed at University of Texas, Austin.

MEOR is one of the built-in features in the simulator. MEOR or bioremediation can be coupled with other chemical features such as the effects from gas, surfactant and polymer. Simulation results for MEOR cases agree well with core flooding experiments (Delshad et al., 2002). Still, thorough simulation studies of MEOR have not yet been presented using UTCHEM.

In the MEOR literature, the oil phase generally consists of oil only. The water phase includes the remaining components being bacteria, substrates and metabolites. The two flowing phases and their components are considered immiscible. Bacteria attach to the pore walls, where they form biofilm. The mathematical description of the bacterial attachment and detachment processes in connection with biofilm formation has overall two approaches. One approach utilizes equilibrium partitioning of bacteria assuming that equilibrium is fast compared to convection. This gives a relation between flowing and adsorbed bacteria. The adsorption is often described by the Langmuir isotherm (Sarkar et al., 1994; Delshad et al., 2002; Desouky et al., 1996; Behesht et al., 2008). The other approach applies rate expressions for the attachment and detachment processes. This implies an extra mass balance for the attached bacteria, where rate processes describe that bacteria grow, enter and leave the biofilm (Chang et al., 1991; Zhang et al., 1992; Islam, 1990). The attachment and detachment rate expressions exist in many versions, but they are generally modified derivations from the colloid filtration theory (Tufenkji, 2007).

The porosity is reduced due to formation of biofilm influencing the absolute permeability. Generally, the permeability is modified according to the Carman-Kozeny equation or modifications thereof. The Carman-Kozeny equation is:

$$\frac{K}{K_0} = \left(\frac{\phi}{\phi_0} \right)^3 \quad (2.1)$$

where K is absolute permeability, ϕ is porosity. The index 0 indicates initial value (Delshad et al., 2002; Zhang et al., 1992).

Some models introduce a limit for how much the water phase pore space can be occupied by biofilm. In the UTCHEM simulator, the biofilm can maximum comprise 90 % of water phase volume.

Nutrients and metabolites adsorb to the pore walls. Their adsorption is also modeled using the Langmuir isotherm (Islam, 1990; Behesht et al., 2008). In MEOR models, it is usually assumed that nutrients do not adsorb (Chang et al., 1991; Sarkar et al., 1994; Islam, 1990). Behesht et al. (2008) let surfactants adsorb in their model. Nutrients and metabolites are generally retained less compared to bacteria (Bryant and Burchfield, 1989).

Surfactant is a metabolite produced within the reservoir and is assumed only to be present in the water phase. When the surfactant concentration reaches a certain threshold, the interfacial tension drops affecting the relative permeabilities (Lake, 1989; Kowalewski et al., 2006). Models take the change in interfacial tension into account by reducing residual oil and residual water. The capillary number depends of IFT and is used to estimate the change in residual oil saturation (Lake, 1989). Often, the approach is empirical, where interpolation is performed between two relative permeability curves for a high and a low interfacial tension (Coats, 1980). The interpolation function depends on either a purely empirical function based on experimental results or the capillary number (Coats, 1980; Islam, 1990; Sarkar et al., 1994).

2.2 The general model

The models for MEOR is based on the general description of isothermal, multiphase, multicomponent fluid flow in porous media from the basic conservation laws (Lake et al., 1984; Lake, 1989).

The mass conservation equation may include a term for accumulation, convective fluxes, and a net production term. The net production covers sources such as injection and production wells, and reaction (Lake, 1989; Orr, 2007; Gerritsen and Durlofsky, 2005). The mass conservation equation is set up for each component i , where its contribution in each phase is included.

$$\frac{\partial}{\partial t} \left(\phi_0 \sum_j \omega_{ij} s_j \right) + \nabla \cdot \left(\sum_j \omega_{ij} \mathbf{u}_j \right) = R_i + Q_i \quad (2.2)$$

where j is the phase, i is the component, ω_{ij} are component mass concentration in phase j , \mathbf{u} is the linear velocity (eqn. (2.3)), t is the time, ϕ_0 is the porosity, and the net production for component i is the reaction term R_i , and well term Q_i .

The Darcy law for a

$$\mathbf{u}_j = - \frac{\mathbf{K} k_{rj}}{\mu_j} \cdot (\nabla P - \rho_j g \nabla D) \quad (2.3)$$

where \mathbf{K} is the absolute permeability tensor, k_{rj} is the relative permeability for phase j , P is pressure, ρ_j is the phase density, and g is gravitational acceleration. The length variables are x , y and z , and the depth is D being downwards positive and equals to the direction of the z axis, The Darcy law (eqn. (2.3)) determines the velocity pattern of the flowing phases based on the pressure gradient, gravitational gradient and the

permeabilities.

For the MEOR system presented here, the fluid flow is one-dimensional and the effect from gravity is excluded. We use the mass balance terms; accumulation, convection and reaction. The reactions are strongly coupled. The source terms also cover injection and production corresponding to the wells.

2.2.1 Fractional flow function

The flow of a phase can be rewritten for a one-dimensional model system, where the capillary pressure and the effect from gravity are considered negligible. The Darcy law is derived from equation (2.3) and becomes (Orr, 2007):

$$u_j = K \lambda_j \left(\frac{\partial P}{\partial x} \right) \quad (2.4)$$

where λ_j is the phase mobility:

$$\lambda_j = \frac{k_{rj}}{\mu_j} \quad (2.5)$$

The total fluid flow is obtained by summing over all flow velocities of the phases, which is given by eq. (2.4). The total fluid flow is:

$$u_t = u_o + u_w \quad \Rightarrow \quad (2.6)$$

$$u_t = -K (\lambda_w + \lambda_o) \left(\frac{\partial P}{\partial x} \right) \quad (2.7)$$

The total mobility λ_t is introduced as the sum of phase mobilities.

$$\lambda_t = \sum_j \lambda_j \quad (2.8)$$

The total mobility changes during the flooding process and therefore the pressure field also changes. The total mobility is determined by the phase relative permeabilities that are functions of saturation (Gerritsen and Durlofsky, 2005).

Combination of equations (2.4) and (2.7) produces the following relation for phase velocity:

$$u_j = u_t f_j \quad (2.9)$$

where f_j is the fractional flow function

$$f_j = \frac{\lambda_j}{\lambda_t} \quad (2.10)$$

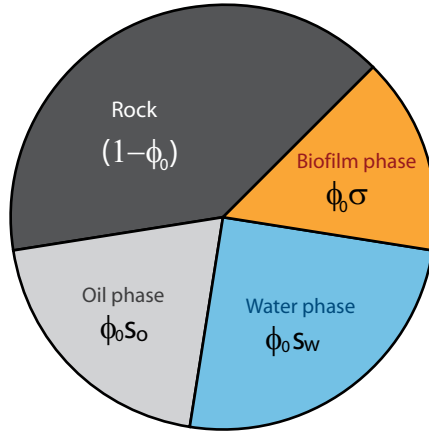


Figure 2.1: Schematic volume distribution of rock and porous volume ϕ_0 . The saturations for oil, water and biofilm are shown.

The fractional flow function describes how much of the total flow is made up by flow of the specific phase. For a system consisting with two phases; oil and water, the fractional flow constraint is as shown below.

$$f_w + f_o = 1 \quad (2.11)$$

Substitution of the phase velocity by the fractional flow function and the total velocity excludes the absolute permeability and the pressure gradient from the equations. The substitution decreases the complexity of the equation system.

2.3 Specific model formulation

The reservoir consists of porous rock $(1 - \phi_0)$ and the pore volume, ϕ_0 , where ϕ_0 is the initial porosity. The pore volume is filled by the three phases. The saturation of a phase is given as the phase volume over the pore volume, where water, oil and biofilm saturations are s_w , s_o and σ . In MEOR literature, the biofilm saturation is generally designated σ . The distribution of occupied pore volume and rock volume fraction is shown in figure 2.1. The phase saturation constraint becomes:

$$s_w + s_o + \sigma = 1 \quad (2.12)$$

Our reactive transport model describes convection, bacterial growth, substrate consumption, and metabolite production, where the metabolite is surfactant. The system consists of two flowing phases and a sessile phase, and comprises five components;

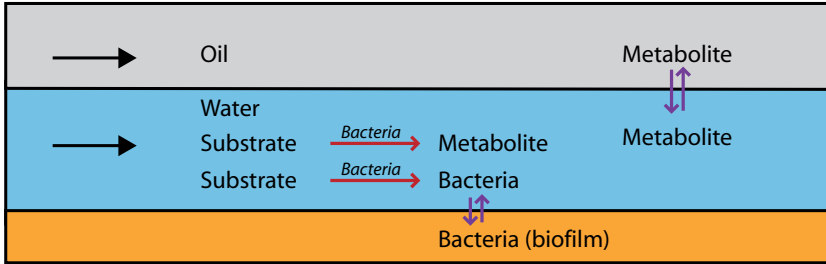


Figure 2.2: Picture illustrating the system consisting of two flowing phases; water and oil, and the sessile biofilm phase. Red arrows indicate the possible reactions, which actually take place in the both water and biofilm phases. Purple arrows indicate reactions, partition between phases by surfactant/metabolite and bacteria.

Phases

- Oil
- Water
- Bacteria

Components

- Oil (o)
- Water (w)
- Substrate (s)
- Bacteria (b)
- Metabolite/surfactant (m)

The mass concentration of component i in phase j is designated ω_{ij} . The biofilm comprises bacteria only, so the biofilm bacteria equal the saturation for the biofilm phase and the symbol for the biofilm bacteria becomes σ .

The water phase may consist of water, bacteria, substrate and metabolite. The oil phase consists primarily of oil, but contains also metabolite. The novel approach is the partition of metabolite between the oil and water phases. Figure 2.2 illustrates components and phases of system. The biofilm bacteria grow, while substrate is consumed directly from the water phase and the metabolite produced is secreted into the water phase.

2.3.1 Assumptions

The model is based on the following assumptions, where some simplifications are introduced:

1. Fluid flow is one-dimensional and takes place in uniform porous medium.
2. Negligible diffusion.
3. Isothermal system as reservoir fluctuations in temperature is regarded minimal (Sarkar et al., 1994).

4. Incompressibility of the fluids meaning that the densities remains constant. Generally, this is a valid assumption for fluid flows (Sarkar et al., 1994; Orr, 2007).
5. *No volume change on mixing* (Orr, 2007), because of the lack of thermodynamical data for most of the components.
6. The simple form of the fractional flow function, eq. (2.10), is used as capillary pressure is considered negligible (Lake, 1989).
7. *No volume change on reaction*, when reaction converts components of same density. When reactants and products have different densities, the volume changes. We choose to use the same densities here, but the code can handle different densities of reactants.
8. Constant viscosity of phases, which is a legitimate assumption for the water phase, when the bacteria concentration is low. The oil phase viscosity is here always assumed constant as no gas is produced and the main carbon source is injected substrates.
9. The pressure difference remains at a level, where injectivity can be maintained.
10. Continuous injection of nutrient and bacteria takes place.
11. The mechanisms responsible for bacterial retainment can be lumped into expression, which then includes the adsorption process during formation of biofilm.
12. Decay of bacteria is left out and instead an effective growth rate is used.
13. Application of anaerobic bacteria as their survivability is considered over aerobic, when exposed to reservoir conditions.
14. No indigenous bacteria present.
15. Bacterial growth rate can be described by Monod kinetics being independent on temperature, pressure, pH and salinity (Ginn et al., 2002; Islam, 1990; Kim, 2006; Nielsen et al., 2003; Zhang et al., 1992).
16. Regarding growth rate, only one substrate is limiting for growth as the other possible substrates is assumed to be in excess.
17. No inhibition of growth by substrates or metabolites.
18. Bacteria adsorb to the pore walls forming a biofilm, which is described by equilibrium partitioning (Behesht et al., 2008). The distribution of bacteria is instantaneous, and the distribution kinetics is neglected.
19. Both flowing and sessile bacteria have the same growth rate (Zhang et al., 1992). Most models assume that similar growth occurs in flowing and sessile phases.

20. Biofilm bacteria take up substrate from the water phase for growth and secrete metabolites directly into the water phase. There is no mass transfer resistance (Chen et al., 1998).
21. Maintenance of bacterial processes is considered negligible. For instance, a low pH reservoir would require a substantial amount of energy to maintain an optimal pH and cellular processes within the bacteria (Molz et al., 1986; Zhang et al., 1992; Sarkar et al., 1994). Therefore, the reservoir conditions is assumed not to stress the bacteria in such a degree that maintenance becomes important (UTCHEM, 2000; Chang et al., 1991).
22. Chemotaxis is considered not to happen.
23. The main metabolite is surfactant and other metabolites are considered negligible.
24. Surfactant can be distributed between both phases. The distribution is instantaneous, and the distribution kinetics is neglected.
25. No substrate and metabolite adsorption on the pore walls. The adsorption of substrates such as molasses and sucrose is limited meaning that negligibility of their adsorption is reasonable (Wo, 1997).

2.3.2 Component mass balances

According to equations (2.2) and (2.3), the mass balances for each component are set up in a one-dimensional system.

Bacteria

Bacteria exist as flowing bacteria in the water phase, ω_{bw} , and as a volume fraction occupied by the biofilm, σ . The bacteria partition between the water phase and the biofilm using equilibrium adsorption. The biofilm saturation is a function of flowing bacteria, and the partitioning is described in details in section 2.3.5. The mass balance covers the total bacteria, which constitute bacteria found in both the water phase and the biofilm.

$$\frac{\partial}{\partial t} (\phi_0 \omega_{bw} s_w + \phi_0 \sigma \rho_b) + \frac{\partial}{\partial x} (u_t \omega_{bw} f_w) = \phi_0 (R_b + Q_b) \quad (2.13)$$

where u_t is the linear velocity, ρ_b is the bacteria density, f_j is the fractional flow function of phase j , x is the length variable, t is the time, ϕ_0 is the initial porosity, R_b is bacteria net production, and Q_b is the bacteria well term. The reaction terms for bacteria, substrate and metabolite are elaborated in section 2.3.4.

Substrate

The substrate is consumed and exists only in the water phase and no adsorption takes place.

$$\frac{\partial}{\partial t} (\phi_0 \omega_{sw} s_w) + \frac{\partial}{\partial x} (u_t \omega_{sw} f_w) = \phi_0 (R_s + Q_s) \quad (2.14)$$

Metabolite

Metabolite exists in both flowing phases and is distributed according to a partitioning coefficient. Metabolite partition is explained in details in section 2.3.6.

$$\frac{\partial}{\partial t} (\phi_0 \omega_{mw} s_w + \phi_0 \omega_{mo} s_o) + \frac{\partial}{\partial x} (u_t \omega_{mw} f_w + u_t \omega_{mo} f_o) = \phi_0 (R_m + Q_m) \quad (2.15)$$

Water

Water is the most abundant component, existing only in the water phase. Water is assumed not to take part in any reactions.

$$\frac{\partial}{\partial t} (\phi_0 \omega_{ww} s_w) + \frac{\partial}{\partial x} (u_t \omega_{ww} f_w) = \phi_0 Q_w \quad (2.16)$$

Oil

The oil is considered only to consist of one component, but in reality oil consists of many different hydrocarbons. Here, the oil has been lumped together constituting one oil. Oil is only present in the oil phase and it is the main constituent.

$$\frac{\partial}{\partial t} (\phi_0 \omega_{oo} s_o) + \frac{\partial}{\partial x} (u_t \omega_{oo} f_o) = \phi_0 Q_o \quad (2.17)$$

2.3.3 Relative Permeability

The relative permeabilities for oil and water are k_{ro} and k_{rw} , respectively. Experimentally determined relative permeability curves exist for systems with specific rock and fluids and are applied to modeling purposes. In many cases, the relative permeability curves are not available, so different empirical correlations are used instead. Many empirical versions of the curves are presented, but a well-established version are the Corey

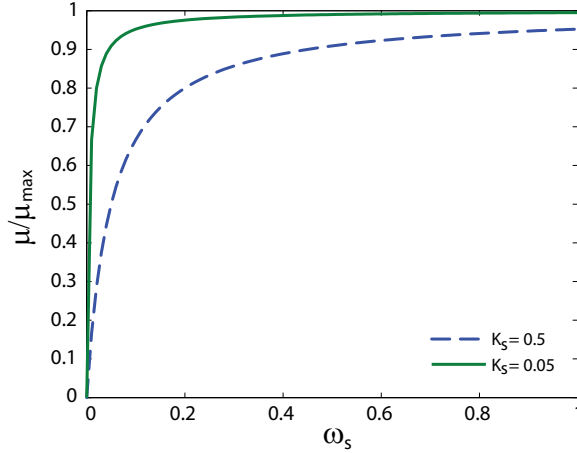


Figure 2.3: Plot of bacterial growth rate μ/μ_{max} as a function of mass concentration of substrate. Two growth rate curves with different K_s are shown.

type relative permeability curves (Lake, 1989):

$$k_{rw} = k_{rwor} \cdot \left(\frac{s_w - s_{wi}}{1 - s_{wi} - s_{or}} \right)^a \quad (2.18)$$

$$k_{ro} = k_{rowi} \cdot \left(\frac{1 - s_w - s_{or}}{1 - s_{wi} - s_{or}} \right)^b \quad (2.19)$$

where s_w is water saturation, s_{wi} is initial water saturation, s_{or} is residual oil saturation, k_{rowi} is endpoint relative permeability for oil at s_{wi} , k_{rwor} is endpoint relative permeability for water at $(1 - s_{or})$, and the exponents for water and oil are a and b , respectively.

2.3.4 Reactions

The growth rate expressions applied for bacteria are often the Monod expression based on the Michaelis-Menten enzyme kinetics and Langmuir expression for heterogeneous catalysis (Chang et al., 1991; Islam, 1990; Nielsen et al., 2003; Zhang et al., 1992). The Monod expression with one limiting substrate is widely used (Islam, 1990; Chang et al., 1991; Behesht et al., 2008), but it is empirical in the context of microbial growth. The Monod expression with two limiting substrates becomes important, when two substrates are not in excess and may limit the growth. The dual substrate Monod expression is applied in e.g. the UTCHEM simulator and by Zhang et al. (1992).

The Monod expression fits the bacterial growth rate characteristics such as having a maximum growth rate, and that the reaction kinetics are first-order processes at

low substrate concentrations (Nielsen et al., 2003). The knowledge about inhibition effects from metabolites is important in order to realize whether a necessary metabolite concentration can be achieved (Deng et al., 1999).

The Monod growth rate for one limiting substrate without any inhibition will be used in this work:

$$\mu = \mu_{max} \cdot \frac{\omega_{sw}}{K_s + \omega_{sw}} \quad [\text{day}^{-1}] \quad (2.20)$$

where μ_{max} is the maximum growth rate, and K_s is the half saturation constant. Figure 2.3 shows the Monod expression for with two different half saturation constants. A larger saturation constant means that the substrate concentration should be larger before half the maximum growth rate is obtained (Nielsen et al., 2003).

Another expression is the semi-empirical Contois equation, which differs from the Monod expression (Sarkar et al., 1994).

$$\mu = \frac{\mu_{max}}{1 + D_c \frac{\omega_{bw}}{\omega_{sw}}} \quad (2.21)$$

where D_c is a constant. The growth rate is inhibited by bacteria themselves, which Nielsen et al. (2003) find very unlikely. They propose that the self-inhibition originates from other unknown factors.

Sugai et al. (2007) presents the modified Moser equation resembling the Monod expression, where it only differs in having exponents on the substrate concentrations. The exponents can be useful for fitting to experimental data (Nielsen et al., 2003). In general, many growth rate expressions rely on batch experiments and the choice of model depends on the best fit with the obtained data point (Chang et al., 1991; Sarkar et al., 1994; Desouky et al., 1996; Sugai et al., 2007).

The reaction term for bacteria depends on the growth rate, where the total production of bacteria is a function of the total bacteria concentration and the growth rate. The corresponding reaction term R_b is expressed as

$$R_b = Y_{sb} (s_w \omega_{bw} + \rho_b \sigma) \mu, \quad (2.22)$$

where the parameter Y_{sb} is the yield of bacteria on substrate, and ω_{bw} is the bacterial mass concentration of the water phase.

During growth, bacteria produce several metabolites and consume different substrates, but only the most important ones are included in the model. Therefore, the model covers only one substrate and one metabolite in the reactions. The reaction terms for

metabolite and substrate are:

$$R_m = Y_{sm} (s_w \omega_{bw} + \rho_b \sigma) \mu, \quad (2.23)$$

$$R_s = -q_b - q_m, \quad (2.24)$$

and Y_{sm} is the yield of surfactant (m) on substrate (Nielsen et al., 2003; Zhang et al., 1992). The yield coefficients determine the fraction of substrate that goes to bacteria and metabolite. Generally, the largest amount of substrate is converted to bacteria. Other researchers have considered production of metabolites when the substrate concentration is only above a threshold point (Zhang et al., 1992; Behesht et al., 2008). The approach originates from the fact that some metabolites are only formed when the surrounding environment is rich in substrate.

In practice, bacterial decay occurs meaning that a portion of the bacteria does not contribute to growth. We assume that the growth rate is the net growth rate.

2.3.5 Bacteria Partition

Many researchers use the additional mass balance for the biofilm bacteria (Islam, 1990; Chang et al., 1991; Zhang et al., 1992; UTCHEM, 2000). We choose equilibrium adsorption to avoid introduction of several parameters whose values are only estimated. Therefore, the effect of bacterial adsorption is investigated using this simpler approach.

Equilibrium adsorption utilizes that a function describes the bacteria partition (Sarkar et al., 1994; Desouky et al., 1996; Delshad et al., 2002; Behesht et al., 2008). The Langmuir equation relates a concentration of bacteria to the amount of bacteria adsorbed to the pore walls. The Langmuir expression is derived from the assumption only one layer of adsorbing components. The biofilm formed by the attached bacteria is assumed to contain no water or other substances, which makes it a cell-dense biofilm. The bacteria exists only flowing in the water phase and as sessile biofilm bacteria. Therefore, the bacteria can only adsorb from the water phase to enter the biofilm. Hence, we assume that the water phase concentration of bacteria, ω_{bw} , determines the amount of bacteria that attach to the pore walls.

The mass of bacteria adsorbed pr. unit area is:

$$\mathcal{M}_b = \frac{w_1 \omega_{bw}}{1 + w_2 \omega_{bw}} \quad [\text{kg}/\text{m}^2] \quad (2.25)$$

where w_1 and w_2 are the Langmuir constants.

The amount of bacteria that adsorbs, depends on the pore wall area available. The specific surface of porous rock \tilde{S} is 10^5 – 10^6 m^2/m^3 total volume. The contact area

between pore walls and the water phase is assumed to reflect the area available for adsorption, so the efficient surface area \mathcal{S} is the specific surface area scaled with the water phase saturation.

$$\mathcal{S} = \frac{\tilde{S}}{\phi_0} \left(\frac{s_w}{s_w^{max}} \right) \quad [\text{m}^2/\text{m}^3 \text{ PV}] \quad (2.26)$$

where the maximum obtainable water saturation is unity.

Combination of equation (2.25) and (2.26) gives the mass of bacteria adsorbing to the pore walls as a function of the water phase concentration of bacteria.

$$\begin{aligned} \sigma \rho_b &= \mathcal{S} \cdot \mathcal{M}_b \quad [\text{kg bacteria adsorbed}/\text{m}^3 \text{ PV}] \\ &= \left(\frac{\tilde{S} \cdot s_w}{\phi s_w^{max}} \right) \frac{w_1 \omega_{bw}}{1 + w_2 \omega_{bw}} \end{aligned} \quad (2.27)$$

The amount of bacteria adsorbed is $(\sigma \rho_b)$. A low concentration of bacteria in the water phase shows linearity between the flowing and adsorbed bacteria. The ratio w_1/w_2 multiplied with the specific surface is the maximum obtainable adsorption of bacteria:

$$(\sigma \rho_b)_{max} = \mathcal{S} \frac{w_1}{w_2} \quad (2.28)$$

2.3.6 Surfactant Partition

The novel approach is partitioning of surfactant. The approach has not been included in other MEOR models so far. Partitioning of surfactant depends of the distribution coefficient K_i (Ravera et al., 2000). The surfactant mass concentration in water and oil phase are ω_{mw} and ω_{mo} , respectively. The surfactant is distributed according to the amounts of water and oil:

$$\frac{\omega_{mw}}{\omega_{mo}} = K_i \frac{\omega_{ww}}{\omega_{oo}} \quad (2.29)$$

Surfactant exists in small amounts compared to water and oil. Partitioning of surfactant takes place, but is dependent on rate of diffusion to obtain equilibrium (Ravera et al., 2000). We assume fast exchange between phases and hence instant equilibrium.

The surfactant concentration in the water phase must reach a certain concentration threshold, before surfactant can reduce the interfacial tension. A large distribution coefficient means that most surfactant is present in the water phase. The relative permeabilities depend on the water phase mass concentration, so when surfactant is moved into the oil phase, there will be a smaller effect from the surfactant. Therefore,

transfer part of the surfactant to oil phase is equivalent to its "disappearance", so that the total effect from surfactant is reduced. The adsorption of surfactant to the pore walls is not directly included in the model, but practically the disappearance also includes this. The model lets surfactant go into the oil phase, where a large part of the oil and subsequently the surfactant in the oil phase do not flow. The oil phase captures the surfactant, but it may as well be adsorbed to the pore walls in the oil phase.

2.3.7 Porosity changes

The initial pore volume ϕ_0 does not change in this model as the rock volume remains unchanged. The actual porosity available for flow is affected by the formation of biofilm. Therefore, the actual porosity ϕ depends on the initial porosity and the biofilm saturation.

$$\phi = \phi_0(1 - \sigma) \tag{2.30}$$

The biofilm phase contribution to the porosity change has been taken into consideration in the definition of saturations. The pore volume consists of saturations of the water, oil and biofilm phases (cf. eq. (2.12)).

2.4 Implementation

This section contains the implementation of the most important mechanisms in MEOR. *Reduction of oil-water interfacial tension* and *fluid diversion* are regarded the primary mechanisms, which leaves out *reduction of oil viscosity* mechanisms. The mechanisms was introduced in section 1.4, and the implementation builds on the model presented earlier in this chapter.

2.4.1 General approaches

In the MEOR literature, there are different approaches for implementation of the mechanisms. There exists literature from other research areas, where these mechanisms are also important. As an example, bioremediation deals with bacteria in the underground working with models that describe the transport and biological processes (Murphy and Ginn, 2000; Tufenkji, 2007). Other EOR processes and generally in the oil industry, many investigations have been performed to clarify the influence of interfacial tensions on the relative permeabilities (Coats, 1980; Kumar et al., 1985; John et al., 2005; Shen et al., 2006).

2.4.2 Reduction of oil-water interfacial tension

In the literature, there is no actual agreement on how the IFT affects the residual saturations and relative permeability curves (Coats, 1980; Kumar et al., 1985; John et al., 2005; Shen et al., 2006). Researchers obtain different effects on the relative permeability curves unable to clarify the influence of the parameters (Al-Wahaibi et al., 2006). Generally, researchers suggest that the relative permeability curves show some dependence on IFT. A lower IFT decreases the capillary resistance, resulting in relative permeability curves with:

- Reduced curvature
- Reduced residual saturations
- Increasing end point relative permeabilities as the lines will approach full miscibility

When IFT goes toward zero, the relative permeability curves approach a unit slope line for which the relative permeability is simply equal to the phase saturation (Coats, 1980; Al-Wahaibi et al., 2006).

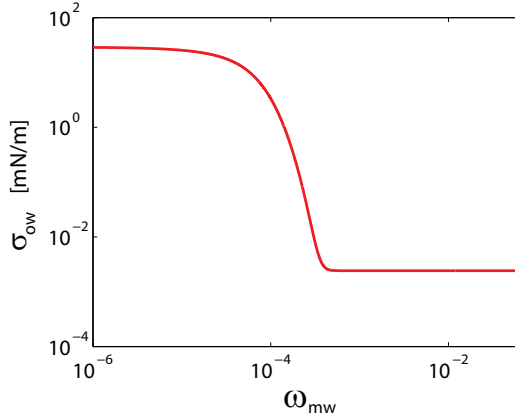


Figure 2.4: Different curves for water phase concentration of surfactant ω_{mw} against interfacial tension σ_{ow} . After a certain concentration of surfactant is reached, further increases in concentration does not change σ_{ow} (Lake, 1989).

The efficiency of a surfactant depends on how much the IFT can be lowered and the concentration where the IFT drops dramatically. In many cases, the correlation curve between surfactant concentration and IFT looks as shown in figure 2.4. The oil-water IFT is designated σ_{ow} , where the equation used is constructed based on the knowledge of typical IFT and surfactant concentration features.

$$\frac{\sigma_{ow}^*}{\sigma_{ow}} = \frac{-\tanh(q_3 \omega_{mw} - q_2) + 1 + q_1}{-\tanh(-q_2) + 1 + q_1} \quad (2.31)$$

where σ_{ow}^* indicates is the calculated IFT, constants are q_1 , q_2 and q_3 . The case without any surfactant has an initial IFT, which is the maximum IFT.

To the best of our knowledge, only the surfactant dissolved in the aqueous phase contributes to the decrease of the oil-water IFT (Tadmouri et al., 2008). In the present work, a simple model is assumed: the surfactant that is dissolved in oil phase, does not affect the IFT. The role of the dissolution in oil is reduction of the effective concentration meaning that IFT only depends on the surfactant concentration in the water phase.

Commonly, the IFTs between oil and water are around 20–30 mN/m (Shen et al., 2006). In order to increase recovery significantly, a good surfactant should decrease IFT three or four orders of magnitude (Fulcher et al., 1985; Shen et al., 2006). Therefore, the ability of the bacteria to produce the threshold surfactant concentration is important to achieve the required reduction of IFT.

Many approaches have been used to implement the effect of IFT reduction on the relative permeability curves, where a variety of functions are used to modify the relative

permeability curves. Often, the Corey relative permeabilities shown in section 2.3.3 are applied. The Corey type permeability curves utilize parameters such as residual saturations and exponents, which are parameters becoming a function of the reduced IFT (Al-Wahaibi et al., 2006). One example is application of the capillary number, which is a function of IFT. The capillary number is related to the residual oil saturation, which is directly applied in the expression for the relative permeability curves (Green and Willhite, 1998; Al-Wahaibi et al., 2006). Another approach proposed by Coats (1980) modifies the relative permeability curves by interpolation between two sets of curves at two different IFTs. The interpolation function ranges between those two IFTs.

Generally, the approach to modify the relative permeability utilize either the capillary number approach or the interpolation approach. However, there are also cases, where the methods are combined e.g. using the capillary number as the interpolation function.

Based on the methods applied to modify the relative permeability, three approaches are presented in the following sections:

1. The capillary number method
2. Coats interpolation between relative permeabilities
3. Interpolation of each parameter in the Corey type relative permeabilities

As suggested in the latter methods, the parameters included in the Corey relative permeability expression are interpolated on its own. Interpolation of various parameters has been performed in other versions (Fulcher et al., 1985; Kumar et al., 1985; Shen et al., 2006).

2.4.2.1 The capillary number method

The capillary number N_{ca} is ratio of viscous to capillary forces and thus being dependent on changes in oil-water interfacial tension σ_{ow} .

$$N_{ca} = \frac{\mu_w v}{\sigma_{ow}} \quad (2.32)$$

where N_{ca} is the dimensionless capillary number, μ_w is viscosity of displacing fluid, and v is the 'characteristic' linear velocity. For general water flooding reservoirs, the capillary number is at about 10^{-6} under normal reservoir conditions (Green and Willhite, 1998). In order to effectively mobilize the residual oil, the capillary number increases to around 10^{-3} . The capillary number increases by velocity increments, increments of water viscosity, and IFT reductions. The reduction of IFT can raise the capillary number

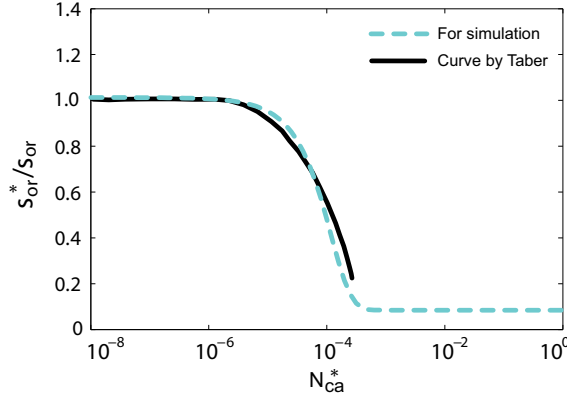


Figure 2.5: Capillary desaturation curve. Green and Willhite (1998) have collected curves for dependencies between $\frac{s_{or}^*}{s_{or}}$ and N_{ca}^* , where s_{or}^* is the modified residual oil saturation. The graph displays the curve (blue, dash) applied in this work and the curve by Taber (1969) (full, black).

significantly, because IFT can be changed far more compared to the other parameters.

Experiments show a dependency between capillary number and normalized residual oil saturation s_{or}^*/s_{or} , where s_{or}^* is the modified residual oil saturation and s_{or} is the residual oil saturation after waterflood. This is also known as the capillary desaturation curve. Green and Willhite (1998) present several data showing this dependency, which is determined for e.g. more rock types. The experiments lead to the different curves, where the reduction of the residual oil saturation differs at each curve. The decline rates differs and different capillary numbers are required before reductions occur, but they produce the same curve behavior.

Figure 2.5 shows one example of the capillary desaturation curve, being an approximation of the curve presented by Taber (1969). The capillary desaturation curve is applied in the simulations. The capillary desaturation curve has the following mathematical description.

$$\frac{s_{or}^*}{s_{or}} = \frac{-\tanh(p_1(N_{ca}^*) - p_3) + 1 + p_2}{-\tanh(p_1(N_{ca}^0) - p_3) + 1 + p_2} \quad (2.33)$$

where $*$ is the index for a modified/calculated variable, N_{ca}^0 is the capillary number at initial conditions also corresponding to minimum capillary number, constants are p_1 , p_2 and p_3 .

Figure 2.6 shows the procedures for the three methods, where the capillary number method is covered by subfigures 2.6(a)–(b). A new residual oil saturation s_{or}^* is predicted from the reduction in IFT. The calculated residual oil is then applied in the Corey equations, equation (2.18) and (2.19), producing the modified relative permeability curves, which are shown in figure 2.6(b). The curves stretch from s_{wi} to $(1 - s_{or}^*)$ and the gradient also become smaller.

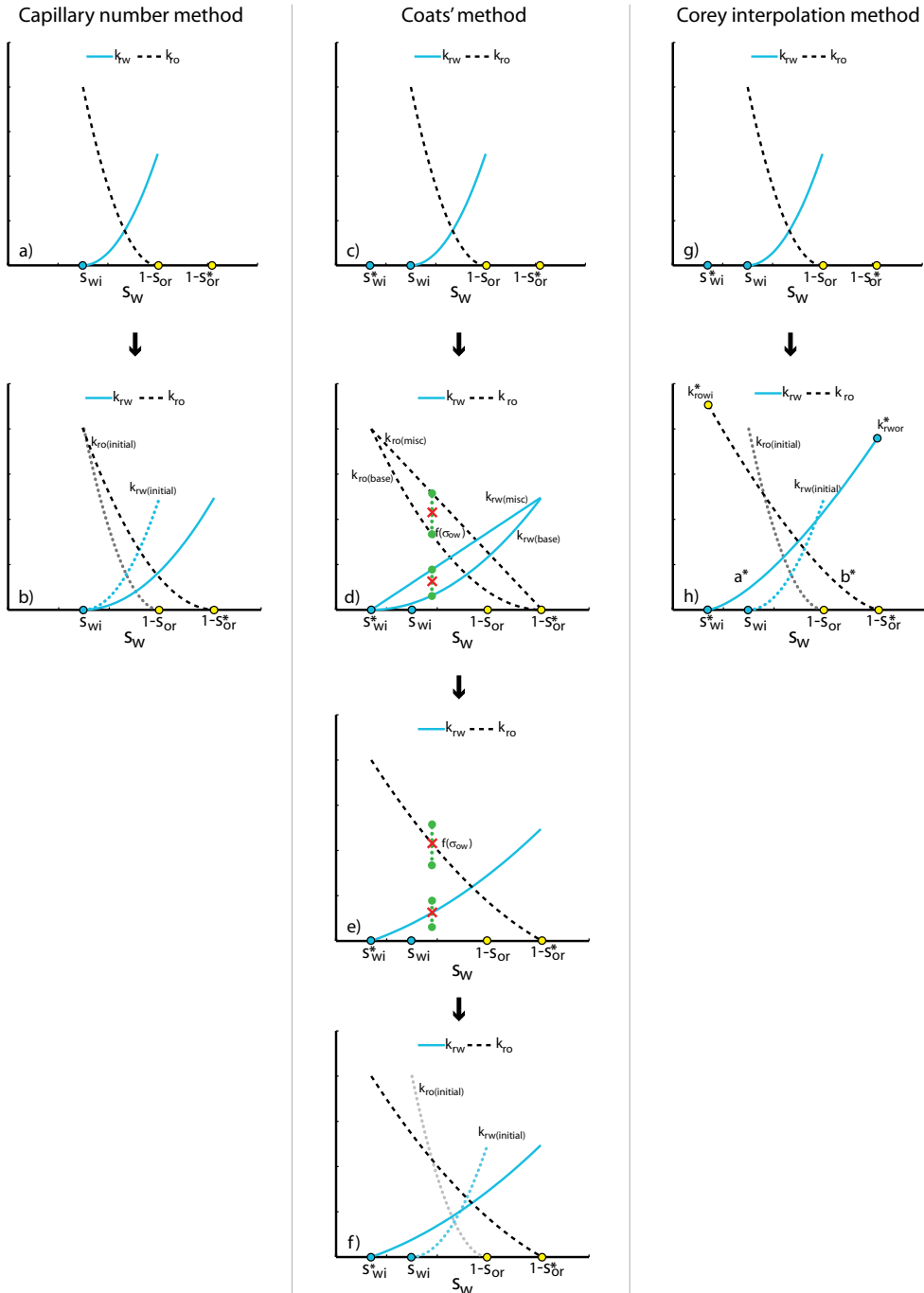


Figure 2.6: Graphic illustration of the procedure for the different interpolation methods; the capillary number method (a–b), Coats' interpolation method (c–f), and Corey interpolation of parameters method (g–h).

2.4.2.2 Coats' interpolation between relative permeability curves

Coats' correlation is stated to be used in many commercial simulators for modeling the effect of miscibility on relative permeability (Al-Wahaibi et al., 2006), even though it is not based on any theory, but developed to describe the changes in the relative permeability curves by IFT reductions (Coats, 1980). Coats (1980) models the changes of two-phase gas and oil relative permeability curves due to reductions of IFT. The method is shown for water and oil:

$$g(\sigma_{ow}) = \left(\frac{\sigma_{ow}}{\sigma_{ow,base}} \right)^{\frac{1}{n}} \quad (2.34)$$

$$s_{wi}^* = g(\sigma_{ow}) s_{wi} \quad (2.35)$$

$$s_{or}^* = g(\sigma_{ow}) s_{or} \quad (2.36)$$

$$k_{rw} = g(\sigma_{ow}) k_{rw(base)} + [1 - g(\sigma_{ow})] k_{rw(misc)} \quad (2.37)$$

$$k_{ro} = g(\sigma_{ow}) k_{ro(base)} + [1 - g(\sigma_{ow})] k_{ro(misc)}, \quad (2.38)$$

where σ_{ow} is current IFT, $g(\sigma_{ow})$ interpolation function with values from unity at the highest IFT towards zero at lower IFT. The index * means modified/calculated values. The modified residual saturations, equations 2.35 and 2.36, are interpolation between zero and the initial residual saturation, where the residual saturations drop as IFT decreases. $k_{r(base)}$ is the relative permeability curve at largest interfacial tension ' $\sigma_{ow,base}$ ' being a function of both residual saturations corresponding to the initial Corey equations, eqns. (2.18) and (2.19)). $k_{r(misc)}$ is the linear relative permeability curve at lowest IFT also being a function of both residual saturations but generally the straight line case approaching full miscibility (Coats, 1980; Al-Wahaibi et al., 2006). n is an adjustable exponent normally in the range of 4–10, which is used to fit to the experimental relative permeability curves. When n is larger, the interpolation function becomes less sensitive toward IFT reductions and thus the relative permeabilities change less toward the full miscibility curves.

Figure 2.6(c)–(f) depicts the procedure for Coats' method. The procedure is initiated by an interpolation, where initial and current IFT are used to create the interpolation function ranging between initial values and zero. The newly calculated residual saturations, s_{or}^* and s_{wi}^* , are found. In figure 2.6d, the interpolation function is used to modify the relative permeability curve to obtain the corrected $k_{rj(misc)}$ and $k_{rj(base)}$. The curves now stretch between s_{wi}^* and $(1 - s_{or}^*)$. Figure 2.6(e) depicts that the interpolation function, eqn. (2.34), is used to interpolate between *base* and *misc* relative permeability curves for water and oil, equations (2.37) and (2.38). In this way, interpolation between the straight line and the curved line corresponds to modifications of curvature. The

initial and final curves are shown in figure 2.6(f), where the final curves has become more straight compared to the initial curves. This means that the residual saturations and to some extent the exponents all are functions of IFT, while the capillary number method only changes residual oil saturation directly.

2.4.2.3 Interpolation of parameters in Corey type relative permeabilities

This method is applied in a similar manner as Shen et al. (2006) presented in their work. However, our inclusion of the parameters results in being a new approach. We apply interpolation of more Corey parameters. One advantage is that experimentally determined changes in the relative permeabilities can more easily be approximated by this method.

The difference between capillary number and Corey interpolation method is the translation of IFT reduction to changes in the relative permeability curves. The methods are different with regard to e.g. sensitivity. We have chosen to use the interpolation function presented by Coats (1980), equation (2.34). The interpolation can be performed for each parameter given in the Corey type permeabilities, cf. eq. (2.18) and (2.19).

$$s_{or}^* = g(\sigma_{ow}) \cdot s_{or} \quad (2.39)$$

$$s_{wi}^* = g(\sigma_{ow}) \cdot s_{wi} \quad (2.40)$$

$$k_{rowi}^* = g(\sigma_{ow}) \cdot k_{rowi} + [1 - g(\sigma_{ow})] \quad (2.41)$$

$$k_{rwor}^* = g(\sigma_{ow}) \cdot k_{rwor} + [1 - g(\sigma_{ow})] \quad (2.42)$$

$$a^* = g(\sigma_{ow}) \cdot a + [1 - g(\sigma_{ow})] \quad (2.43)$$

$$b^* = g(\sigma_{ow}) \cdot b + [1 - g(\sigma_{ow})] \quad (2.44)$$

Again, the residual saturations are interpolated between zero and initial saturations like performed by Coats (1980). A modified approach could be another usage of interpolation function in relation to residual water, because the residual water saturation changes differently than the residual oil saturation (Amaefule and Handy, 1982; Kumar et al., 1985). As the curves are supposed to go towards the straight line curve, the end point values, equations (2.41) and (2.42), are interpolations between the initial end point values and unity, and the exponents is interpolated between unity and initial value, which in our case is two.

Figure 2.6(g)–(h) depicts the procedure for the Corey parameter interpolation method. Similar to Coats' method, the procedure is initiated by creating an interpolation function. The interpolated parameters, equations (2.39)–(2.44), are applied to the Corey

relative permeability equations. The resulting curves are shown in figure 2.6(h), where the curves straighten and span broader on the water saturation axis due to reductions in residual saturations, increased end point values at residual saturations, and reduction of exponents.

2.4.2.4 *Applicability*

This section has presented a method for implementing the reduction of IFT. Three approaches have been presented for modifying the relative permeability for water and oil. The approaches have some resemblance, so we regard that they perform similar. In chapter 4, we illustrate the performance of the different approaches for changing IFT in context of MEOR.

2.4.3 Permeability Modifications

Bacteria form biofilm, reducing the porosity and thus the permeability. In the MEOR literature, the general approach is application of the Carman-Kozeny equation and modifications thereof (Chisholm et al., 1990; Zhang et al., 1992; UTCHEM, 2000).

The following version of the Kozeny-Carman relation has been used in work concerning MEOR (Chisholm et al., 1990; Zhang et al., 1992):

$$\frac{K}{K_0} = \left(\frac{\phi}{\phi_0} \right)^\gamma \quad (2.45)$$

The exponent γ is normally around 3 (Chisholm et al., 1990; Zhang et al., 1992), but is used with values between 2 and 5 (Clement et al., 1996). In bioremediation, many investigations have been performed on the applicability of the Kozeny-Carman equation or similar expressions. Generally, they are performed on systems with only one phase (Clement et al., 1996; Thullner, 2009). Overall, the results show reasonable fits, but they propose no final conclusion (Thullner, 2009).

Several other approaches have also been proposed. Sarkar et al. (1994) suggest a permeability reduction model applying effective medium theory, which utilizes the distribution function for pore sizes and permeabilities. Islam (1990) proposes empirical relationship to modify the permeabilities for pluggable and non-pluggable pores as a function of attached bacteria.

Generally, the porosity reductions is considered only to influence the absolute permeability. However, Wo (1997) proposes modifications of the relative permeability for the water phase only, because bacteria are present in the water phase. They enter the biofilm phase due to adsorption from the water phase.

Different approaches for modifying the permeabilities have been introduced. The following sections go through two approaches:

- Modifications of absolute permeability
- Modifications of the relative permeability for the water only

2.4.3.1 Absolute permeability

According to the approach coming from one phase studies, the porosity modification affects both phases equally, influencing the absolute permeability (Thullner, 2009). The

total Darcy velocity \mathbf{u}_t can also be written as:

$$\mathbf{u}_t = -\mathbf{K} \lambda_t \nabla P \quad (2.46)$$

where \mathbf{K} is absolute permeability, λ_t is total mobility (eq. (2.8)), and P is pressure (cf. section 2.2).

The total Darcy velocity shows that a reduction of the absolute permeability influences the other variables contained in the expression above. The reduced permeability forces either the pressure difference to become larger or the total flow to decrease. In our system of equations, the fractional flow function is applied, so the change in either flow rate or the pressure gradient will not influence the system. The fractional flow is a function of only the relative permeabilities and the viscosities. For the one-dimensional system, we will see no effect from modifications of the absolute permeability.

Simulations with changes in absolute permeability should not be performed in only one dimension as this is basically unrealistic (Islam, 1990). In one dimension, the absolute permeability starts to drop near injection site when bacteria are injected. Therefore, the flow through the entire reservoir is determined by the lowest permeability found near the injection site and plugging can take place. On the other hand, simulations performed in two or three dimensions create realistic cases, where the full fluid diversion mechanism can be investigated. In conclusion, absolute permeability changes should only be studied in two or three dimensions (Islam, 1990).

The considerations reveal that the effect from modifying the absolute permeability is not investigated here. In the context of this approach, we only study the influence from the formation of biofilm. Meanwhile, we hold the assumption that the actual modifications that would happen, does not influence the total flow rate and keeps the pressure within a sound range.

Saturation

The presence of biofilm encompasses that the relative permeability should remain unchanged. The relative permeability is calculated based on the water phase saturation, but the biofilm phase reduces the actual pore volume available for flow. The presence of the biofilm should be taken into account in order to obtain the same relative permeability curves independent of the biofilm saturation.

The bacteria exist only in the water and biofilm phases. Formation of biofilm occurs by bacteria leaving the water phase and enter the biofilm phase, but what happens in the water and biofilm phases does not influence the oil phase. Therefore, the water phase

saturation that would have existed if no biofilm had formed, is:

$$\hat{s} = s_w + \sigma \quad (2.47)$$

Application of \hat{s} in the relative permeability calculations gives unchanged relative permeability curves k_{rj} for both oil and water phases:

$$k_{rj} = k_{rj}^0(s_w + \sigma) = k_{rj}(\hat{s}) \quad (2.48)$$

In the context of studying the influence from biofilm, the relative permeabilities do not experience a distinction between absence or presence of the biofilm.

2.4.3.2 Water phase relative permeability

The formation of biofilm is a process that involves bacteria coming from the water phase and adsorb to the pore walls. Similar to the previous approach, the oil phase is not affected by the processes taking place in the water and biofilm phases, and the relative permeability for oil stays the same. The absolute permeability remains unchanged. The lumped saturation for the water and biofilm phases defined in equation (2.47) is used.

$$k_{ro} = k_{ro}(\hat{s}) \quad (2.49)$$

2.4.3.3 The original Kozeny-Carman equation

The Kozeny-Carman equation is used to relate the pressure drop of a fluid through a packed bed column of solids (McCabe et al., 2005).

$$u_j = \frac{1}{180} \alpha_s^2 d^2 \frac{\phi^3}{(1 - \phi)^2} \left(\frac{\Delta P}{\ell} \right) \quad (2.50)$$

where u_j is the velocity of the fluid phase j , α_s is the sphericity coefficient being in the order of unity, d is an effective sphere diameter of solid grains, ϕ is porosity, P is pressure, and ℓ is the length of the column. From this equation, other authors have derived the Kozeny-Carman relation, equation (2.45).

Combining the Kozeny-Carman equation with the Darcy law in the form shown as equation (2.3) gives the following expression for the permeability (Wang and Tarabara, 2009) :

$$(k_{rw} \cdot K) = \frac{1}{180} \alpha_s^2 d^2 \frac{\phi^3}{(1 - \phi)^2} \quad (2.51)$$

The result is that the product of absolute and relative permeability can be written as a function of sphericity, grain diameter and porosity.

2.4.3.4 The modified Kozeny-Carman relation

We use equation (2.51) to produce the ratio between the permeability with and without the formation of biofilm. This leads to an expression for the relative permeability for water, as only the relative permeability for water is changed.

$$\frac{k_{rw}}{k_{rw}^0} = \frac{d^2 \phi^3 (1 - \phi_0)^2}{d_0^2 \phi_0^3 (1 - \phi)^2} \quad (2.52)$$

The relative permeability for water becomes a function of grain size and porosity, while it excludes the absolute permeability from the expression. The index 0 indicates the initial case, associated with no bacterial adsorption. No index indicates the current state with biofilm formation.

The presence of biofilm reduces the pore volume available for fluid flow. This implies that more solid is produced. Before any biofilm formation takes place, the solid is only rock $(1 - \phi_0)$. The formation of biofilm adds volume to the solid $(\phi_0\sigma)$:

$$\begin{aligned} \text{Solid: Rock} & \quad (1 - \phi_0) \\ \text{Solid: Rock with biofilm} & \quad (1 - \phi_0) + \phi_0\sigma \end{aligned}$$

The ratio between the actual porosity with biofilm and the initial porosity is found by rewritings of porosity definition, equation (2.30).

$$\frac{\phi}{\phi_0} = (1 - \sigma) \quad (2.53)$$

The porosity decreases as more biofilm forms.

Assume that the addition of non-flowing volume of the solid material is uniformly distributed between all the spherical rock grains, meaning that all grains grow equally. Volume addition to a grain increases the diameter, where the volume corresponds to the diameter to power one third, according the formula for sphere volume. The diameter ratio is determined from the volume ratio:

$$\frac{d}{d_0} = \sqrt[3]{\frac{1 - \phi_0 + \phi_0\sigma}{1 - \phi_0}} = \sqrt[3]{1 + \frac{\phi_0\sigma}{1 - \phi_0}} \quad (2.54)$$

where d and d_0 are grain diameters with and without biofilm, respectively.

The ratios, equations (2.53) and (2.54), are substituted into equation (2.52) that de-

scribes the ratio for the water relative permeability. After rearrangements, the modified relative permeability for the water phase becomes:

$$k_{rw}(\hat{s}, \phi) = k_{rw}^0(\hat{s}) \cdot \left[\left(1 + \frac{\phi_0 \sigma}{1 - \phi_0} \right)^{8/3} (1 - \sigma)^3 \right] \quad (2.55)$$

where $k_{rw}^0(\hat{s})$, is the relative permeability for water *without* biofilm formation. Therefore, it is also a function of initial relative permeability for water, where the lumped saturation \hat{s} is applied.

Comparison

We assume that the Kozeny-Carman equation can also be directly applied for changing the relative permeability for the water phase only. Thullner (2009) reviews several relations between porosity and permeability changes of one-phase flow in porous media, but concludes that no final correlation exists. A comparison between the regularly used and the modified Kozeny-Carman equation is shown in figure 2.7, equation (2.45) and equation (2.55), respectively. The curves differ a little, where the regular version is more concave compared to the modified version. The curves reveal that the effect on the relative permeability becomes significant, when the biofilm saturation reaches around 0.1 for the regular version and around 0.2 for the modified version. Generally, the biofilm formation should be extensive in order to modify the permeability significantly.

We choose to continue working the modified Kozeny-Carman expression, eq. (2.55), to include the effect from biofilm formation.

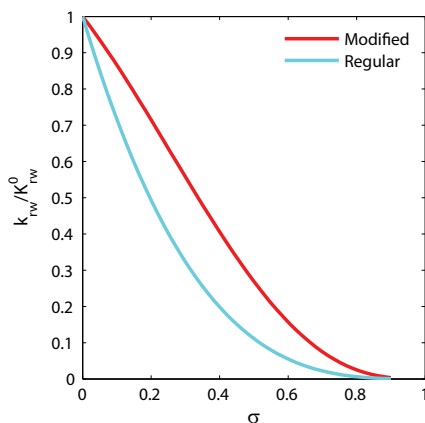


Figure 2.7: Comparison of *modified* and *regular* Kozeny-Carman relation for water relative permeability, respectively eqn. (2.55) and eqn. (2.45) with $\gamma = 3$.

2.4.4 Microscopic fluid diversion

The formation of biofilm promotes fluid diversion. This mechanism is explained in details in section 1.4.3. Fluid diversion utilizes the changes of flow paths, and thus it can only be fully investigated in a multidimensional system (Islam, 1990). As we only look at a one-dimensional system, we do not investigate the full effect of fluid diversion.

In relation to fluid diversion, the modification of the relative permeability of water occurs in the thief zones, where biofilm grows in the beginning. We study the effect taking place on the microscopic level. While the relative permeability for water is reduced, the relative permeability for oil remains the same. This entails mobilization of more oil causing the fractional flow of oil to increase. We designate this effect *microscopic fluid diversion*, because the incremental flow of oil takes place on the microscopic level. Microscopic fluid diversion partly contributes to the overall process of fluid diversion. The contribution from microscopic fluid diversion is investigated in chapter 4.

2.5 Summary of model

The reactive transport model set up in this chapter describes convection, bacterial growth, substrate consumption, and surfactant production. It is two-phase flow comprising five components; oil, water, bacteria, substrate, and surfactant. The water phase may consist of water, bacteria, substrate and surfactant. In the context of MEOR, a novel approach is the partition of surfactant between both phases. The oil phase consists primarily of oil, but contains also surfactant. We apply the fractional flow function, and the relative permeabilities are the Corey type expressions.

The reactions are substrate consumption, bacteria multiplication and surfactant production. The bacterial growth rate is the Monod expression for one limiting substrate, so the reaction rate depends on the bacteria and substrate concentrations.

Surfactant reduces IFT, modifying the relative permeabilities. We have looked into three methods how to translate the IFT reduction into changes of the relative permeabilities; the capillary number method, Coats' method, and the Corey relative permeability interpolation method. The surfactant concentration in the water phase must reach a certain concentration threshold, before surfactant can reduce the interfacial tension. A large distribution coefficient means that most surfactant is present in the water phase. The relative permeabilities depend on the water phase concentration, so when surfactant is moved into the oil phase, there will be a smaller effect from the surfactant on the flow. Therefore, transfer part of the surfactant to oil phase is equivalent to its "disappearance", so that the total effect from surfactant is reduced.

The bacteria partition between phases according to the Langmuir expression dependent on the bacteria concentration in the water phase. The adsorbed bacteria constitute the biofilm phase. The surface available for adsorption is scaled by the water saturation, as bacteria only adsorb from the water phase. We assume no transport limitations in the biofilm, causing the bacteria in the water and biofilm phases to have the same growth rate.

The formation of biofilm leads to porosity reduction, which is coupled to the modification of permeability. The modification of absolute permeability that could take place, is not investigated as the model is one-dimensional. An effect contributing to the fluid diversion mechanisms, is microscopic fluid diversion, where the relative permeability for water only, is modified. This happens due to the fact that the biofilm is formed only at the water-occupied zones or pores where bacteria live. Bacteria only influence the water and biofilm phases, while the oil phase remains the same.

Solution procedure

The model for MEOR was developed in chapter 2. The mathematical model comprises three phases; oil and water are the flowing phases, and biofilm is the sessile phase. Some components belong to more phases, but this is only the case for bacteria and metabolite. The main constituents, oil and water, do not mix. The possible combinations of component and phases are shown in table 3.1.

Table 3.1: Phases and constituent components.

Component	Phase		
	Oil	Water	Biofilm
Water	-	ω_{ww}	-
Oil	ω_{oo}	-	-
Substrate	-	ω_{sw}	-
Bacteria	-	ω_{bw}	ω_{ba}
Metabolite	ω_{mo}	ω_{mw}	-

The component mass concentrations in the phase are ω_{ij} [kg/m³ phase]. Another form of the variable concentrations are

$$\Omega_{ij} = \omega_{ij} \cdot s_j \quad (3.1)$$

This is mass concentration which is then related to the pore volume [kg/m³ PV]. The

overall concentration of a component comes by summation:

$$\Omega_i = \sum_j \Omega_{ij} = \sum_j \omega_{ij} \cdot s_j \quad (3.2)$$

During the solution procedure, application of the different mass concentrations are useful.

The program coding is performed in Fortran, and Matlab is used for visualization of the results.

3.1 Dimensionless form

The transport equations (2.13)–(2.17) are rewritten in dimensionless form.

An important parameter is α describing the duration before the one reservoir pore volume has been injected. This is a parameter that measures the progress of the flooding process.

$$\begin{aligned} \alpha &= \frac{\phi_0 L}{u_{inj}} \\ &= \frac{\phi_0 A L}{Q_{inj}} \end{aligned} \quad (3.3)$$

where u_{inj} is the linear injection velocity, Q_{inj} is the volumetric injection velocity, A is the reservoir cross sectional area, L is the length of the reservoir, and ϕ_0 is the initial porosity. One of the dimensionless variables is the reservoir length:

$$\xi = \frac{x}{L} \quad (3.4)$$

The fraction, ξ , can also be interpreted as the volumetric fraction of the total pore volume. The dimensionless time τ is *pore volumes injected* [PVI]:

$$\begin{aligned} \tau &= \frac{Q_{inj}}{\phi_0 A L} \cdot t \\ &= \frac{t}{\alpha} \end{aligned} \quad (3.5)$$

The dimensionless injection velocity u_d is defined as:

$$u_d = \frac{u_t}{u_{inj}} \quad (3.6)$$

The injection velocity is here shown as the linear velocity relation, but the volumetric

velocity fraction is primarily used during the calculations.

Application of the dimensionless variables turns the transport equations into the dimensionless form. The transport equation for component i in all phases j is:

$$\frac{\partial}{\partial \tau} \left(\sum_j \omega_{ij} s_j \right) + \frac{\partial}{\partial \xi} \left(u_d \sum_j \omega_{ij} f_j \right) = \alpha (R_i + Q_i) \quad (3.7)$$

The transport equations easily become more compact using the overall component concentration, Ω_i , and F_i , which as the overall component flux. The compact transport equation is:

$$\frac{\partial \Omega_i}{\partial \tau} + \frac{\partial F_i}{\partial \xi} = \alpha (R_i + Q_i) \quad (3.8)$$

where

$$F_i = u_d \sum_j \omega_{ij} f_j \quad (3.9)$$

3.2 Discretization scheme

The mathematical model equations, eq. (3.8), are solved numerically using a semi-implicit finite difference technique, where the component mass balances and the total volume balance are satisfied.

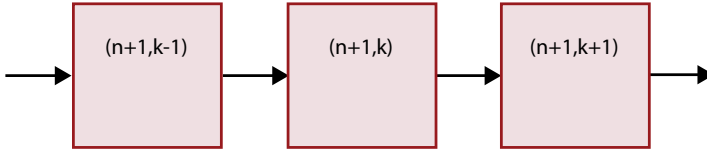


Figure 3.1: Subdivision of volumes.

The reservoir volume is subdivided into volume blocks $\Delta \xi$, where ξ both relates the volume and the length fraction of the reservoir. The time step is $\Delta \tau$. The spatial and time indices are k and n , respectively. Each discretization point ξ^k corresponds to a volume block at a specific time τ^{n+1} . This is illustrated in figure 3.1. It is assumed that each block is well-mixed, having the same composition in the entire block.

The general implicit scheme of discretization for component i becomes (Aziz et al., 2003), when the new step to be calculated is $(n + 1, k)$:

$$\Omega_{i,k}^{n+1} - \Omega_{i,k}^n + \frac{\Delta \tau}{\Delta \xi} \cdot (F_{i,k}^{n+1} - F_{i,k-1}^{n+1}) = \Delta \tau \cdot \alpha \cdot (R_{i,k}^{n+1} + Q_{i,k}^{n+1}) \quad (3.10)$$

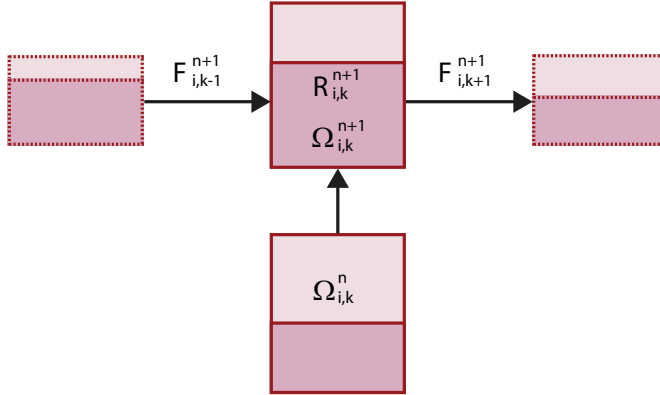


Figure 3.2: Tanks-in-series approach. The composition of block k at the present time $(n + 1)$ is $\Omega_{i,k}^{n+1}$ and depends on; the composition of that block in the previous time $\Omega_{i,k}^n$, the influx F_i determined by the previous block $(k - 1)$ at present time τ^{n+1} , and the efflux F_i from the current block k at present time τ^{n+1} . The reaction R_i also relies on the composition of the current block.

The implicit discretization produces a fully coupled system of equations. The tanks-in-series approach is applied meaning that the solution of all blocks at one time step is not calculated simultaneously. Instead, the volume blocks are solved in a sequential manner. The approach is illustrated in figure 3.2, where the composition of a block k at a new time $(n + 1)$ depends on; the composition of that block k in the previous time n , the influx from the beforehand block $(k - 1)$ at this time step $(n + 1)$, and the efflux from the current block $(n + 1, k)$. The reaction R_i also relies on the composition of the current block $(n + 1, k)$.

The tanks-in-series approach entails that the fully implicitness is retarded. There are some forward mixing of components from the initial injection, but this is regarded minor. Therefore, the method is considered semi-implicit. The choice of method implies that large matrix operations is avoided and the calculation load is reduced.

Injection and production wells are located in the first and the last block, respectively. The injection well is taken into account in the influx to the first block. Similarly, the production well is included considering the efflux from the last block.

3.3 Application of Newton-Raphson procedure

The multivariable Newton-Raphson method applies to solve the system of equations for each discrete block k at each time step $(n + 1)$. Therefore, the primary variables and the corresponding equations have to be specified.

Primary variables

The model utilizes a mass balance for each of the five components. The main dependent variables are selected to be total concentrations. The total volume balance is also taken into account. The volumetric flow u_d is added as a variable to include the possibility for volume changes, if a component reacts and the density of the product differs. Therefore, the primary variables are:

$$\Omega_w, \Omega_o, \Omega_m, \Omega_s, \Omega_b, \text{ and } u_d$$

The relation between total and phase concentrations are as shown in equation (3.2).

Flash calculations

Usually, the flash calculations utilize the total composition, temperature, pressure, and thermodynamical data to distribute the components between phases. Due to lack of thermodynamical data and *no volume change on mixing*, the flash calculations use partitioning coefficients, making up a simple flash without the necessity for iterating.

Sections 2.3.5 and 2.3.6 presented the partitioning of bacteria and metabolite, respectively. The bacteria and metabolite fractions in each phase are initially calculated. The components are divided between the phases, and the volume of each phase is calculated by adding the partial volumes for components in that phase.

The saturations are necessary for calculating the fractional flow function. For a block, the relation between the volume of a phase V_j and total pore volume V_T gives the saturations:

$$\sigma = \frac{V_a}{V_T} \quad (3.11)$$

$$s_w = \frac{V_w}{V_T} \quad (3.12)$$

$$s_o = 1 - (s_w + \sigma) \quad (3.13)$$

Reaction term

In block k , reactions take place during the time $\Delta\tau$ and depend on the composition at time τ^{n+1} . The Monod expression, equation (2.20), determines the bacterial growth rate. The total concentration of bacteria enter the reactions, because bacteria grow equally whether they are located in the water or the biofilm phase. The reaction terms

for bacteria, metabolite and substrate are the discrete version of eqs. (2.22)–(2.24):

$$R_{b,k}^{n+1} = Y_{sb} \Omega_{b,k}^{n+1} \mu \quad (3.14)$$

$$R_{m,k}^{n+1} = Y_{sm} \Omega_{b,k}^{n+1} \mu \quad (3.15)$$

$$R_{s,k}^{n+1} = -R_{b,k}^{n+1} - R_{m,k}^{n+1} \quad (3.16)$$

The bacterial growth rate is calculated as shown below, where the phase concentration of substrate at present time is estimated from the overall concentration and the water saturation from the previous time step.

$$\mu = \frac{\mu_{max} \frac{\Omega_{b,k}^{n+1}}{s_{w,k}^n}}{K_s + \frac{\Omega_{b,k}^{n+1}}{s_{w,k}^n}} \quad (3.17)$$

Mass and volume conservation

Application of the Newton-Raphson method on each block $(n + 1, k)$ calculates the six primary variables. The procedure requires six equations, which is the discrete component mass balances and the total volume balance. Importantly, the solution scheme is set up such that the mass and volume balances are satisfied.

The Newton-Raphson method is explained in details in appendix B. The system is set up as a multivariable Newton problem, where a numerical Jacobian matrix is used. Iterations are performed until convergence. The function that is searched to become zero, is the check function vector, \mathcal{F} :

$$\mathcal{F} = \begin{cases} V_T - \sum_j V_j = 0 \\ \Omega_{i,k}^n + \frac{\Delta\tau}{\Delta\xi} \cdot F_{i,k-1}^{n+1} + \Delta\tau \alpha R_{i,k}^{n+1} - \Omega_{i,k}^{n+1} - \frac{\Delta\tau}{\Delta\xi} \cdot F_{i,k}^{n+1} = 0 \end{cases} \quad (3.18)$$

where $i = \{w, o, b, s, m\}$. The different terms was shown in figure 3.2.

The procedure for the solution of each block volume is listed below.

1. Guess on variables $\Omega_w, \Omega_o, \Omega_m, \Omega_s, \Omega_b$ and u_d .
2. From equation (2.29), the mass concentration of metabolite in water and oil phases are calculated.
3. The bacteria are distributed between water and biofilm phases according to equation (2.27). The saturation from the previous step $s_{w,k}^n$ is used for producing the water phase concentration of bacteria.

4. Water, oil and biofilm phase volumes are found.
5. In order to obtain the fractional flow function, the saturations are found.
6. Influx $F_{i,k-1}^{n+1}$ is determined from previous calculation step.
7. Efflux from current step $F_{i,k}^{n+1}$ is calculated.
8. Net production $R_{i,k}^{n+1}$ is found according to the reactions eqs. (3.14)-(3.16).
9. Calculation of the check function \mathcal{F} , eq. (3.18) and the application of the Newton-Raphson method, cf. appendix B.
10. Find the next guess on primary variables.
11. Estimate the error from the check function.

Repetition of steps until convergence.

Often, convergence occurs fast due to quadratic convergence of the method, but convergence requires a starting guess reasonably close to the solution (Aziz et al., 2003). Therefore, convergence takes place, when the time step size $\Delta\tau$ remains small compared to the block volume.

One-dimensional simulations

Several mechanisms govern the MEOR process. It is difficult to distinguish between the contributions of the different mechanisms. The simulation studies enable us to investigate each mechanism separately and in combination. We look at the effect from surfactant production, biofilm formation and microscopic fluid diversion. Simulations are performed revealing the characteristics for the most important MEOR mechanisms and their contribution to the overall enhancement of oil recovery.

The mathematical model was set up in chapter 2, and specifically the implementation of mechanisms was described in section 2.4. The system of equations are solved as presented in chapter 3.

4.1 Selection of parameters

Before simulations are carried out, the selection parameters are presented to produce simulation results as close as possible to the reality. The selected parameters are listed in table 4.1 (p. 58).

Reservoir properties

The reservoir simulation is considered to be one-dimensional. The reservoir part has the length 400 m and the cross section is 100×100 m. The porosity is 0.40. This gives

Table 4.1: Parameters.

Parameter	Value
ϕ	0.4 -
Reservoir length	400 m
Reservoir width	100 m
Reservoir height	100 m
Volumetric injection velocity	800 m ³ /day
Y_{sm}	0.18 kg/kg
Y_{sb}	0.82 kg/kg
K_s	1 kg/m ³
μ_{max}	0.2 day ⁻¹
K_i	1 -
\tilde{S}	$3 \cdot 10^5$ m ² /m ³ total volume
w_1, w_2	{0, 0} [m, m ³ /kg]
μ_w	1 mPa·s
μ_o	3 mPa·s
ρ_w	1000 kg/m ³
ρ_o	800 kg/m ³
ρ_s	1000 kg/m ³
ρ_b	1000 kg/m ³
ρ_m	1000 kg/m ³
σ_{base}	29 mN/m
n	6 -
p_1, p_2, p_3	{ $6.5 \cdot 10^3$, 0.1, 0} -
Surfactant A:	
q_1, q_2, q_3	{ $1 \cdot 10^{-4}$, 0.2, $1.5 \cdot 10^4$ }
Surfactant B:	
q_1, q_2, q_3	{ $41 \cdot 10^{-4}$, 2, 180}
Surfactant C:	
q_1, q_2, q_3	{ $30 \cdot 10^{-4}$, 2, $1.5 \cdot 10^4$ }
$v_{bw, inj}$	$0.5 \cdot 10^{-5}$ m ³ /m ³
$v_{sw, inj}$	10^{-5} m ³ /m ³
$v_{mw, inj}$	0 m ³ /m ³
k_{rwor}	0.5 -
k_{rowi}	0.8 -
a	2 -
b	2 -
s_{wi}	0.3 -
s_{or}	0.4 -

a pore volume (PV) of $1.6 \cdot 10^6 \text{ m}^3$. The injection is $800 \text{ m}^3/\text{day}$ implying that injection of one PV takes 5.5 years.

Injection fluid

The injection fluid consists primarily of water. A small fraction comprises substrate and bacteria. The injection mode is continuous, even though many field tests utilize slug injection. The reservoir is assumed not to contain any indigenous bacteria.

Besides in MEOR, injection of bacteria with substrates also takes place in research areas such as bioremediation and water technology. Many different injection concentrations are used, ranging from 10^{-5} to $10^1 \text{ kg substrate/m}^3$ (Behesht et al., 2008; Chang et al., 1991; Soleimani et al., 2009; Sen et al., 2005; Sarkar et al., 1994), which also corresponds to 10^{-8} to 10^{-2} volume fraction. Volume fraction is the injection parameter $v_{sw,inj}$ used in the program code. We have chosen a substrate volumetric fraction 10^{-5} thus being in the low end of the interval. The injection fraction of bacteria is assumed to be similar to the substrate concentration.

Fluid properties

The main constituent of the water phase is water. Therefore, the water phase viscosity is regarded to be constant. Under high bacteria concentrations, the viscosity could be more affected, but this is assumed not to be the case. Similarly, the main constituent of the oil phase is oil, and the oil viscosity is considered to be constant. The densities are also listed in table 4.1, where oil has a lower density than the other components.

Properties for bacterial growth and reaction

Different constants have been used in earlier MEOR models. The maximum growth rate μ_{max} is found to range between 0.02 to 14.4 day^{-1} (Zhang et al., 1992; Desouky et al., 1996; Wo, 1997; Delshad et al., 2002). The maximum growth rate is chosen to be kept low at 0.2 day^{-1} , because it is assumed that these are anaerobic bacteria, which grows slower than aerobic bacteria. In addition, the reservoir is a stressful environment for bacterial influencing the growth rate. The half saturation constant K_s is found to range between 0.045 to 8 kg/m^3 (Islam, 1990; Delshad et al., 2002; Sen et al., 2005). A median value at 1 kg/m^3 is chosen.

Zhang et al. (1992) presents a value for the yield of bacteria on substrate Y_{sb} to be 0.82 kg/kg, which is a value used in several other simulation studies (Sharma and Georgiou, 1993; Delshad et al., 2002). This leaves the yield of metabolite on substrate Y_{sm} to be 0.18 kg/kg.

Adsorption

Bacteria adsorb to the pore walls and form biofilm. The equilibrium partitioning distributes the bacteria between the biofilm and water phases according to the Langmuir expression, eq. (2.27). For low bacteria concentrations, the adsorption is linear.

The specific surface is determined as the surface area available for adsorption. Section 2.3.5 presents that the range is 10^5 – 10^6 m²/m³, which originates from the many small pores surfaces in the porous rock. We choose a value of $3 \cdot 10^5$ m²/m³.

The derivation of the full Langmuir expression for our case is performed in section 2.3.5. The Langmuir values, w_1 and w_2 , are chosen in such a way that 75 % of the porous volume can become saturated with biofilm, corresponding to $(\sigma \rho_b)_{max}$, eq. (2.28). We select the value of w_2 , so approximately half of the bacteria adsorb. The values are listed in table 4.1, and another approach to obtain the same parameter values, are shown in appendix A.

When no bacteria adsorb and form biofilm, the bacteria only exist in the water phase. This results in that constant w_1 in the Langmuir type equilibrium expression is zero.

Reduction of interfacial tension

The correlation between IFT and the mass concentration of surfactant is earlier shown as equation (2.31). We use a very efficient *surfactant A* and a less efficient *surfactant B*. Both sets of constants are listed in table 4.1. The choice of parameters entails curves that have a critical micelle concentration (CMC) at $1 \cdot 10^{-4}$ and $3 \cdot 10^{-2}$ kg/m³ with the minimum obtainable IFT at $2 \cdot 10^{-3}$ mN/m and $6 \cdot 10^{-2}$ mN/m for surfactant A

Table 4.2: Overview over surfactant parameters and properties. CMC is critical micelle concentration.

Surfactant	q_1	q_2	q_3	CMC [kg/m ³]	σ_{min} [mN/m]
A	$1 \cdot 10^{-4}$	0.2	$1.5 \cdot 10^4$	$1 \cdot 10^{-4}$	$2 \cdot 10^{-3}$
B	$41 \cdot 10^{-4}$	2	180	$3 \cdot 10^{-2}$	$6 \cdot 10^{-2}$
C	$30 \cdot 10^{-4}$	2	$1.5 \cdot 10^4$	$4 \cdot 10^{-4}$	$4 \cdot 10^{-2}$

and surfactant B, respectively. Surfactant A and surfactant B are used in the one-dimensional simulations, while surfactant C is used in chapter 5 for the multidimensional streamline simulations.

Capillary desaturation curve

For the capillary number method, the dependence between normalized residual oil saturation and capillary number is given by equation (2.33). The curve was shown earlier as figure 2.5 (p. 36). The constants are chosen such that a reasonable description of the original curve is obtained. However, it should be mentioned that the curve levels off and has a minimum achievable saturation. The original curve has no information above a concentration. After this concentration, we let the curve level off, not lowering the saturation further. Our minimum residual saturation then becomes 0.08 of the initial residual saturation.

4.2 Verification of simulator

Before application of the developed model, verification of the simulator is performed, which is conducted by comparison between the analytical and numerical solution of the well-known Buckley-Leverett equation.

The system is a reservoir containing water and oil only, which make up the the two flowing phases. Injection of pure water takes place, displacing oil. The sum of the oil and water saturation is unity, which is why solution of one transport equation is required. The transport of water is described by equation (2.16). In the absence of other components in the water phase, the equation written in dimensionless coordinates using eqs. (3.4) and (3.5), reduces to:

$$\frac{\partial s_w}{\partial \tau} + \frac{\partial f_j}{\partial \xi} = 0 \quad (4.1)$$

where the fractional flow function depends on the water saturation. The velocity always equals injection velocity removing the dimensionless velocity, eq. (3.6).

The analytical solution is shortly derived in appendix C according to Bedrikovetsky (1993):

$$\frac{\xi}{\tau} = f'_w(s_w), \quad \text{for } 0 < \frac{\xi}{\tau} < D_f \quad (4.2)$$

$$s_w = s_{wi}, \quad \text{for } \frac{\xi}{\tau} > D_f \quad (4.3)$$

where the value of D_f is

$$D_f = f'_w(s_f) \quad (4.4)$$

The front water saturation is s_f . The saturation determines D_f , which describes the location of the front for a given time.

Comparison of analytical and numerical solutions

The necessary parameters from table 4.1 is applied for the simulation of the displacement of oil by pure water. The number of blocks will be 400 corresponding to Δx is 1 m. The time step $\Delta\tau$ is 1.2 days.

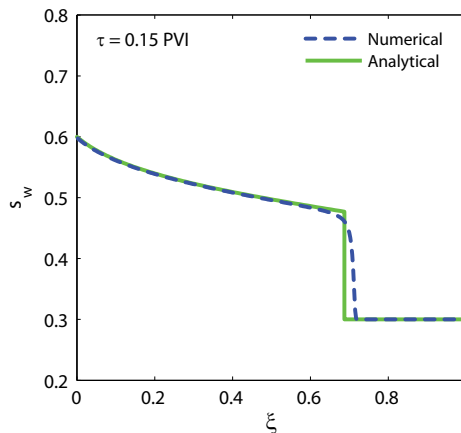


Figure 4.1: Comparison between analytical and numerical solution to Buckley-Leverett equation. The number of blocks is 400.

Figure 4.1 shows both the analytical and numerical solution. The curves nicely follow each other, but there is expectedly a discrepancy between the fronts. The analytical solution has a discontinuity, which can never be made by the numerical solution, because it cannot produce discontinuities and has a degree of numerical dispersion. The numerical front is reasonably steep and as the number of blocks is increased, the numerical front approaches the analytical front.

Based on the consistency of the produced curves for the Buckley-Leverett solution, the simulator developed is considered validated.

4.3 Surfactant effect

One of the important mechanisms is reduction of oil-water interfacial tension due surfactant production, where bacteria produce the surfactant within the reservoir. This chapter presents the simulation studies for surfactant effect (cf. section 2.4.2). The aim of the investigations deals with the effect of surfactant produced in situ on the saturation profiles, residual oil saturation and the oil recovery curves. These simulations assume no attachment of bacteria and thus no biofilm formation.

To begin with the MEOR characteristics created by the surfactant production are explored, where we use a very efficient surfactant denominated *surfactant A* (cf. section 4.1). The sensitivity of different process parameters are investigated in order to determine how the parameters influence the profiles, residual saturations and oil recovery curves, but also which parameters seem important.

4.3.1 Characteristics due to surfactant effect

A prime example of the water phase saturation profile can be seen in figure 4.2. The capillary number method is applied to introduce the surfactant effect using this very efficient *surfactant A*. The parameters applied are listed in table 4.1 (p. 4.1).

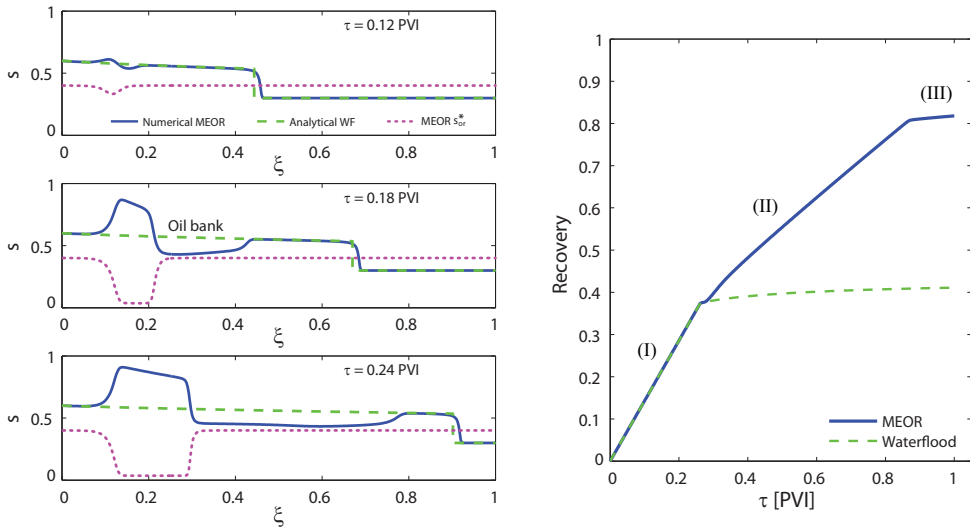


Figure 4.2: Saturation profiles at different dimensionless times, τ . The dimensionless reservoir length is ξ . The curves are the analytical Buckley-Leverett solution for pure waterflood, numerical MEOR water phase saturation, and the corresponding MEOR residual oil saturation s_{or} . The viscosity used for oil and water is 1 mPa·s, which differs from the parameters listed in table 4.1. Recovery curves are for MEOR and waterflooding.

The MEOR solution is injected, producing a water front like during waterflooding. As bacteria and substrate penetrate the reservoir, more bacteria and surfactant are produced. When enough surfactant is produced, the interfacial tension reduces significantly affecting the relative permeabilities. The interfacial tension reduction mobilizes oil creating the *oil mobilization point*. More water will accumulate producing a second water front with surfactant. This results in a traveling oil bank, which occasionally catches up with the first front as a consequence of different front velocities. If the oil bank catches up with the first front, the water front now having a new saturation will be slowed down. On the other hand, as long as the oil bank does not catch up, the water front will be located at the position of the front for pure waterflooding and breakthrough occurs at the time for pure waterflooding breakthrough.

The recovery curve is also shown in figure 4.2. When the oil bank catches up with the waterfront, it results in production with steepest incline in recovery curve for an extra period of time (I), as water breakthrough occurs later. The second part of the curve (II) has a smaller inclination than the first part (I), which results from a larger water cut relative to the first part of the recovery curve. The water saturation is lower until breakthrough of the surfactant water front, where the recovery curve levels off (III). If the oil bank does not catch up with the water front, the recovery curve follows the waterflooding recovery curve until the oil bank breakthrough. Islam (1990) produces a recovery curve similar to the latter curve, where the oil bank does not catch up with the water front. Our incremental recovery is around 40% OOIP using the very efficient surfactant. It should be emphasized, that the incremental recovery depends on the

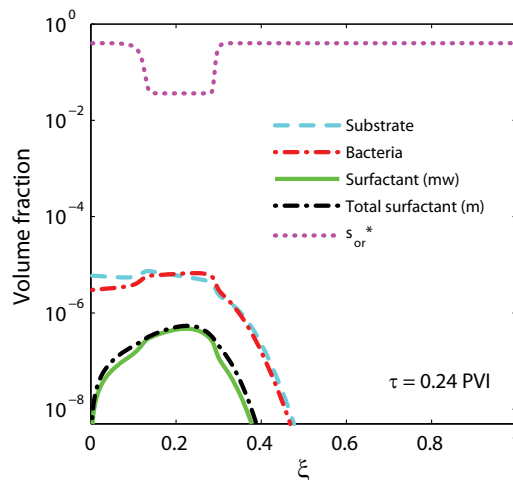


Figure 4.3: The volume fraction of constituents. The surfactant is shown both as total surfactant and surfactant in the water phase. The calculated residual oil is shown as well in order to see the effect from surfactant.

specific surfactant and the actual reservoirs. A less efficient surfactant mobilizes less oil.

Due to no adsorption of bacteria, the substrate and bacteria are transported together in the water phase. The substrate is consumed by the bacteria during the flooding. If the bacteria concentration is high enough, all substrate is consumed before the outlet and no reaction can occur.

Figure 4.3 shows the volume fractions of substrate, bacteria, total metabolite and metabolite existing in the water phase. The volume fractions are shown in a semilog plot to be able to compare the smaller and the larger amounts. The calculated residual oil is shown as well to see the effect from surfactant. The residual oil decreases around the threshold concentration.

4.3.2 Effect of surfactant partitioning

Partitioning of surfactant between phases is a novel approach. Figure 4.4 shows saturation profiles (left) and recovery curves (right) for the different cases of partitioning. When the distribution coefficient is small, surfactant is mainly located in the oil phase. Less surfactant is then present in the water phase and more surfactant should be produced in order to decrease residual oil saturation markedly. The time before changes in residual oil occur, is longer, but the mobilization point is located at the same distance from the inlet (not shown). The time delay means that the oil bank is created later, and the recovery curve follows pure waterflooding recovery until breakthrough of the oil bank. This becomes even more clear for the case with $K_i = 10^{-1}$, where the oil bank is produced later giving a oil bank breakthrough time around 0.7 PVI. However,

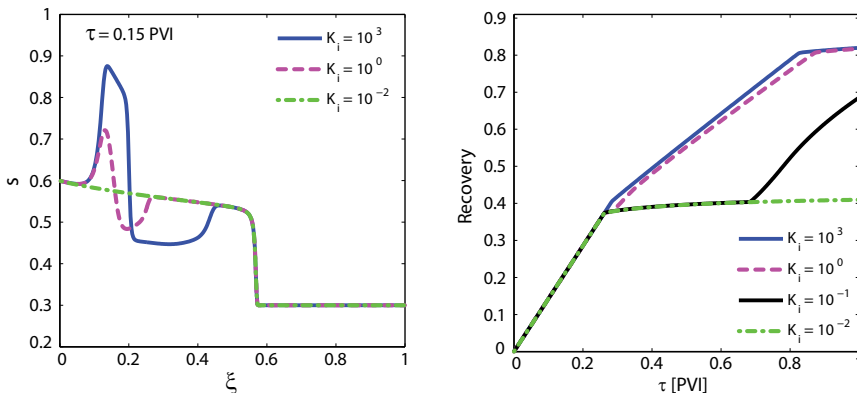


Figure 4.4: Water phase saturation profiles and recovery curves for different values of distribution coefficient K_i .

the final recovery will become equal to the case with the larger partitioning coefficients after 2 PVI, as the mobilization points are alike.

When surfactant is mainly present in the oil phase ($K_i = 10^{-2}$), sufficient surfactant cannot be produced in order to obtain a water phase surfactant concentration large enough to mobilize oil. No effect from surfactant takes place at these conditions. The water phase saturation profile and recovery curve result in being the same as during waterflooding. Therefore, the performance of MEOR is dependent on how surfactant partitions between the phases.

4.3.3 Effect of growth rate

The growth rate can be difficult to maintain in a reservoir as reservoir conditions may change. We demonstrate the effect of growth rate only by changing the maximum growth rate μ_{max} .

Cases for different maximum growth rates are shown in figure 4.5. A larger growth rate at 2 day^{-1} results in a faster surfactant production and the mobilization point appears closer to the inlet. An order of magnitude reduction of the growth rate to 0.2 day^{-1} prolongs the time before the surfactant effect can be seen, but also determines the distance from the inlet before the residual oil decreases. Another order of magnitude reduction in growth rate to 0.02 day^{-1} shows no effect from surfactant as an insufficient amount of surfactant is produced. The oil recovery curve is then equal to the recovery curve for pure waterflooding.

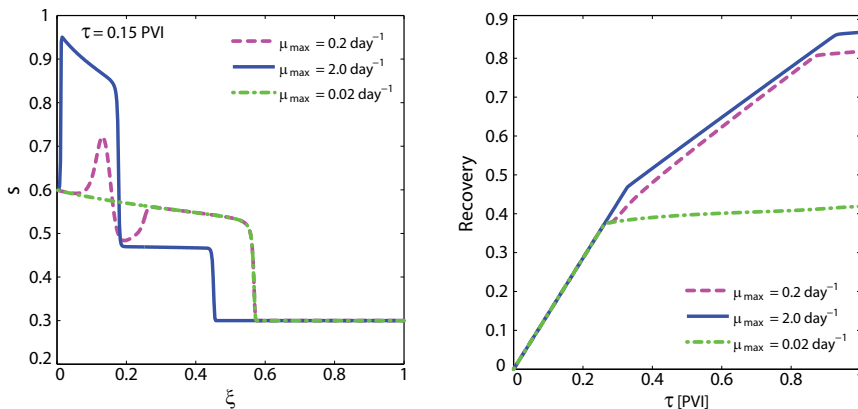


Figure 4.5: Water phase saturation profiles and recovery curves for different maximum growth rates μ_{max} .

A high level of oil recovery can only be achieved, if we are able to maintain a certain growth rate. This should be considered, as reservoirs are often heterogeneous and thus many environmental factors influence the growth rate.

4.3.4 Effect of substrate and bacterial injection concentrations

The bacterial growth rate is dependent on both substrate and bacteria concentration. Therefore, the recovery is expected to be dependent on the injection concentrations. The injected amounts of substrate and bacteria also set the upper limit for how much surfactant that can be produced. Figure 4.6 shows saturation profiles and recovery curves using the capillary number method at different concentrations. Doubling of the injection concentration ($2\times$) initiates the surfactant effect at an earlier time, and the oil mobilization point emerges closer to the inlet. The largest difference between double and regular injection concentrations ($1\times$) relies on the residual oil that is not mobilized from the inlet to the mobilization position. For half the injection concentration ($0.5\times$), we see a significant delay before the surfactant effect initiates. Here, the incremental oil is approximately only half the incremental recovery compared to the two other cases. The mobilization position is found around half the reservoir length (not shown graphically) meaning that large amounts of oil will not be mobilized.

The injection concentrations determine the time before residual oil becomes mobilized, and the point of initial mobilization. Between the inlet and the mobilization point, a large amount of residual oil is not mobilized, which reduces the final recovery. This clearly demonstrates that injection concentrations should be considered carefully to utilize the full potential of MEOR.

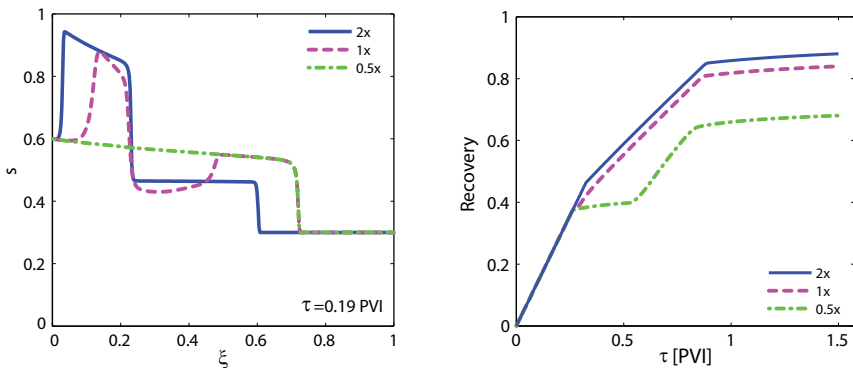


Figure 4.6: Water phase saturation profiles and recovery curves capillary number method for different injection concentrations that is given relative to the injection concentration listed in table 4.1.

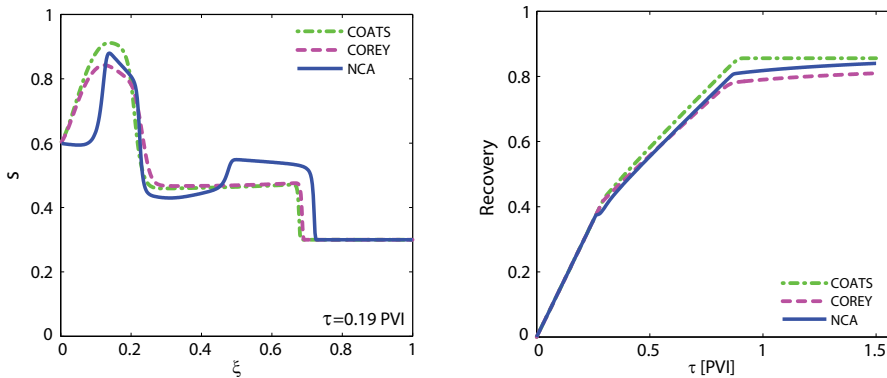


Figure 4.7: Water phase saturation profiles and recovery curves for the three methods. NCA is the capillary number method.

4.3.5 Comparison of interpolation methods

The three methods affect saturation profiles in the same way, but the capillary number method makes sharper profile changes, cf. figure 4.7. Coats' method and the Corey interpolation method are smoother producing larger zones of a reduced residual oil saturation. The sensitivity for Coats and Corey interpolation methods depends on the parameter n . In our case, n is 6. A larger n produces curves that are less sensitive to changes in interfacial tension, producing a smaller reduction of the residual oil. The final recovery for the three methods is very similar, but there are small differences. The minimum residual oil differs a little between the methods, but also the mobilization points are unlike. Coats' method and the Corey interpolation method have mobilization points closer to the inlet. As an example, Coats' method produces a lower residual oil saturation and the mobilization point is very near the inlet resulting in a recovery being a little larger than the two other methods.

All methods investigated are sensitive to distribution of surfactant, growth rate, substrate and bacterial concentration. The incremental recovery for the three methods has only minor differences ranging between 38–44 % OOIP, so the recovery outcomes are very alike. Due to this interpolation approach, the best method for making simulations depends on the specific case to model. Therefore, the choice of method should rely on experimental data in order to have a method that describes the specific cases.

4.3.5.1 Interpolation of Corey parameters

So far, the curves presented using interpolation of the Corey parameters only includes modification of residual oil. This project also uses interpolation of the remaining parameters.

The saturation profile for the case with interpolation of residual oil only and both residual saturations are shown in figure 4.8(a). Interpolation of the residual water saturation mobilizes less oil in terms of producing a smaller oil bank and less water accumulates. Moreover, the water saturation profile becomes more smooth when applying the interpolation of residual water. The smoothness is also seen for the Coats interpolation method, which interpolated both residual saturations.

The modification of residual water may be too extensive. Some researchers suggest that the residual water changes less with the reduction of IFT (Kumar et al., 1985). This change implies a different interpolation function for residual water, which could be less sensitive to IFT reductions.

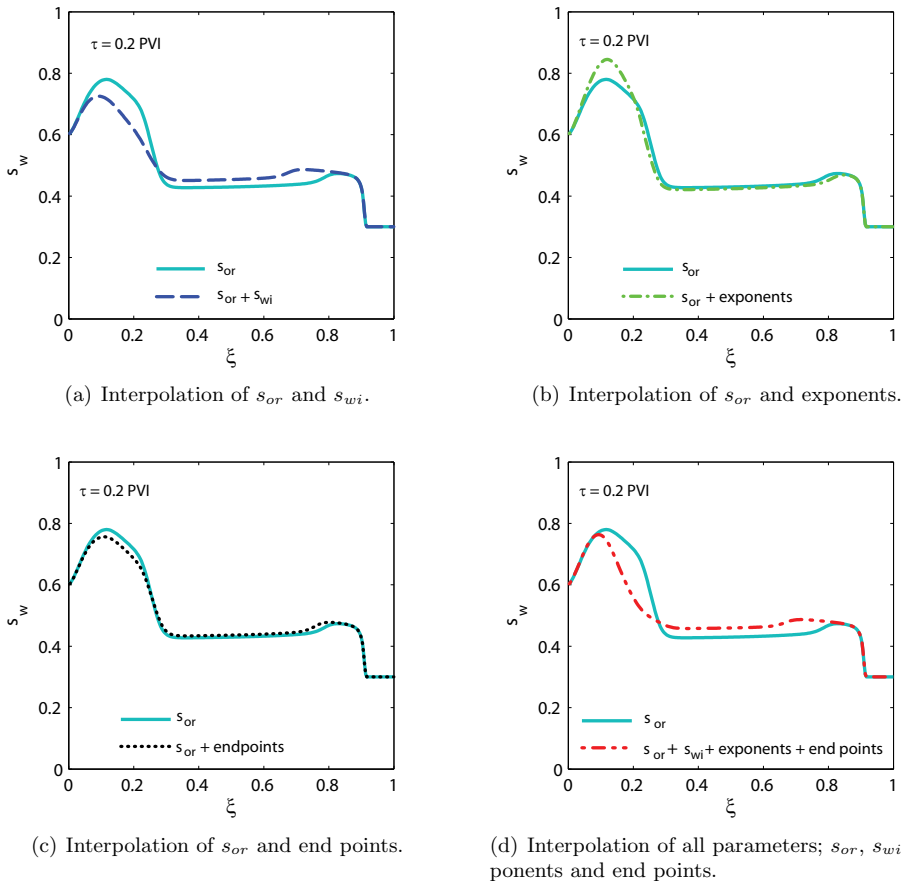


Figure 4.8: Interpolation of different parameters in the Corey relative permeabilities. The parameter are residual saturations, s_{or} and s_{wi} , the exponents and the endpoints, where the effect from different combinations of interpolated parameters are shown. All curves are compared against the Corey interpolation method for residual oil only (cyan full line).

Figure 4.8(b) depicts the saturation profile, where the residual oil saturation and the exponents are interpolated. Applying interpolation of both exponents gives more linear relative permeability curves. The water saturation profile reveals an increment of accumulated water and thus a bigger oil bank from oil mobilization. Interpolation of both residual saturations and of the exponents produces a saturation profile (not shown), which is a cross between the two curves shown as figures 4.8(a) and figure 4.8(b).

In the chosen procedure, interpolation of end points takes place between their initial value and unity. Initially, the lowest end point value is for water and therefore its endpoint value will be increased more. The profile is depicted in figure 4.8(c). A slight reduction water accumulation and the oil bank is noticeable, so the profiles is not very sensitive to interpolation of the end points. The influence of end point interpolations should be verified by experimental studies such as proposed by Shen et al. (2006).

Figure 4.8(d) presents the saturation profile, where all parameters are selected for interpolation. The profile reveals that the oil bank is smaller due to the interpolation of residual water and endpoints.

4.3.6 Effect of surfactant efficiency

In our work, the surfactant produced by the bacteria is designated *surfactant A* and is considered very efficient having both a low threshold before oil-water interfacial tension starts to drop, and produce a several orders of magnitude reduction of the interfacial tension. We have specially restricted ourselves with this case of extremely efficient MEOR, in order to demonstrate the influence of the different physical phenomena and model approximations on the process. The recovery achieved in the laboratory studies is usually lower (Chisholm et al., 1990; Banat, 1995; Zekri and Almehaideb, 1999; Sen, 2008). This is explained by the fact that the threshold concentration, which should be obtained before the effect of surfactant takes place, is higher than in our simulations.

Applying MEOR has a dramatical effect on the oil recovery, when using the very efficient surfactant presented. It clearly demonstrates that surfactant partitioning, growth rate and injection concentration of substrate and bacteria are critical process parameters. The way how the surfactant influence the saturation profiles and oil recovery curves becomes very apparent using this very efficient surfactant.

Figure 4.9 shows simulation results for a less efficient surfactant, which is designated *surfactant B*. A larger amount of surfactant B is required (around 10 mg surfactant/L) (Youssef et al., 2007) and the lowest interfacial tension obtainable is 0.06 mN/m (Gray et al., 2008). The incremental recovery is 9 % OOIP over that of waterflooding. Similar to the first case, the saturation profiles and the oil recovery curves are still sensitive

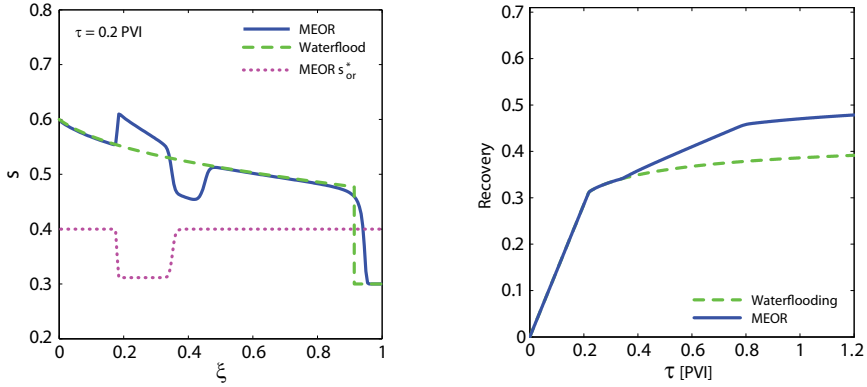


Figure 4.9: Water phase saturation profiles and recovery curves for a less efficient surfactant having both a high threshold before oil-water interfacial tension starts to drop, and produce a less orders of magnitude reduction of the interfacial tension.

to surfactant partitioning, bacterial growth rate and injection concentrations. The oil recovery for this less efficient surfactant is lower being in accordance with experimental results (Chisholm et al., 1990; Banat, 1995; Zekri and Almehaideb, 1999; Sen, 2008). In the experiments, the lower recovery may amongst others originate from the efficiency of the surfactant produced, the actual growth rate and actual production rate of both bacteria and surfactant. These are factors that certainly influence the performance of the MEOR process, but they are subjects for other separate investigations.

4.4 Effect of biofilm formation

The main question for this section is how the retention of the bacteria changes the saturation profile and the recovery curve.

Several studies have been conducted on one-phase flow systems in porous medium using microorganisms in the context of bioremediation (Vandevivere et al., 1995; Clement et al., 1996; Thullner, 2009). One of the big challenges is predicting the modification of the absolute and relative permeabilities according to pore space plugging and porosity reduction due to biofilm formation in the porous medium.

4.4.1 Parameters revisited

The parameters applied when modeling biofilm formation only *without* any surfactant is listed in table 4.1 (p. 58). The exceptions from that is explained below.

Injection of a very high bacteria concentration applying biofilm-forming bacteria entails a risk of plugging the injection area severely and damaging the formation rock. Aslam (2009a) suggest that the injected bacteria concentration should be maximum 10^9 cell/ml. This corresponds to a volumetric fraction of $1 \cdot 10^{-12} \text{ m}^3/\text{m}^3$, when using a bacteria size of $1 \text{ }\mu\text{m}^3$. However, actual biofilm consists of a large fraction of stagnant water captured inside the biofilm (Madigan et al., 2003). In practice, the required bacterial count could be significantly smaller, depending on the biofilm structure and thus its actual composition.

The injected substrate concentration is $8 \cdot 10^{-3} \text{ m}^3/\text{m}^3$. Metabolite is also produced, but we consider it to be an inert tracer compound distributed between the two flowing phases. This leaves out the effect generated by surfactant.

The attachment of bacteria to form a biofilm is determined by the Langmuir adsorption expression, eq. (2.27). As highlighted the parameters are chosen in such a way that bacteria can maximum occupy 75 % of the pore volume, and the bacteria is almost evenly distributed between the biofilm and the water phase. Simulations are also used to conclude on the influence of parameters for bacterial adsorption.

Application of the Langmuir expression to maintain a maximum 75 % occupation of pore volume utilizes the basic parameters:

$$\begin{aligned} w_1 &= 1 \cdot 10^{-3} \cdot w_2 \quad [\text{m}] \\ w_2 &= 1.7 \cdot 10^{-3} \text{ m}^3/\text{kg} \end{aligned} \quad (4.5)$$

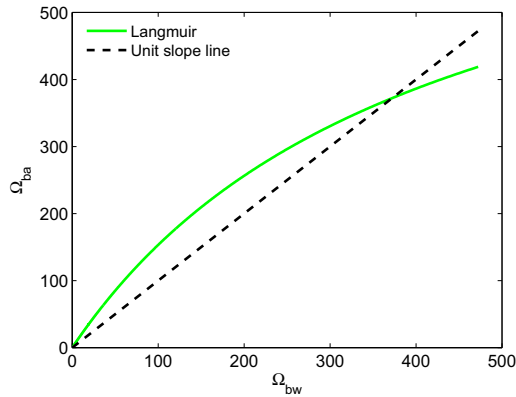


Figure 4.10: The Langmuir expression for the base case shown with the unit slope line. The saturation is set to 0.6.

For the linear case, the parameters are

$$\begin{aligned} w_1 &= 4 \cdot 10^{-6} \text{ m} \\ w_2 &= 0 \text{ m}^3/\text{kg} \end{aligned} \quad (4.6)$$

so w_1 is the same as w_1 found in equation (4.5).

The expression using the current values is depicted in figure 4.10. The initial part of the curve changes almost linearly, while it goes toward the maximum occupation of 75 % corresponding to 750 kg/m^3 pore volume, if the porous medium is fully saturated with water.

4.4.2 Effect of bacteria adsorption

The goal of this section is to investigate the effect of bacteria adsorption and disappearance from the flow alone, without the effect on the absolute or relative permeability. We compare the transport of biofilm-forming bacteria compared to the transport without bacterial adsorption. The adsorption of bacteria depends on the water phase saturation (cf. section 2.4.3).

Figure 4.11 shows the difference between the case without adsorption of bacteria and the case with bacteria forming biofilm. Bacterial transport is retarded as the bacteria attach to the pore walls, while no adsorption entails that bacteria travel together with the substrate. The area with the high concentration of bacteria has a high consumption rate, resulting in utilization of all the substrate around.

A peak of bacteria emerges at some distance from the inlet, as it takes time before a substantial amounts of bacteria have been produced. The biofilm formation causes faster transport of substrate relative to the bacteria, leading to unconsumed substrate bypassing the bacteria. This is in accordance with experimental results (Youssef et al., 2007). Due to equilibrium partition, the bacteria leave the biofilm when the concentration of flowing bacteria becomes smaller. Generally, the equilibrium approach corresponds to a method of stalling the bacterial transport increasing their breakthrough time (Tufenkji, 2007).

The profiles using the Langmuir relation and the linear relation gives the same results (not shown), because the bacteria concentration mainly remains in the linear region. Thus, we will not present the curves for linear part as they do not result in new information.

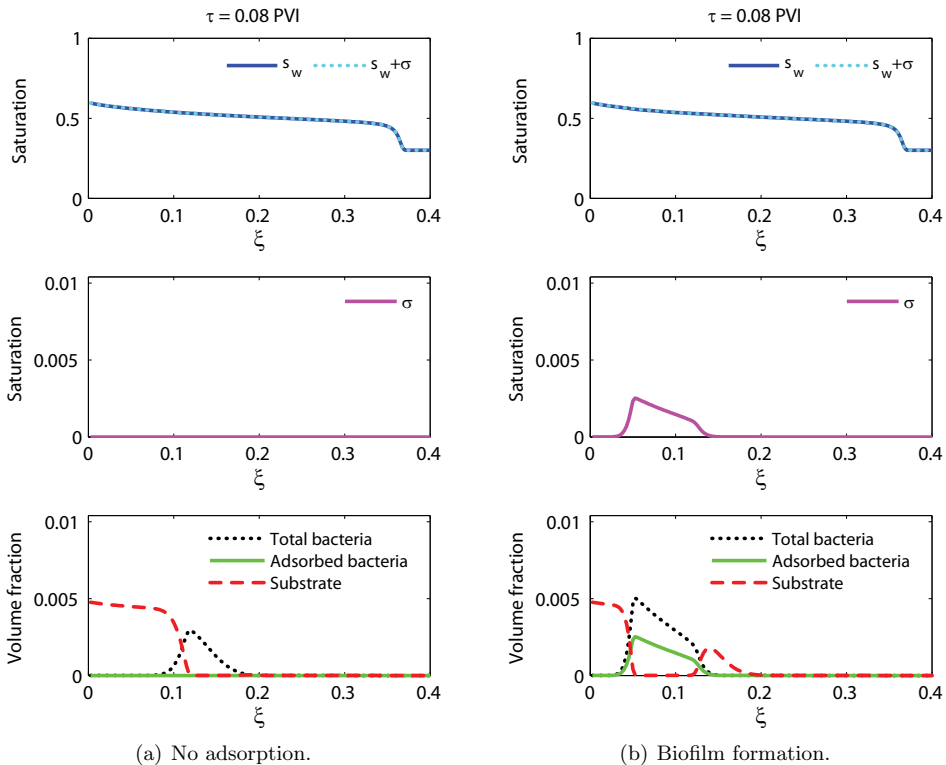


Figure 4.11: Influence of biofilm on the retention of bacteria. Graphs are for water saturation, biofilm saturation and volumetric fractions of the pore volume for substrate and bacteria.

4.4.3 Effect of water relative permeability

The other approach modifies the relative permeability for water only, according to the biofilm-induced porosity reduction. This effect is microscopic fluid diversion: it reduces permeability for water only, since bacteria adsorb only form water-filled pores. Thus, the formation of biofilm alone helps decreasing the fraction of water in the flow and increasing the recovery. The approach was presented in section 2.4.3.

The presence of biofilm produces a delay in bacterial breakthrough. According to the presentation of this approach in section 2.4.3, the biofilm is estimated to occupy around 20 % of the pore space, before the relative permeability for water is reduced enough to enhance the oil recovery. The surface available for adsorption is scaled with the water saturation, entailing that less biofilm is formed at small biofilm saturations.

First task is to investigate how much the porosity should change before there is a markedly effect on the saturation profiles and recovery curves. In the next numerical experiment, we inject bacteria that are independent of substrate concentration and growth. It should be noted that the injection concentration is too high for practical applications but it is purely used for illustration.

Figure 4.12 depicts both the saturation profile and oil recovery for injection with bacteria alone. The saturation profile in figure 4.12(a) shows the regular displacement front and,

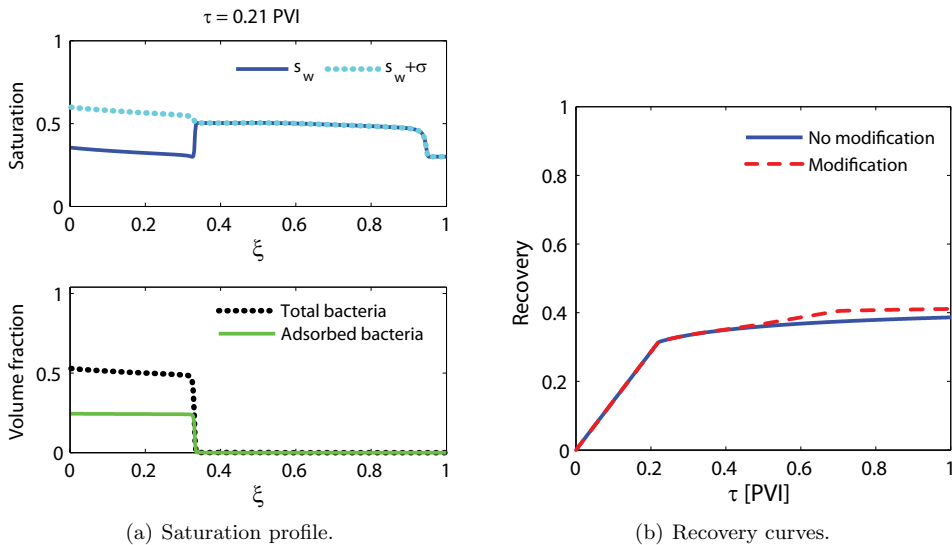


Figure 4.12: Injection bacteria only in order to study the effect of high bacterial concentration. The recovery curve is compared with the recovery without any modification of the relative permeability.

additionally, a small second front appears. The total volumetric fraction of bacteria is 0.5 and the adsorbed bacteria result in a biofilm saturation at 0.24. The small second front leads to a minor enhancement of the oil recovery.

The recovery curves for cases with and without modification of the water relative permeability curves are depicted in figure 4.12(b). The curves show that the oil recovery is improved compared to waterflooding. The recovery curves follows the curve for waterflooding until breakthrough of the second water front. A biofilm saturation at 0.24 is reached, which produces an incremental oil recovery of 1.9 % OOIP. The result is listed in table 4.3 together with a similar simulation example.

The other simulation example displays less adsorption, which is introduced by a lower w_2 . The biofilm saturation is 0.17, leading to an incremental recovery of 1.2 % OOIP. To obtain a significant improvement of oil recovery, the biofilm saturation should be at around 0.2 or preferably higher to improve the oil production. Thus, a relatively large amount of bacteria needs to be injected, or in the realistic case, a large amount of bacteria is required to be produced by growing within the reservoir, before an incremental oil recovery is obtained.

The results rely on the reduced porosity that modifies the relative permeability for water only. This effect is microscopic fluid diversion (cf. section 2.4.3). It partially contributes to the overall fluid diversion process. However, it will only contribute, when the biofilm formation is substantial.

Table 4.3: Incremental recovery by changing water relative permeability.

Bacteria volume fraction	w_2	Biofilm saturation	Incremental recovery
0.48	$1.7 \cdot 10^{-3}$	0.17	1.2 % OOIP
0.50	$1 \cdot 10^{-2}$	0.24	1.9 % OOIP

4.4.3.1 MEOR simulations

In order to obtain a sufficiently high concentration of bacteria, large amounts of substrate have to be injected. When the volumetric injection fraction of bacteria is as low as $10^{-12} \text{ m}^3/\text{m}^3$, the bacteria have to multiply extensively to achieve the necessary saturation. Therefore, it is important to inject sufficient amounts of substrate in order to secure growth.

Figure 4.13 illustrates the curve obtained for MEOR with a substrate injection fraction of 0.4. Due to the availability of substrate, the bacteria grow fast leading to formation of biofilm that changes the porosity.

Substrate is consumed during its transportation through the reservoir. A peak of sub-

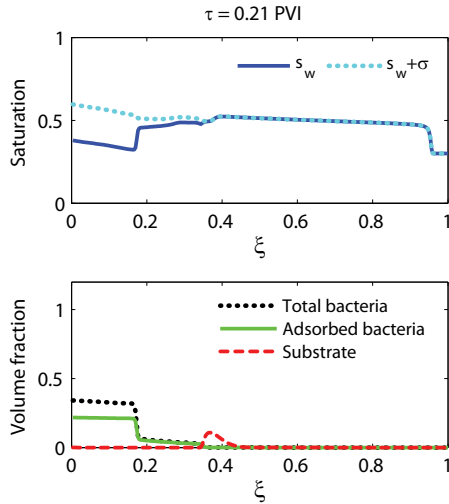


Figure 4.13: MEOR saturation profile.

strate is found at some distance from the inlet, whilst all substrate has been consumed between the inlet and the peak of substrate. The substrate travels faster than bacteria, because bacteria are retained. The bacteria distribution consists of two areas; a high and a low concentration area. The area with the high bacteria concentration originates from the first burst of bacteria multiplying rapidly resulting in a bacteria peak. The bacteria grow and the peak widens until the substrate is consumed. At inlet, there is a constant injection of substrate and bacteria, so bacteria will continue growing. When the bacteria peak is formed, the substrate peak is transported from the retained bacteria. Some bacteria are transported along with the flow. A part of them travels with the substrate peak, where they consume substrate. As substrate is slowly consumed, the production rate of bacteria decreases resulting in the decline in the low concentration part. There is a small bacteria front at the edge of the substrate peak.

The two areas with high and low concentration of bacteria produce changes in the water phase saturation profile, mobilizing more oil. After 1.4 PVI, the incremental oil recovery is 1.5 % OOIP over that of waterflooding.

4.4.4 Assumption about constant viscosities

As mentioned earlier, when reaching injection volumes percents around 20 %, the amount of bacteria is large. The question is whether this large amount of bacteria modifies the density and the viscosity of water, so that the assumption about constant viscosity is violated. Most likely, the production of metabolite increases water viscosity. A larger water phase viscosity influences the fractional flow of oil positively, giving rise

to increase in oil recovery. The incremental oil recovery due to biofilm formation can be around 2 % OOIP. Therefore, underestimation of the viscosity actually corresponds to underestimation of the oil recovery.

4.5 Combination of mechanisms

Both MEOR mechanisms are combined in this section. Surfactant is produced and biofilm is formed. The amount of surfactant produced strongly influences the residual oil saturation and improves the oil recovery. The surfactant is responsible for modifications of the relative permeability curves due to surfactant-induced reduction of IFT. Modification of the relative permeability for water induces the effect from microscopic fluid diversion, which partly contributes to the overall fluid diversion mechanism (cf. section 2.4.3).

4.5.1 Parameters revisited

The general parameters used in the simulations are listed in table 4.1 (p. 58). The bacterial surfactant is *surfactant B*, which is the least efficient surfactant investigated. The surfactant properties are shown in table 4.2 (p. 60). The surfactant concentration is translated into modifications of the relative permeabilities utilizing the capillary number method (cf. section 2.4.2).

The exceptions concerning biofilm is the same as presented earlier in section 4.4.1. The injection concentration of substrate is $2 \cdot 10^{-2} \text{ m}^3/\text{m}^3$, which is a little lower than previous. The Langmuir expression for bacterial partitioning utilizes $w_2 = 10^{-2}$.

4.5.2 Biofilm formation with surfactant effect

Surfactant is produced both by sessile and flowing bacteria. The bacteria are retained as they form a biofilm, and this can have a positive effect on the surfactant concentration.

Figure 4.14(a) shows the saturation profiles for the case without adsorption of bacteria. The substrate is consumed by the peak of bacteria. After that point, the bacteria are transported without any reactions taking place. As shown in section 4.3 about the surfactant effect, there is a distance from the injector to the point of mobilization, before the residual saturation decreases. The saturation profile characteristically contains two displacement fronts and formation of an oil bank.

Figure 4.14(b) shows the same case except that bacteria form biofilm. The bacteria are retained leading to a higher bacteria concentration near the inlet. The biofilm bacteria produce surfactant implying that the sufficient surfactant concentration is achieved faster and closer to the inlet. A small amount of substrate is not fully consumed and bypasses the bacteria. The biofilm formation leads to reduction of IFT already at the inlet due the increased concentration of bacteria producing surfactant. The formation

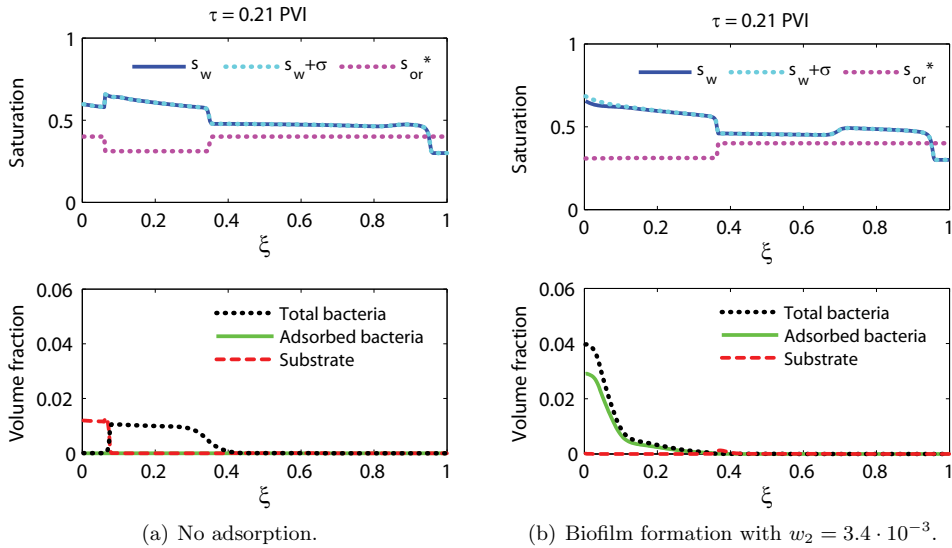


Figure 4.14: Comparison between MEOR cases with and without biofilm formation. The surfactant effect is included.

of biofilm moves the point of mobilization closer to the inlet. The effect is seen as the decrease in residual oil saturation at the inlet, especially comparing with the residual oil saturation curve in figure 4.14(a).

The case with surfactant alone to change the relative permeabilities produces after 1.4 PVI an incremental recovery of 13.0 % OOIP over that of waterflooding. When biofilm is formed, the incremental recovery becomes 13.6 % OOIP. The increase of another 0.6 % OOIP in oil recovery is produced due to the sessile bacteria producing surfactant near the inlet. Bacteria adsorbing to the pore walls improve the effect from surfactant due to the increased local concentration of surfactant. However, the influence on the recovery is minor.

4.5.3 Microscopic fluid diversion with surfactant effect

We consider the combined effect of surfactant production, formation of biofilm and microscopic fluid diversion. As shown previously in section 4.4.3 about the effect from biofilm, the biofilm saturation has to reach around 0.20 before a positive influence on the recovery can be attained with the microscopic fluid diversion.

Figure 4.15 depicts the results of computations for this case. In order to show a successful scenario, the injection concentration of substrate has been increased to $0.2 \text{ m}^3/\text{m}^3$. The biofilm saturation is 0.2 in the area with the high bacteria concentration. The residual oil

saturation drops like in the previous case with the combined effect of biofilm formation and surfactant production (figure 4.14). In addition, the biofilm formation introduces the effect from microscopic fluid diversion, which reduces the residual oil saturation further. After 1.4 PVI, the incremental oil recovery becomes 14.9 % OOIP over that of waterflooding, which is an improvement of another 0.7 % OOIP compared to the case with the effect from surfactant and biofilm formation (not shown). The effect from biofilm and microscopic fluid diversion together contributes with an improvement of 1.3 % OOIP.

In conclusion, an incremental oil recovery of almost 15 % OOIP can be achieved by the combined effect of surfactant, biofilm formation and the resulting microscopic fluid diversion. Each mechanism contributes to the overall effect, where the main contribution comes from production of surfactant.

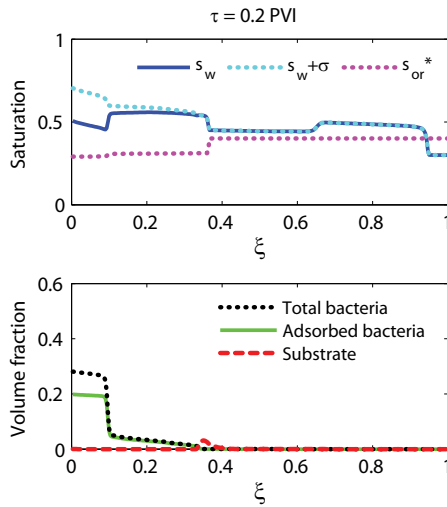


Figure 4.15: Saturation profile indicating the effect from surfactant, biofilm formation, and modification of relative permeability for water.

4.6 Summary of 1D results

The illustrative simulation results show the characteristics of the water phase saturation profiles and the corresponding oil recovery curves for MEOR. To begin with we have looked into the mechanism that reduces the oil-water interfacial tension. Surfactants are produced by the bacteria, while biofilm formation does not take place. The water phase saturation profile is found to contain a waterfront initially following the waterfront for pure waterflooding. At the *oil mobilization point* – where the surfactant effect starts to take place – surfactant has been built up mobilizing residual oil producing a second waterfront also containing bacteria, substrate and surfactant. An oil bank is created, and in some cases, it catches up with the waterfront. The recovery curve consists of several parts. The recovery curve follows pure waterflooding recovery until breakthrough of the oil bank. The next part of the recovery curve continues until breakthrough of the second waterfront containing surfactant. The incline is still relatively steep due to a low water cut. In the last part, the curve levels off.

Partitioning of surfactant between the oil and water phase is a novel approach in the context of MEOR. The partitioning coefficient only determines the time lag before the surfactant effect can be seen. For a surfactant mainly present in the water phase, the delay is small, but for cases with the main part being located in oil phase, it takes longer before the surfactant effect occurs. The position for the surfactant effect does not change final recovery with different partitioning, but a smaller partitioning coefficient gives a larger time lag before the same maximum recovery is reached. However, if too little surfactant stays in the water phase ($K_i = 10^{-2}$), we cannot obtain the surfactant effect.

It has been found that the final recovery depends on the distance from the inlet to the oil mobilization point. Additionally, it depends on, how much the surfactant-induced IFT reduction lowers the residual oil. The surfactant effect position is sensitive to changes in maximum growth rate, and injection concentrations of bacteria and substrate, which then determine the final recovery. Variations in growth rate and injection concentration also affect the time lag until mobilization of residual oil occurs, influencing how long the MEOR recovery follows the pure waterflooding recovery curve. For the cases investigated, the recovery curves are less affected.

We have investigated three methods for implementing reductions of interfacial tension; the capillary number method, Coats' method, and the Corey relative permeability interpolation method. The final oil recovery is similar for the three methods, producing an incremental recovery of 38–44 % OOIP. The differences in recovery are due to method variations in the minimum obtained residual oil, the attained distance from the inlet to the position for the initial surfactant effect, and the sensitivity to IFT reduction.

The method that interpolates the parameters of the Corey relative permeabilities, ap-

pears promising. Interpolation of residual oil and the exponents only, increases the water accumulation, and more oil is mobilized. The second front produced due to IFT reduction becomes more steep. When residual oil together with residual water and the endpoint saturations are applied as interpolation parameters, the second front becomes smoother. Less water accumulates, decreasing the mobilization of residual oil. The sets of interpolation parameters influence the saturation profiles in different ways. This leads to a suggestion for application of a modified interpolation function for e.g. residual water, which could improve the fit with experimental relative permeability curves for different interfacial tensions.

A less efficient surfactant is also investigated, where this surfactant has a higher threshold concentration, before the effect from the surfactant takes place, and a smaller IFT reduction. This results in an incremental oil recovery of 9 % OOIP. Compared to the increment of around 40 % OOIP for the more efficient surfactant, this improvement of oil recovery is lower, but it is still considered significant.

Bacterial transport is slowed down, when biofilm is formed. The biofilm saturation increases due to the continuous injection of bacteria and substrate, and to the growth of bacteria in both the biofilm and water phase. When biofilm is formed together with production of surfactant, the saturation profile is affected. The biofilm formation implies that the concentration of bacteria near the inlet increases. At the same time, these bacteria produce surfactant, resulting in attainment of a larger surfactant concentration near the inlet. The effect from surfactant only displays an incremental oil recovery of 13.0 % OOIP. In comparison, the effect from both biofilm formation and surfactant production leads to an increment of 13.6 % OOIP, so biofilm formation enhances the oil recovery by another 0.6 % OOIP. The formation of biofilm removes or shortens the distance, before the oil mobilization takes place, but the influence on the oil recovery is minor.

An effect contributing to the fluid diversion mechanisms, is microscopic fluid diversion. This happens due to the fact that the biofilm is formed only at the water-occupied zones or pores where bacteria live. The porosity decreases due to biofilm formation, and the relative permeability for the water phase only is reduced according to our modified version of the Kozeny-Carman equation. Simulations illustrate that the biofilm saturation should reach about 0.2, before a markedly improvement of the oil recovery can be seen. The incremental oil recovery is 1.3 % OOIP. Combination of biofilm formation, microscopic fluid diversion, and surfactant production improves the oil recovery even more. We achieve an increment in recovery of almost 15 % OOIP, having the main contribution from the surfactant effect.

Streamline simulations

The two-phase model for MEOR in one dimension is presented earlier in chapter 2. The model includes the most important MEOR mechanisms, where bacteria produce surfactant and can adhere to the pore walls forming biofilm. The interesting question is whether the same characteristics that appeared in the one-dimensional case, also occurs when the model is extended to two and three dimensions.

A streamline simulator is an excellent tool for fast upscaling from one dimension to two or three dimensions, because of its utilization of one-dimensional solutions along the streamlines. Therefore, the MEOR solver for one dimension is implemented in an existing streamline simulator. The existing streamline simulator additionally comprises a finite difference simulator. The two types of simulators are subject for comparison.

The implementation includes only the effect from surfactant as the biofilm formation is a phenomenon not well dealt with in the streamline simulator due to its strong influence on permeabilities and thus the streamline paths. We set up simulation examples to illustrate the multidimensional MEOR performance.

The simulators used have been put at my disposal by the Chemical Engineering Department, University of Southern California, USA. The simulators are modified to be able to contain more components, include reactions, and to perform correct gravity calculations. Gravity is included using an operator splitting approach.

5.1 Introduction

Today's streamline methods have been developed from the streamtube approach. The flow domain is divided into streamtubes and the geometry of the tubes is taken into account (Datta-Gupta, 2000). Their geometry delivers a side of disadvantages, when simulating in multiple dimensions. The streamline application has gone through several steps of development since the streamtubes were used. The details of development in the streamline approach can be found in Batycky (1997) or Thiele (1991), and Datta-Gupta (2000) has produced an excellent review on the application of streamline simulators. The current streamline technology now utilizes the *time-of-flight* concept, which eliminates the necessity of keeping track of the geometry. The time of flight is the travel time for a tracer along a streamline. The application of streamlines decouples a 2D or 3D problem into multiple 1D equations, which are less heavy to solve. The space coordinate is the time-of-flight variable (Datta-Gupta, 2000).

One phenomena that often acts across the streamlines is the effect from gravity. Therefore, the streamline simulators often underestimate gravity effect. To properly account for the gravity cross flow, operator splitting is a good option (Batycky, 1997; Berenblyum, 2004).

An advantage of the streamline simulation over the finite difference approach is that the computation time is often smaller and has a smaller impact of numerical dispersion (King and Datta-Gupta, 1998). On the other hand, the finite difference simulators better handle physical phenomena that transport fluid across the streamlines (Batycky, 1997).

The conventional simulators are often based on a finite difference methods, where many variations exist. An example is UTCHEM developed by University of Texas, Austin. The latter also has a wide utilization range for both waterfloodings and chemical EOR methods. UTCHEM has the possibility for applying both MEOR and bioremediation (Delshad et al., 2002), but more extensive studies could be presented using UTCHEM.

Comparison of the two simulation approaches gives a possibility to see the differences in the methods and verify the simulators against each other.

5.2 The multi-dimensional model

The general transport model in more dimensions was shown earlier in section 2.2. The assumptions presented in section 2.3 is considered still to hold, except that the model is extended to multiple dimensions.

Summations of the Darcy velocity for the phases, eq. (2.3), gives the total velocity:

$$\mathbf{u}_t = -\mathbf{K} (\lambda_t \nabla P - \lambda_g \nabla D) \quad (5.1)$$

where

$$\lambda_g = \lambda_w \rho_w + \lambda_o \rho_o \quad (5.2)$$

The Darcy velocity vector is \mathbf{u}_t , \mathbf{K} is the absolute permeability tensor, λ_t is the total mobility earlier described in equation (2.8), P is pressure, D is depth. The total gravity mobility λ_g depends on the phase mobilities and the phase densities ρ_j (Berenblyum, 2004). The depth is assumed to be equal to the z coordinate.

For an incompressible fluids and non-deformable rock, the gradient of the total velocity must be equal to zero (Batycky, 1997):

$$\begin{aligned} \nabla \cdot \mathbf{u}_t &= 0 \\ \nabla \cdot [-\mathbf{K} (\lambda_t \nabla P - \lambda_g \nabla D)] &= 0 \end{aligned} \quad (5.3)$$

In the well area, eq. (5.3) equals the total well volumetric flow rate \mathbf{Q}_t .

$$\nabla \cdot \mathbf{u}_t = \mathbf{Q}_t \quad (5.4)$$

Thus, the multidimensional system of equations are the pressure equation (5.4) combined with a mass balance equations for each component, equation (2.2).

5.2.1 Solution methods

The reservoir is divided into grid blocks in a conventional manner, where each grid block has a porosity, permeability and initial composition assigned.

Several solution methods have been used for solving the system of equations. A fully implicit method can be applied, but it produces a substantial amount of numerical dispersion (Aziz et al., 2003). Therefore, the solution procedure for both simulators is based on the standard IMPEC framework (implicit pressure explicit composition). The outline of the IMPEC solution procedure is presented below (Berenblyum, 2004):

1. The pressure equation, eq. (5.3) or eq. (5.4), is solved implicitly for the pressure values in each grid block based on mobilities determined by block composition from previous time step.
2. The velocity field is computed by using the Darcy velocity for each phase, eq. (2.3).
3. The reactions are calculated based on the composition of the previous time step.

4. The mass balances, eq. (2.2), for each component are solved applying the pressures calculated in step 1 and the reactions in step 3.
5. Return to step 1.

The solution of the pressure equation produces a coupled system of linear equations, where the IMPEC method produces coefficient matrices with diagonal bands only containing numbers. The number of diagonal bands increase with the number of dimensions. The pressure equation are mainly solved using iterative methods for sparse linear systems, but solving the equations is still a substantial part of the computational load (Aziz et al., 2003).

5.2.1.1 Finite difference procedure

The finite difference (FD) simulator requires solution of the pressure equation, eq. (5.3), each time the composition has been updated during a time step. This often leads to large computation times (Berenblyum, 2004). Gravity is taken into account through the velocity field, when the pressure equations are solved.

5.2.1.2 Streamline procedure

In the streamline (SL) simulator, the pressure equations are also solved using IMPEC. The solution in composition can be propagated several time steps along the streamlines, before an update of the pressures is required. The time step between pressure updates is thus much larger in the SL simulator compared to the FD simulator (Datta-Gupta, 2000).

In the SL simulator, the numerical solution procedure is:

- The pressure equation is solved implicitly on the finite difference grid using the composition from the previous time step.
- The Darcy velocities of each block are computed based on the pressure.
- Streamlines are traced from injection wells.
- The resulting 1D component equations are solved along the streamlines with time-of-flight as a coordinate variable (Datta-Gupta, 2000).
- The component composition is mapped back from the streamline grid to the finite difference grid.

- Due to operator splitting between convective flux and gravity flux, the gravity lines are made based on columns in the finite difference grid. The 1D gravity equations are solved along each gravity line (Jessen and Orr, 2004).
- The component composition is updated.

Mapping between the finite difference grid and the streamline grid can also produce some amount of dispersion that negatively influences the effect from surfactant in the MEOR process. Therefore, the pressure updates should be kept to a minimum avoiding too many smearing out translations between the grids.

5.2.2 Gravity

The total velocity field is also based on the gravity and determines the streamlines. The gravity effect is driven by the density differences between the flowing phases, but the propagation of the fluids along the streamlines does not account for the gravity effect. The fractional flow function could include the gravity, but operator splitting is an excellent alternative for including gravity in a streamline simulator (Batycky, 1997; Jessen and Orr, 2004). The method has earlier shown good agreement with results produced by the conventional simulator Eclipse.

The convective and the gravity fluxes can be separated by means of operator splitting resulting solution of component mass balances in a sequential manner. A time step starts with a convective step, which is shown here as a modified version of eq. (2.2).

$$\phi_0 \frac{\partial \Omega_i}{\partial t} + \nabla \mathbf{F}_i = R_i + Q_i \quad (5.5)$$

Earlier, the overall concentration Ω_i was defined in eq. (3.2) and the overall flux \mathbf{F}_i in eq. (3.9). The overall flow is based on the fractional flow function, which does not contain gravity.

The convective step is followed by the gravity step, which only accounts for the gravity effects:

$$\phi_0 \frac{\partial \Omega_i}{\partial t} + \nabla \mathcal{G}_i = 0 \quad (5.6)$$

where

$$\mathcal{G}_i = K_z \sum_j \omega_{ij} \lambda_j \left(\frac{\lambda_g}{\lambda_t - \rho_j g} \right) \frac{\partial D}{\partial z} \quad (5.7)$$

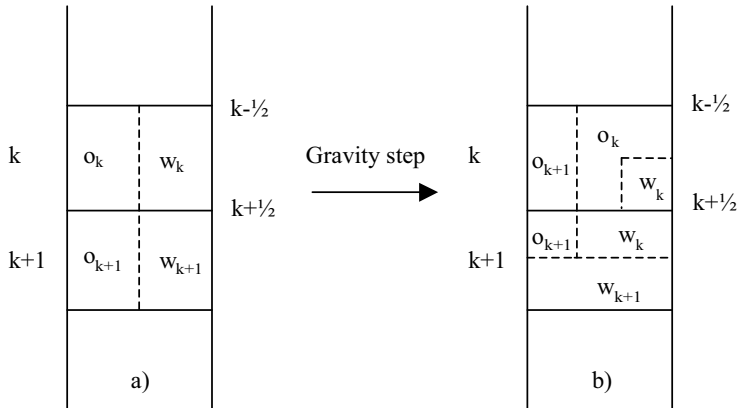


Figure 5.1: Blocks are designated k and $k+1$. Each block contains a segment of the oil phase and a segment of the water phase, which for instance for block k are o_k and w_k . a) Initial state. b) The segments are moved according to the fluxes, and the block composition can be calculated from the segments contained in the block after the gravity step. Adapted from Jessen and Orr (2004).

The density phase density is ρ_j , \mathcal{G}_i is the gravity flux vector, K_z is absolute permeability in z direction, ω_{ij} is the phase concentration for component i , λ_t is total mobility, λ_g is gravity mobility, and the gradient $\frac{\partial D}{\partial z}$ equals unity as the z axis equals the depth direction D , which is also the direction for the gravity.

The gravity segregation utilizes a pseudo-immiscible approach (Jessen and Orr, 2004), where phase segment fluxes along gravity lines are found based on their phase density differences and mobilities corresponding to overall phase compositions. Figure 5.1 depicts the idea of the method, where figure 5.1(a) illustrates the initial state with two immiscible segments for the oil (o) and water (w) phases for two neighboring blocks k and $(k+1)$. The segments are moved between blocks according to the calculated fluxes, which results in the segment distribution shown in figure 5.1(b). The new overall composition can now be calculated from the segments now contained in the block (Jessen and Orr, 2004). In this way, the phase equilibrium calculation is avoided.

5.3 Parameters

The parameters used in the simulations are shown in table 5.1. The reservoir is initially assumed not to contain any bacteria or other indigenous microorganisms. Bacteria and substrate in solution are continuously injected into the reservoir. The injection composition is given in terms of volumetric fractions $v_{ij,inj}$. The surfactant produced by the bacteria is assumed to be *surfactant C*. The details of the surfactant can be found the section 4.1.

Table 5.1: Parameters used in the SL and FD simulations.

μ_{max}	0.2	day ⁻¹
K_s	1	kg/m ³
Y_{sm}	0.18	kg/kg
Y_{sb}	0.82	kg/kg
ϕ	0.4	-
Reservoir length (1D)	400	m
Reservoir width (1D)	100	m
Reservoir height (1D)	100	m
Volumetric injection velocity (1D)	800	m ³ /day
$\Delta x, \Delta y, \Delta z$ (for 2D and 3D)	1	m
μ_w	0.5	mPa·s
μ_o	0.7	mPa·s
ρ_w	1000	kg/m ³
ρ_o	800	kg/m ³
ρ_s	1000	kg/m ³
ρ_b	1000	kg/m ³
ρ_m	1000	kg/m ³
σ_{base}	29	mN/m
n	6	-
p_1, p_2, p_3	{6.5 · 10 ³ , 0.1, 0}	-
K_i	1	-
Surfactant C:		
q_1, q_2, q_3	30 · 10 ⁻⁴ , 2, 1.5 · 10 ⁴	-
$v_{bw,inj}$	0.5 · 10 ⁻⁵	m ³ /m ³
$v_{sw,inj}$	10 ⁻⁵	m ³ /m ³
$v_{mw,inj}$	0	m ³ /m ³
k_{rwor}	0.6	-
k_{rowi}	0.9	-
a	2	-
b	2	-
s_{wi}	0.2	-
s_{or}	0.2	-

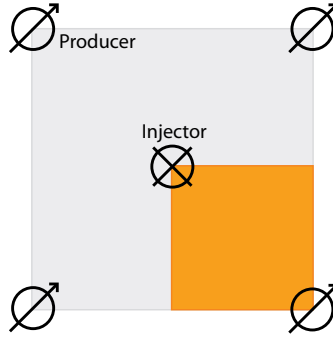


Figure 5.2: Five spot well pattern is shown as the gray area, where one injector is located in the center and four producers are located in each corner. *The quarter of a five spot well pattern is the orange area.*

In both SL and FD simulations, injection is performed with a specified rate at the injection well and the production has a specific pressure (22500 kPa). For horizontal 2D and 3D simulation cases, the sample reservoirs are a quarter of a five spot well pattern. This well pattern is illustrated in figure 5.2.

Gravity number

The gravity number N_g is the characteristic ratio for fluid to flow in the vertical direction due to gravity forces to that in the horizontal direction due to convective viscous forces (Green and Willhite, 1998; Zhou et al., 1994). The gravity number is defined as:

$$N_g = \frac{K_{av} \Delta \rho g H}{u \mu_o L} \quad (5.8)$$

where K_{av} is the average absolute permeability, $\Delta \rho$ is the density difference between the water and the oil phase, g is gravitation, H is height of the reservoir, u_t is the Darcy velocity, μ_o is the viscosity of oil (the displaced phase), and L is the reservoir length (Green and Willhite, 1998; Zhou et al., 1994).

The gravity number indicates the influence of gravity segregation. A low gravity number corresponds to only a small effect from gravity.

The Darcy velocity without the gravity term earlier shown as eq. (2.3), is rearranged in order to isolate the pressure difference ΔP . Insertion into eq. (5.8), gives the following equation for the gravity number:

$$N_g = \frac{\Delta \rho g H}{\Delta P} \quad (5.9)$$

The pressure difference in the 3D simulations performed later in this chapter, is in

average 4600 kPa, and the gravity is 9.81 m/s^2 . The remaining parameters are listed in table 5.1. We apply an oil density of both 800 and 500 kg/m^3 , resulting in gravity numbers at 0.004 and 0.01 , respectively. These gravity numbers indicate that the effect from convection mainly dominates. Therefore, we only expect a moderate effect from gravity on the saturation profiles and oil recovery.

5.4 Verification of implementation

In figure 5.3, results from the explicit 1D simulator, the SL simulator, and the FD simulator show that the simulators produce the same water phase saturation profiles in 1D displacement. It confirms that the 1D model has been properly implemented into the multidimensional schemes in both simulators.

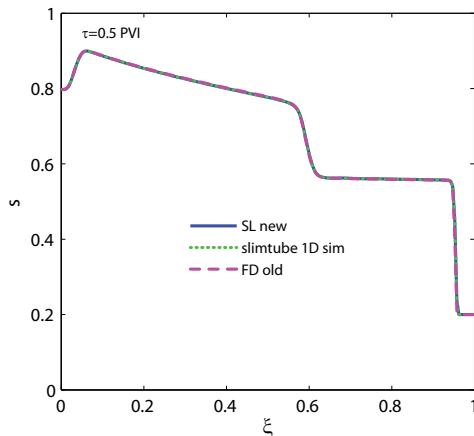


Figure 5.3: Comparison between original 1D simulator (explicit version), the streamline simulator (SL), and finite difference simulator (FD) for MEOR with 200 blocks. All three curves are located at the top of each other.

5.5 Comparison of 2D results

Comparison between the SL and FD simulators is performed by running MEOR simulations in a homogeneous square "reservoir", with injection into the upper left corner and production from the lower right corner (figure 5.4). Comparison between the simulators shows that their solutions are similar with only minor differences. The FD simulator produces a smoother propagation front compared to the SL simulator, due to higher numerical dispersion.

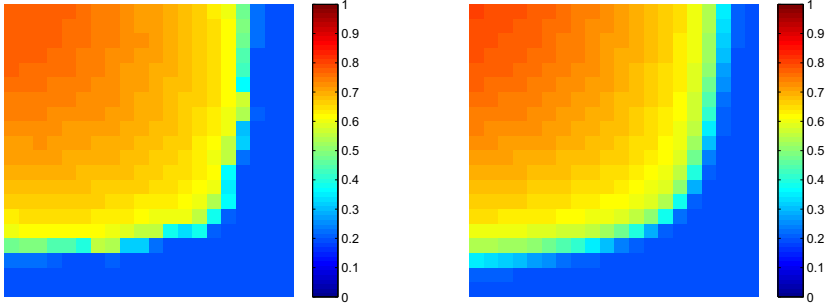


Figure 5.4: Waterflooding in 2D. Streamline simulation (left) and finite difference simulation (right) showing water phase saturation after 0.31 PVI. The horizontal reservoir is 20×20 with injection in upper left corner (1,1) and production from lower right corner (20,20) in a homogenous reservoir.

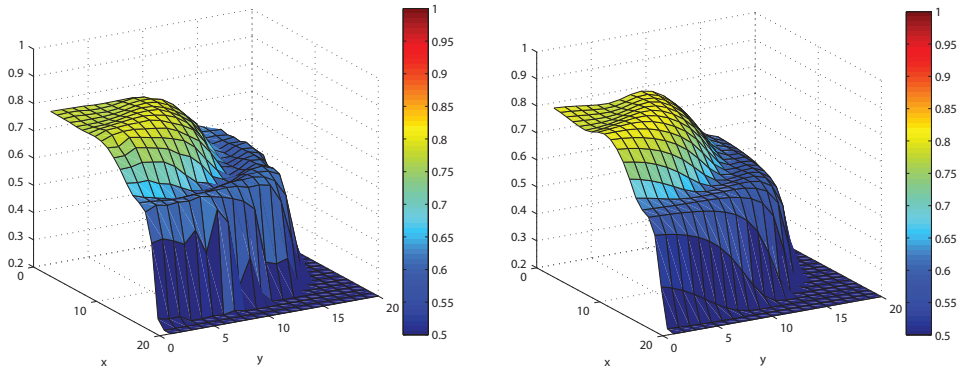


Figure 5.5: Water phase saturation profiles for 2D horizontal MEOR with the SL simulator (left) and the FD simulator (right). Injection in block (1,1). The specific MEOR features are the water phase accumulation producing a traveling oil bank and two displacement fronts.

5.6 The MEOR characteristics

Production of the metabolite results in the specific MEOR characteristics. Figure 5.5 shows the water phase saturation profiles for the SL and FD simulators. The profiles are characterized by generation of the oil bank due to water accumulation, creating the second water front. This effect is rather pronounced for the homogeneous permeability field. It is very important to see that the effects in 1D is also found for the 2D case.

One issue that has to be considered carefully is the effect from dilution on the MEOR process. The MEOR performance is sensitive to surfactant concentration and the total growth rate which is dependent on substrate and bacteria concentration. The further away from the inlet, the more initial water is met by the substrate, bacteria and surfactant. The incoming water phase mixes with the initial water, which can lead to some extent of dilution of the water phase components in low concentration. The dilution effect could result in a smaller growth rate and less bacteria to produce the surfactant, entailing less mobilized oil.

Figure 5.5 indicates that the effect from dilution seems minor in the simulation case. This probably results from the lower initial water saturation in the reservoir. A larger initial water saturation could weaken the MEOR performance, but the extent has not been investigated further.

It should be mentioned that the pressure updates in SL should be performed as less times as possible due to smearing out the concentrations when mapping from the finite difference grid to the streamline grid and vice versa. In the context of MEOR, smearing out entails a smaller effect from the bacterial surfactant, as this effect is dependent on the local surfactant concentrations. For that reason, we have kept the pressure solves to a minimum.

5.7 Simulations in 2D with gravity effect

We consider the same homogeneous square-shaped "reservoir" as above, but now it is put vertically. Displacement is carried out from the lower left to the upper right corner of the reservoir. In general, gravity is expected to support the oil displacement, when water is injected from the bottom and production occurs at the top.

The results for waterflooding without bacteria, produced by the SL simulator, are presented in figure 5.6. As the flowing phases are oil and water, water injection is conducted from the lower part of the injection well and production from the upper part of the production well in a 50×50 grided vertical field. There is a minor effect from the

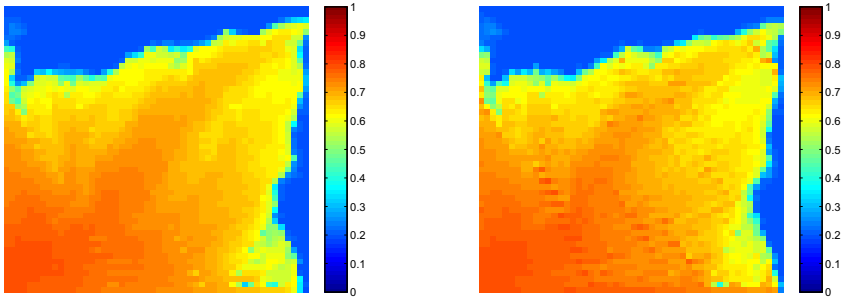


Figure 5.6: Vertical 2D waterflooding (WF) at 0.4 PVI using the SL simulator. (Left) Waterflooding. (Right) Waterflooding with gravity. Water injection is conducted from the lower part of the injection well (1,43:50) and production from the upper part of the production well (50,1:5) in a 50×50 vertical field with a block side length of 1 m. Injection rate is $0.2 \text{ m}^3/\text{day}$.

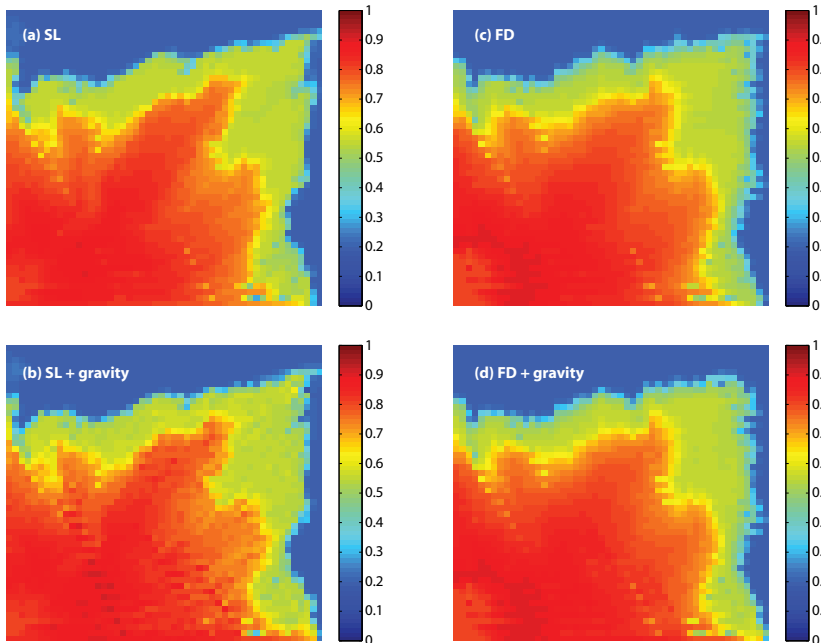


Figure 5.7: MEOR flooding at 0.4 PVI. (a) SL (b) SL + gravity (c) FD (d) FD + gravity. Water injection is conducted from the lower part of the injection well (1,43:50) and production from the upper part of the production well (50,1:5) in a 50×50 vertical field with a block side length of 1 m. Injection rate is $0.2 \text{ m}^3/\text{day}$.

gravity. The FD simulator gives similar results (not shown), where fingering towards the production well occurs less markedly.

MEOR 2D simulations

Figure 5.7 shows 2D MEOR with and without gravity carried out by both simulators. The standard MEOR case without gravity supports the fact that the FD fronts become smoother and the SL produces more fingering. This was also seen at the previous MEOR flooding simulations. The MEOR characteristics are also present the 2D vertical case with gravity.

The SL simulation with gravity shows small perturbations in the saturations, but the figure illustrates basically the same features as the FD simulation. It can be seen that gravity to some extent stabilizes the displacement of oil. For the current case, the gravity effect results in a slightly larger oil production, but the improvement is only 1 % OOIP after 1 PVI for both waterflooding and MEOR.

The incremental oil recovery after 1 PVI is 9 % OOIP, when comparing MEOR with waterflooding under the influence of gravity. The maximum attainable recovery during waterflooding (1D) after infinite time is 75 % OOIP and this is already achieved after 1 PVI during MEOR. This demonstrates the potential of MEOR. The MEOR recovery after 2.4 PVI reaches 88 % OOIP for the current set-up.

5.8 Simulations in 3D with gravity effect

Figure 5.8 illustrates some layers of the heterogeneous permeability field used for the 3D simulations, which are performed only by the SL simulator. The grid is $50 \times 50 \times 10$ with injection in (1,1,1:10) being located in upper left corner and production occurs in blocks (50,50,1:2). The water phase saturations for the layers located in the top, middle and bottom are presented in figure 5.9 and figure 5.10 without and with gravity, respectively. Importantly, both profiles show two displacement fronts characterizing the MEOR displacement. This is seen as shifts from blue to green area and from green to red area.

As expected with gravity, more water is located in the bottom layers. Recovery after 1 PVI is 78 % OOIP without gravity and 79 % OOIP with gravity. The recovery is only slightly increased due to gravity, which was also seen for the vertical 2D case. The recovery for waterflooding is 69 % OOIP. Thus, also for this case MEOR results in a noticeable increment of recovery.

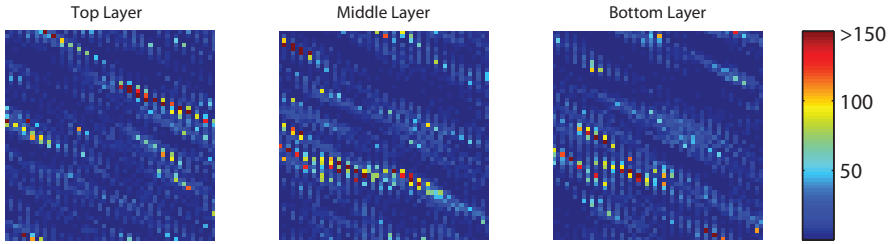


Figure 5.8: Illustration of permeability field for 3D simulations.

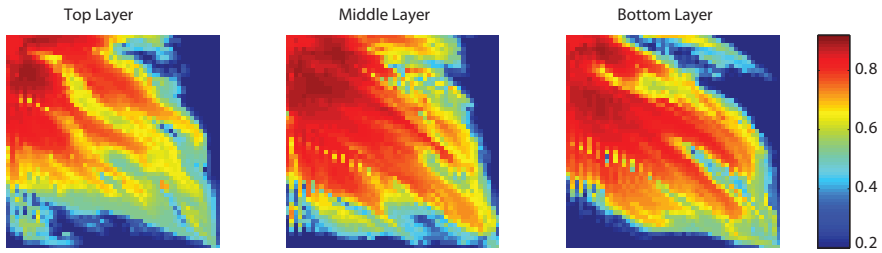


Figure 5.9: MEOR 3D simulation results **without** gravity after 0.5 PVI. Grid is $50 \times 50 \times 10$ with injection in $(1,1,1:10)$ being located in upper left corner and production occurs in blocks $(50,50,1:2)$. Injection rate is $2 \text{ m}^3/\text{day}$.

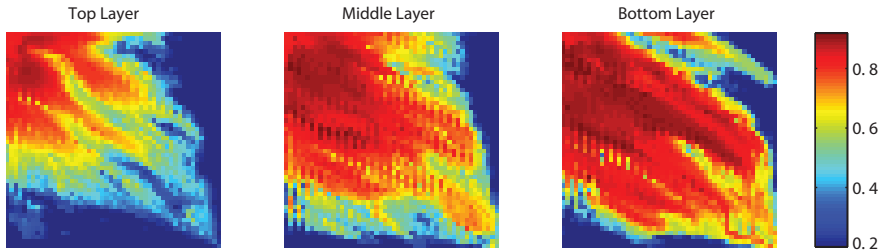


Figure 5.10: MEOR 3D simulation results with gravity after 0.5 PVI. Grid is $50 \times 50 \times 10$ with injection in $(1,1,1:10)$ being located in upper left corner and production occurs in blocks $(50,50,1:2)$. Injection rate is $2 \text{ m}^3/\text{day}$.

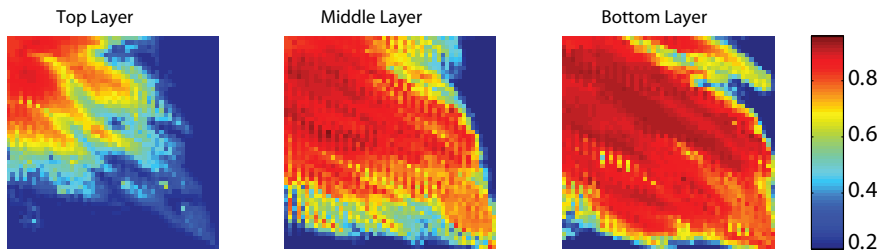


Figure 5.11: MEOR 3D simulation results like fig. 5.10 with gravity after 0.5 PVI. Only the oil density is reduced from 800 kg/m^3 to 500 kg/m^3 .

Table 5.2: Incremental recovery over that of waterflooding after 1 PVI.

After 1 PVI	ρ_o [kg/m ³]	÷ gravity	+ gravity
Waterflooding	800	-	1 % OOIP
MEOR	800	10 % OOIP	11 % OOIP
MEOR	500	10 % OOIP	14 % OOIP

The influence from the heterogeneous permeability field becomes evident on the saturation profile of the layers (figure 5.8). The variations in permeability produce multiple fronts compared to e.g. the horizontal 2D case with a homogeneous permeability field (fig. 5.5). The high permeable path easier leads the water through and the fronts have reached furthest. Fingering also happens for conventional waterflooding in 3D (not shown). The 3D MEOR flooding in the heterogeneous permeability field has a lower sweep efficiency compared to the 1D case. The 1D reservoir is basically constructed to have a full sweep by the water flow. This indicates that the SL simulator is a good candidate for studying both microscopic and macroscopic displacement efficiency of MEOR.

Figure 5.11 shows the same simulation case again, except that the oil density is reduced from 800 to 500 kg/m³. The larger density difference facilitates that gravity can play a role. The incremental recoveries for the different 3D scenarios is shown in table 5.2. The incremental recovery increases from 11 to 14 % OOIP, where the effect from gravity becomes significant. Therefore, the density difference should be at the current value or larger, before the gravity effect has a markedly positive influence on the recovery.

5.9 Summary of multidimensional results

The SL simulator has been extended to include the MEOR two-phase model, enabling the study of MEOR in two and three dimensions. The SL simulator is found to produce similar results with the corresponding finite difference simulator. The general characteristics found for MEOR in one-dimensional simulations are also demonstrated both in two and three dimensions: It is accumulation of water together with mobilization of residual oil producing a traveling oil bank, and the creation of two displacement fronts.

The effect from dilution when the fluids move from the injector toward the producer could be important for the MEOR performance. For our simulation examples, the effect of dilution appears to be insignificant.

In the SL simulator, the effect of gravity is introduced using an operator splitting technique. The gravity effect stabilizes the oil displacement causing slight incremental oil recovery, which is also indicated from the gravity number. Decreasing the oil density prompts that gravity may play a role. This leads to markedly improvement of incremental oil recovery.

Overall, the MEOR process produces more oil compared to waterflooding. Three-dimensional simulations, compared to one-dimensional, make it possible to not only study the sweep efficiency, but also the displacement efficiency on the reservoir scale, affected by the three-dimensional geometry and reservoir heterogeneities.

Conclusion

A generic model has been set up to include the two main mechanisms in the MEOR process; *reduction of IFT* due to surfactant production, and *microscopic fluid diversion* as a part of the overall fluid diversion mechanism due to formation of biofilm.

In the context of MEOR, our novel approach is the partition of surfactant between oil and water. Surfactant is the key component in order to reduce interfacial tension (IFT). We have looked into three methods how to translate the IFT reduction into changes of the relative permeabilities: the capillary number method, Coats' method, and the Corey relative permeability interpolation method. These methods produce similar results, with small variations in the minimum obtained residual oil, the attained distance from the inlet to the position for the initial surfactant effect, and the sensitivity to interfacial tension reduction.

Separate investigations of the surfactant effect have been performed through exemplifying simulation cases, where no biofilm is formed. The water phase saturation profiles are found to contain a waterfront initially following the saturation profile for pure waterflooding. At the *oil mobilization point* – where the surfactant effect starts to take place – sufficient surfactant has been built up mobilizing residual oil producing a second waterfront. An oil bank is created, and in some cases, it catches up with the waterfront. The recovery curve consists of several parts. Initially, the recovery curve follows pure waterflooding recovery until breakthrough of the oil bank. The next part of the recovery curve continues until breakthrough of the second waterfront. The incline is still relatively steep due to a low water cut. In the last part, the curve levels off.

The surfactant concentration in the water phase must reach a certain concentration

threshold before surfactant can reduce the interfacial tension. The relative permeabilities depend on the water phase concentration, so when surfactant is moved into the oil phase, there will be a smaller effect from the surfactant on the flow. Therefore, transfer part of the surfactant to oil phase is equivalent to its “disappearance”, so that the total effect from surfactant is reduced. The oil phase captures the surfactant, but it may as well be adsorbed to the pore walls in the oil phase.

The influence from partitioning of surfactant only determines the time lag before the surfactant effect can be seen. The position for the surfactant effect does not change final recovery with different partitioning. However, if too little surfactant stays in the water phase, we cannot obtain the surfactant effect.

It has been found that the final recovery depends on the distance from the inlet to the oil mobilization point. A long distance means that oil in the beginning of the reservoir is not recovered. The surfactant effect position is sensitive to changes in growth rate, and injection concentrations of bacteria and substrate. Variations in growth rate and injection concentration to a smaller extent affect the time lag until mobilization of residual oil occurs.

Additionally, the final recovery depends on, how much the surfactant-induced IFT reduction lowers the residual oil, which is also a result of efficiency of the surfactant. A super efficient surfactant produces an incremental recovery recovery around 40 % OOIP over that of waterflooding. Application of a less efficient – and probably more realistic – surfactant results in an incremental oil recovery of 9 % OOIP, but it is still considered a significant improvement.

The adsorbed bacteria adhere to the pore walls and constitute the biofilm phase. The biofilm formation implies that the concentration of bacteria near the inlet increases. In combination with surfactant production, the biofilm results in a higher surfactant concentration in the initial part of the reservoir. The oil that is initially bypassed in relation to the surfactant effect, can be recovered as formation of biofilm shortens the distance to the oil mobilization point. In a sample simulation, the effect from surfactant only displays an incremental oil recovery of 13.0 % OOIP. In comparison, the effect from both biofilm formation and surfactant production leads to an increment of 13.6 % OOIP. The formation of biofilm to a minor extent enhances the oil recovery.

The formation of biofilm promotes fluid diversion. A contribution to this mechanism is *microscopic fluid diversion*, which is possible to investigate in a one-dimensional system. This happens due to the fact that the biofilm is formed only at the water-occupied zones or pores where bacteria live. The porosity decreases due to biofilm formation, and the relative permeability for the water phase alone is reduced, according to our modified version of the Kozeny-Carman equation. This results in decreasing the mobility of water and, correspondingly, a higher fraction of oil in the flow. Simulation cases study the

effect from biofilm formation together with microscopic fluid diversion. The biofilm saturation should reach about 0.2, before there is a markedly improvement of the oil recovery. The incremental oil recovery is 1.3 % OOIP.

Combination of biofilm formation, microscopic fluid diversion, and surfactant production improves the oil recovery even more. We achieve an increment in recovery of almost 15 % OOIP.

The one-dimensional studies for the mechanisms separately and in combination show that all the mechanisms contribute to improvement of the oil recovery. The mechanisms produce their characteristic effect on the saturation profile and thus on the recovery curve. When sufficient amounts of surfactant can be produced, the effect from surfactant generates a larger effect compared to microscopic fluid diversion.

To study the MEOR performance in multiple dimensions, the 1D model with the surfactant effect only has been implemented into existing simulators; a streamline simulator and a finite difference simulator. In the streamline simulator, the one-dimensional simulator is used for propagating the solution along each streamline, which makes it easier to implement the model. In addition, the effect of gravity is introduced using an operator splitting technique. The gravity effect stabilizes oil displacement causing markedly improvement of the oil recovery, when the oil density becomes relatively low. The general characteristics found for MEOR in one-dimensional simulations are also demonstrated both in two and three dimensions. Overall, the MEOR in multiple dimensions in heterogeneous reservoirs also produces more oil compared to waterflooding. In our simulations for model reservoirs, characteristic effects and orders of magnitude of recovery improvement were found to be similar to one-dimensional simulations. This will probably change if more heterogeneous reservoirs will be considered.

Future work

The model developed in this thesis is generic building on general knowledge of microbial and reservoir processes. For achieving the long-term goal of designing a robust MEOR process, the model should be modified to describe MEOR with specific bacteria under specific reservoir conditions. The model should be “fed” with necessary particular information coming from laboratory experimental data and field tests. In order to obtain the necessary information, collaboration with other researchers in petroleum microbiology and engineering should be established. Other collaborators could be researchers working with bioremediation or ground water contamination, where they possess some expertise on transport of bacteria in the underground. One subject that should be focused on, is arrangement of field trials. Obtaining specific information on the basis of the field trial data is a specific task that needs a separate development.

Microscopic fluid diversion has been investigated as a part of the fluid diversion mechanism. We suggest that the model should be extended to two or three dimensions to see the full effect of fluid diversion. Especial attention should be paid to highly heterogeneous media where formation of biofilm may lead to not only microscopic, but also meso- and macroscopic fluid diversion: hindering water breakthrough through high permeable zones or systems of fractures.

Fluid diversion is supposed to increase areal sweep, while the effect of surfactant is to recover more oil, where the water has already flown. The two effects are clearly complementary. Their combination in three dimensions should also be investigated.

In this work, it is assumed that biofilm consists of bacteria only. As mentioned, the actual biofilm is also composed of a water-filled matrix, sticky polysaccharides, and

many substrates and metabolites. All these additions may affect biofilm growth rate and thickness, as well as surfactant production in it. Therefore, they are suggested to be included in later models. Especially, the water content should be included, in order to estimate the influence from biofilm.

The porous media are composed of pores of different sizes. Therefore, the transport of bacteria through the reservoir also depends on processes such as straining and physical filtration. The straining process is a function of the pore geometry, where a bacterium too large to allow passage through a pore is trapped. Physical filtration is the removal of particle mass from solution via collision with and deposition on the internal porous surface (Ginn et al., 2002). Investigations should be performed to be able to describe physical transport of the bacteria. The attachment process for initiating a biofilm, is an excellent target for further studies. This gives rise to a new direction in the MEOR modeling, where bacterial transport is modeled in the framework of the deep bed filtration theory. Relevant deterministic or stochastic models may be applied.

In connection to MEOR, future models should also be able to include the presence of different bacteria. Oil fields do contain indigenous bacteria, or bacteria enter the reservoir during water injection. The indigenous bacteria may comprise different types of bacteria representing a bacterial community. For activating the community in a specific way, knowledge about the community collaboration is important. In addition, bacteria injected into the reservoir should also be able to properly compete with the indigenous bacteria or well site bacteria. Generally, there is a need for models that can deal with bacterial communities, because it can very likely be important for the performance of the MEOR process. Interaction between the different bacterial populations may need development of new approaches, similar to population balance models, but taking into account multiphase character of the flow and bacterial filtration.

Injection of substrates should be done with care to secure that the substrates will favor the growth of specific MEOR bacteria. A model that combines different substrates with the bacterial diversity is another step on the way toward designing a robust MEOR process.

Parameters in Langmuir expression

To support the choice of parameters for the Langmuir expression in section 4.1, we look at the parameters differently. The same result is obtained by approaching it another way.

Assume that we have bacteria with a diameter of $d_b = 1 \mu\text{m}$, and the bacteria density is as given in table 4.1. The maximum amount of bacteria per area becomes a product of the number of bacteria per surface area and the mass of one bacteria, when one bacterium is considered a cube with the side length d_b , and covers the surface in one layer:

$$\mathcal{M}_{b,max} \approx \frac{1}{(d_b)^2} \cdot (d_b^3 \rho_b) = d_b \rho_b \quad (\text{A.1})$$

where ρ_b is the density of the bacterium given in table 4.1.

Application of equation (2.28) gives a maximum pore volume of 75 %, which agrees with the result found using the other approach.

Multivariable Newton iteration

The Newton iteration solves the matrix system below (Aziz et al., 2003). The correction factor δ is found, which is the correction to the new variable vector y to approach the solution of the system.

$$\mathbf{J}(y_n) \cdot \delta = -\mathcal{F}(y_n) \tag{B.1}$$

$$y_{n+1} = y_n + \delta \tag{B.2}$$

This will be repeated until convergence, which is evaluated from an error estimate $|\mathcal{F}(y)|^2$. Often, $|\delta|^2$ is used as error estimator, but I choose $|\mathcal{F}(y)|^2$, because it takes different scales of components into account. The tolerance is set to 10^{-8} . The Newton iteration is characterized by showing quadratic convergence, when the initial guess is close enough to the true zero. In this case, the initial guess is considered reasonable, when conditions from the previous time step and position are used, and concurrently small time steps are taken, so changes will be small.

In order to setup the matrix system above, the Jacobian should be manufactured. The definition of the Jacobian is:

$$J_{ij} = \frac{\partial \mathcal{F}_i}{\partial y_j} \tag{B.3}$$

The Jacobian is chosen to be numerical as this makes the system more flexible. The numerical Jacobian will be calculated as shown in equation (B.4).

$$J_{ij} = \frac{\Delta \mathcal{F}_i}{\Delta y_j} = \frac{\mathcal{F}_i(y + \epsilon_j) - \mathcal{F}_i(y)}{\epsilon_j} \tag{B.4}$$

The perturbation ϵ_j will be in the order of 10^{-5} .

Analytical solution of Buckley-Leverett equation

The analytical solution is derived by Bedrikovetsky (1993).

The Buckley-Leverett equation describing displacement:

$$\frac{\partial s_w}{\partial \tau} + \frac{\partial f_j}{\partial \xi} = 0 \quad (\text{C.1})$$

The analytical solution is derived using the similar transformation, where the new variable η is applied.

$$\eta = \frac{\xi}{\tau} \quad (\text{C.2})$$

The water saturation only becomes a function on the new variable:

$$s_w = s_w(\eta) \quad (\text{C.3})$$

Variable substitution into equation (4.1) replaces ξ and τ by the new variable η and turns the water transport equation into an ordinary differential equation.

$$\frac{d s_w}{d \eta} (\eta - f'_w(s)) = 0 \quad (\text{C.4})$$

Rearrangement of the equation reveals the analytical solution.

$$\eta = f'_w(s_w), \quad \text{for } 0 < \eta < D_f \quad (\text{C.5})$$

$$s_w = s_{wi}, \quad \text{for } \eta > D_f \quad (\text{C.6})$$

where the value of D_f is

$$D_f = f'_w(s_f) \quad (\text{C.7})$$

Here, the front water saturation is s_f . The saturation determines D_f , which describes the location of the front in terms of η . It is known that the fractional flow is zero at initial saturation s_{wi} , and the tangent on the fractional flow curve at the front saturation $f_w(s_f)$ goes through the initial point.

The front water saturation is determined from the knowledge about the fractional flow first derivative.

$$f'_w = \frac{f_w(s_f) - 0}{s_f - s_{wi}} \quad (\text{C.8})$$

Nomenclature

a	Exponent in Corey relative permeabilities
b	Exponent in Corey relative permeabilities
D	Depth, downwards positive [m]
d	Grain diameter [m]
D_c	Constant in Contois expression for bacterial growth rate
D_f	Location of the water front
F_i	Overall component flux
f_j	Fractional flow function for phase j
f'_j	First derivative of fractional flow function wrt. saturation
\mathcal{F}	Zero function in Newton-Raphson iteration procedure
g	Gravitational acceleration [m/s ²]
$g(\sigma_{ow})$	Interpolation function
\mathcal{G}_i	Gravity flux
H	Height of the reservoir [m]
i	Index for component
j	Index for phase
\mathbf{J}	Jacobian matrix in Newtons method
K	Absolute permeability [mDa]
K_i	Partitioning coefficient for surfactant
K_s	Half saturation constant in Monod expression [kg/m ³]
K_z	Vertical absolute permeability [mDa]
K_{av}	Average absolute permeability of the reservoir [mDa]
k_{rj}	Phase relative permeability
$k_{r_{owi}}$	Endpoint relative permeability for oil at s_{wi}

k_{rwor}	Endpoint relative permeability for water at $(1 - s_{or})$
L	Length of the reservoir [m]
ℓ	The length of the column, where the pressure drop is investigated [m]
n	Exponent in Coats' interpolation function
n_c	Number of components
N_g	Gravity number
n_p	Number of phases
P	Pressure [kPa]
p_1	Constant in surfactant concentration - IFT correlation
p_2	Constant in surfactant concentration - IFT correlation
p_3	Constant in surfactant concentration - IFT correlation
q_1	Constant in expression for the desaturation curve
q_2	Constant in expression for the desaturation curve
q_3	Constant in expression for the desaturation curve
Q_i	Well term for component [m^3/day]
Q_t	Total well volumetric flow rate [m^3/day]
R_i	Reaction meaning net production of component
\hat{s}	Sum of water and biofilm saturations [m^3/m^3]
s_f	Saturation of the water front [m^3/m^3]
s_j	Saturation of phase j [m^3/m^3]
s_{or}	Residual oil saturation [m^3/m^3]
s_{wi}	Initial water saturation [m^3/m^3]
\tilde{S}	Specific surface [m^2/m^3 totalvolume]
S	Efficient specific surface [m^2/m^3 PV]
t	Time [day]
u_d	Dimensionless velocity
u_j	Phase velocity [m/s]
u_t	Total flow velocity [m/s]
u_{inj}	Injection velocity [m/day]
v	Linear velocity [m^3/day]
V_j	Volume of a phase in a block [m^3]
V_T	Total pore volume of a block [m^3]
$v_{ij,inj}$	Volumetric injection fraction
w_1	Constant in the Langmuir expression for partitioning of bacteria [m]
w_2	Constant in the Langmuir expression for partitioning of bacteria [m^3/kg]

x	Horizontal axis in sample reservoir [m]
y	Horizontal axis in sample reservoir [m]
Y_{sb}	Yield of bacteria on substrate [kg/kg]
Y_{sm}	Yield of surfactant/metabolite on substrate [kg/kg]
z	Vertical axis in sample reservoir [m]
α	Constant describing the time for injection of one pore volume
α_s	Sphericity coefficient
$\Delta\rho$	Density difference between water and oil
δ	Adjustment vector for variable correction in Newtons method
ϵ	Perturbation in Newtons method to make a numerical Jacobian
η	Similar transformation variable; ξ/τ
γ	Exponent in the Carman-Kozeny equation found between 2 and 5
λ_g	Gravity mobility
λ_j	Phase mobility
λ_t	Total mobility
μ_{max}	Maximum growth rate in Monod expression [day^{-1}]
μ	Growth rate for bacteria [day^{-1}]
μ_j	Phase viscosity [Pa·s]
Ω_{ij}	Overall component concentration in the phase [kg/m^3 PV]
ω_{ij}	Concentration of component i in phase j [kg/m^3 phase]
Ω_i	Overall component concentration [kg/m^3 PV]
ϕ	Porosity
ρ_i	Component density [kg/m^3]
ρ_j	Phase density [kg/m^3]
σ	Volumetric concentration of biofilm bacteria [m^3/m^3]
σ_{ow}	Interfacial tension between oil and water [mN/m]
τ	Dimensionless time [PVI]
ξ	Dimensionless length
*	Estimated/predicted value
<i>base</i>	Standard case at highest IFT, Coats' interpolation method
<i>inj</i>	Index indicating injection
<i>k</i>	Index for position/block

<i>misc</i>	Linear case at lowest IFT, Coats' interpolation method
<i>n</i>	Index for time step
0	Index indicating the initial state
<i>b</i>	Index for bacteria
<i>m</i>	Index for metabolite/surfactant
<i>o</i>	Index for oil
<i>s</i>	Index for substrate
<i>w</i>	Index for water
EOR	Enhanced oil recovery
IFT	Interfacial tension
MEOR	Microbial enhanced oil recovery
NRB	Nitrate reducing bacteria
OOIP	Original oil in place
PV	Pore volume
PVI	Pore volumes injected
SRB	Sulfate reducing bacteria

Bibliography

Al-Wahaibi, Y. M., C. A. Grattoni, and A. H. Muggeridge (2006, September). Drainage and imbibition relative permeabilities at near miscible conditions. *J Petrol Sci Eng* 53, 239–253.

Amaefule, J. O. and L. L. Handy (1982). The effect of interfacial tensions on relative oil/water permeabilities of consolidated porous media. *SPE J* 22, 371–381.

Amro, M. M. (2008). Multidisciplinary challenge for microbial enhanced oil recovery (MEOR). *SPE-120820 presented at Saudi Arabia Section Technical Symposium, Al-Khobar, Saudi Arabia, 10–12 May*.

Aslam, U. (2009a). Mechanisms of microbe propagation in heterogeneous porous media and analysis of various MEOR processes involved in microbe transportation. *SPE-119010 presented at Middle East Oil and Gas Show and Conference, Bahrain, Kingdom of Bahrain, 15–18 March*.

Aslam, U. (2009b). Microbial plugging: A cost-effective approach for improved sweep efficiency through permeability reduction. *SPE-119023 presented at Production and Operations Symposium, Oklahoma City, Oklahoma, USA, 4–8 April*.

Aziz, K., L. Durlofsky, and H. Tchelepi (2003). *Notes on petroleum reservoir simulation*. Department of Petroleum Engineering, School of Earth Sciences, Stanford University, California, USA.

Banat, I. M. (1995). Biosurfactants production and possible uses in microbial enhanced oil recovery and oil pollution remediation: A review. *Bioresour Technol* 51, 1 – 12.

Bao, M., X. Kong, G. Jiang, X. Wang, and X. Li (2009). Laboratory study on activating indigenous microorganisms to enhance oil recovery in Shengli Oilfield. *J Petrol Sci Eng* 66, 42 – 46.

Batycky, R. P. (1997). *A three-dimensional two-phase field scale streamline simulator*. Ph. D. thesis, Department of Petroleum Engineering, Stanford University, California, USA.

Bedrikovetsky, P. G. (1993). *Mathematical theory of oil and gas recovery*. Kluwer

Academic Publishers, London.

Behesht, M., R. Roostaazad, F. Farhadpour, and M. R. Pishvaei (2008). Model development for MEOR process in conventional non-fractured reservoirs and investigation of physico-chemical parameter effects. *Chem Eng Technol* 7, 953–963.

Berenblyum, R. A. (2004). *Streamline simulation with capillary effects applied to petroleum engineering problems*. Ph. D. thesis, Department of Chemical Engineering, Technical University of Denmark, Denmark.

Blanchet, D., A. Grabowski, and J.-P. Vandecasteele (2001). Microbiology of oil degradation in reservoirs. *SPE-71449 presented at ATCE, New Orleans, Louisiana, USA, 30 September–3 October*.

Bordoloi, N. and B. Konwar (2008). Microbial surfactant-enhanced mineral oil recovery under laboratory conditions. *Colloid Surface B* 63(1), 73 – 82.

Brown, F. (1992). Microbes: The practical and environmental safe solution to production problems, enhanced production, and enhanced oil recovery. *SPE-23955 presented at Permian Basin Oil and Gas Recovery Conference, Midland, Texas, USA, 18–20 March*.

Brown, L. R. (2010). Microbial enhanced oil recovery (MEOR). *Curr Opin Microbiol* 13, 1–5.

Brown, L. R. and A. A. Vadie (2002). Slowing production decline and extending the economic life of an oil field: New MEOR technology. *SPE Reserv Eval Eng* 5, 33–41.

Bryant, R. and T. Burchfield (1989). Review of microbial technology for improving oil recovery. *SPE Reservoir Eng* 4, 151–154.

Bryant, R., T. Burchfield, K. Chase, K. Bertus, and A. Stepp (1989). Optimization of oil mobilization, transport of microbes and metabolites, and effects of additives. *SPE-19686 presented at ATCE, San Antonio, Texas, USA, 8–11 October*.

Bryant, R. S. and J. Douglas (1988). Evaluation of microbial systems in porous media for EOR. *SPE Reservoir Eng* 3, 489–495.

Bryant, S. L. and T. P. Lockhart (2002). Reservoir engineering analysis of microbial enhanced oil recovery. *SPE-63229 presented at ATCE, Dallas, Texas, USA, 1–4 October*.

Buciak, J., A. Vazquez, R. Frydman, J. Mediavilla, and R. Bryant (1995). Enhanced oil recovery by means of microorganisms: Pilot test. *SPE Advanced Technology Series* 4, 144–149.

Chang, M.-M., F. Chung, R. Bryant, H. Gao, and T. Burchfield (1991). Modelling and laboratory investigation of microbial transport phenomena in porous media. *SPE-22845 presented at ATCE, Dallas, Texas, USA, 6–9 October*.

Characklis, W. G. and P. A. Wilderer (Eds.) (1989). *Structure and function of biofilms*. John Wiley and Sons.

Chen, B., J. Wang, and S. Wo (1998). A generalized Godunov method for enhanced oil recovery processes with microbial permeability modification in 1-D coreflood models.

Iterative Methods in Scientific Computation. EMACS Publication.

Chilingarian, G. V. and M. R. Islam (1995). A three-dimensional numerical simulator for microbial enhanced oil recovery. *Scientia Iranica* 2, 55–64.

Chisholm, J., S. Kashikar, R. Knapp, M. McInerney, and D. Menzie (1990). Microbial enhanced oil recovery: Interfacial tension and gas-induced relative permeability effects. *SPE-20481 presented at ATCE, New Orleans, Louisiana, USA, 23–26 September*.

Clement, T. P., B. Hooker, and R. S. Skeen (1996). Macroscopic models for predicting changes in saturated porous media properties caused by microbial growth. *Ground Water* 34, 934–942.

Coats, K. H. (1980, October). An equation of state compositional model. *SPE J* 20, 363–376.

Crescente, C., A. Rekdal, A. Abraiz, O. Torsaeter, L. Hultmann, A. Stroen, K. Rasmussen, and E. Kowalewski (2008). A pore level study of MIOR displacement mechanisms in glass micromodels using *Rhodococcus* sp. 094. *SPE-110134 presented at the IOR Symposium, Tulsa, Oklahoma, USA, 19–23 April*.

Crescente, C., O. Torsaeter, L. Hultmann, A. Stroem, , K. Rasmussen, and E. Kowalewski (2006). An experimental study of driving mechanisms in MIOR processes by using *Rhodococcus* sp. 094. *SPE-100033 presented at the IOR Symposium, Tulsa, Oklahoma, USA, 22–26 April*.

Datta-Gupta, A. (2000). Streamline simulation: A technology update. *SPE-65604. J Petrol Technol* 52, 68–73.

Davidova, I., M. Hicks, P. Fedorak, and J. Sufлита (2001). The influence of nitrate on microbial processes in oil industry production waters. *J Ind Microbiol Biot* 27, 80–86.

Delshad, M., K. Asakawa, G. A. Pope, and K. Sepehrnoori (2002). Simulations of chemical and microbial enhanced oil recovery methods. *SPE-75237 at the IOR Symposium, Tulsa, Oklahoma, USA, 13–17 April*.

Deng, D., C. Li, Q. Ju, P. Wu, F. L. Dietrich, and Z. H. Zhou (1999). Systematic extensive laboratory studies of microbial EOR mechanisms and microbial EOR application results in Changqing Oilfield. *SPE-54380 presented at Asia Pacific Oil and Gas Conference and Exhibition, Jakarta, Indonesia, 20–22 April*.

Desouky, S. M., M. M. Abdel-Daim, M. H. Sayyoub, and A. S. Dahab (1996). Modelling and laboratory investigation of microbial enhanced oil recovery. *J Petrol Sci Eng* 15, 309–320.

Dietrich, F., F. Brown, Z. Zhou, and M. Maure (1996). Microbial EOR technology advancement: Case studies on successful projects. *SPE-36746 presented at ATCE, Denver, Colorado, USA, 6–9 October*.

Eckford, R. and P. Fedorak (2002). Planktonic nitrate-reducing bacteria and sulfate-reducing bacteria in some western Canadian oil field waters. *J Ind Microbiol Biot* 29, 83–92.

- Feng, Q., F. Ni, B. Qin, X. Ma, C. Ji, and X. Wang (2006). Review of MEOR technology application in Dagang Oilfield for the last decade. *SPE-100791 presented at the SPE Asia Pacific Oil and Gas Conference and Exhibition, Adelaide, Australia, 11–13 September*.
- Feng, Q., J. Zhou, Z. Chen, X. Wang, F. Ni, and H. Yang (2002). Study on EOR mechanisms by microbial flooding. *SPE-79176 presented at ATCE, Abuja, Nigeria, 5–7 August*.
- Fulcher, R. A., T. Ertekin, and C. D. Stahl (1985). Effect of capillary number and its constituents on 2-phase relative permeability curves. *J Petrol Technol* 37(2), 249–260.
- Gandler, G. L., A. Gbosi, S. L. Bryant, and L. N. Britton (2006). Mechanistic understanding of microbial plugging for improved sweep efficiency. *SPE-100048 presented at the IOR Symposium, Tulsa, Oklahoma, USA, 22–26 April*.
- Gerritsen, M. G. and L. J. Durlofsky (2005). Modeling fluid flow in oil reservoirs. *Annu Rev Fluid Mech* 37, 211–238.
- Ghojavand, H., F. Vahabzadeh, E. Roayaei, and A. K. Shahraki (2008). Production and properties of a biosurfactant obtained from a member of the *Bacillus subtilis* group (PTCC 1696). *J Colloid Interf Sci* 324, 172 – 176.
- Ginn, T., B. Wood, K. Nelson, T. Scheibe, E. Murphy, and T. Clement (2002). Processes en microbial transport in the natural subsurface. *Adv Water Resour* 25, 1017–1042.
- Gray, M. R., A. Yeung, J. M. Foght, and H. W. Yarranton (2008). Potential microbial enhanced oil recovery processes: A critical analysis. *SPE-114676 presented at ATCE, Denver, Colorado, USA, 21–24 September*.
- Green, D. W. and G. P. Willhite (1998). *Enhanced oil recovery*, Volume 6. SPE Textbook Series.
- Grula, E. A., H. H. Russell, D. Bryant, and M. Kenaga (1989). Oil displacement by anaerobic and facultatively anaerobic bacteria. *Microbial enhanced oil recovery*, pp. 113–124. Elsevier Science Publishers B. V.
- Gullapalli, I. L., J. H. Bae, K. Hejl, and A. Edwards (2000). Laboratory design and field implementation of microbial profile modification process. *SPE Reserv Eval Eng* 3, 42–49.
- Halim, A. Y., U. D. Fauzi, S. Siregar, E. Soewono, A. Y. Gunawan, D. I. Astuti, and N. Juli (2009). Microbial enhanced oil recovery: An investigation of bacteria ability to live and alter crude oil physical characteristics in high pressure condition. *SPE-123506 presented at Asia Pacific Oil and Gas Conference and Exhibition, Jakarta, Indonesia, 4–6 August*.
- Hitzman, D. O., M. Dennis, and D. C. Hitzman (2004). Recent successes: MEOR using synergistic H₂S prevention and increased oil recovery systems. *SPE-89453 presented at the IOR Symposium, Tulsa, Oklahoma, USA, 17–21 April*.
- Ibrahim, Z., M. I. Omar, K. S. Foo, E. J. Elias, and M. Othman (2004). Simulation

- analysis of microbial well treatment of Bokor Field, Malaysia. *SPE-88453 presented at Asia Pacific Oil and Gas Conference and Exhibition, Perth, Australia, 18–20 October.*
- Islam, M. (1990). Mathematical modeling of microbial enhanced oil recovery. *SPE-20480 presented at ATCE, New Orleans, Louisiana, USA, 23–26 September.*
- Islam, M. R. and A. Gianetto (1993). Mathematical modelling and scaling up of microbial enhanced oil recovery. *J Can Petrol Technol 32*, 30–36.
- Jack, T. R., J. Shaw, N. Wardlaw, and J. W. Costerton (1989). Microbial plugging in enhanced oil recovery. *Microbial Enhanced Oil Recovery*, pp. 125–148. Elsevier Science Publishers B. V.
- Jang, L.-K., M. M. Sharma, and T. F. Yen. (1984). The transport of bacteria in porous media and its significance in microbial enhanced oil recovery. *SPE-12770 presented at California Regional Meeting, Long Beach, California, USA, 11–13 April .*
- Jenneman, G., R. Knapp, M. McInerney, D. Menzie, and D. Revus (1984). Experimental studies of in-situ microbial enhanced recovery. *SPE-10789. SPE J 24*, 33–37.
- Jenneman, G. E. (1989). The potential for in-situ microbial applications. *Microbial enhanced oil recovery*, pp. 37–74. Elsevier Science Publishers B. V.
- Jessen, K. and F. M. Orr (2004). Gravity segregation and compositional streamline simulation. *SPE-89448 presented at the IOR Symposium, Tulsa, Oklahoma, USA, 17–21 April.*
- John, A., C. Han, M. Delshad, G. A. Pope, and K. Sepehrnoori (2005). A new generation chemical-flooding simulator. *SPE J 10*, 206–216.
- Kim, S.-B. (2006). Numerical analysis of bacterial transport in saturated porous media. *Hydrol Process 20*, 1177–1186.
- King, M. J. and A. Datta-Gupta (1998). Streamline simulation: A current perspective. *In Situ 22*, 91–140.
- Kowalewski, E., I. Rueslåtten, K. Steen, G. Bødtker, and O. Torsæter (2006). Microbial improved oil recovery – bacterial induced wettability and interfacial tension effects on oil production. *J Petrol Sci Eng 52*, 275–286.
- Kumar, S., S. J. Torabzadeh, and L. L. Handy (1985). Relative permeability functions for high- and low-tension systems at elevated temperatures. *SPE-13670 presented at the California Regional Meeting, Bakersfield, California, USA, 27–29 March.*
- Lake, L. W. (1989). *Enhanced oil recovery*. Prentice-Hall, Inc.
- Lake, L. W., G. A. Pope, G. F. Garey, and K. Sepehrnoori (1984). Isothermal, multi-phase, multicomponent fluid flow in permeable media. *In Situ 8*, 1–40.
- Lazar, I., I. G. Petrisor, and T. F. Yen. (2007). Microbial enhanced oil recovery (MEOR). *Petrol Sci Technol 25*, 1353–1366.
- MacLeod, F., H. Lappin-Scott, and J. Costerton (1988). Plugging of model rock system

by using starved bacteria. *Appl Environ Microb* 54, 1365–1372.

Madigan, M., J. Martinko, and J. Parker (2003). *Brock: Biology of microorganisms* (Tenth ed.). Prentice-Hall.

Magot, M., B. Ollivier, and B. Patel (2000). Microbiology of petroleum reservoirs. *Anton van Lee* 77, 103–116.

Marshall, S. L. (2008). Fundamental aspects of microbial enhanced oil recovery: A literature survey. Technical report, CSIRO Land and Water, Floreat, Western Australia.

Maudgalya, S., R. M. Knapp, and M. J. McInerney (2007). Microbially enhanced oil recovery technologies. A review of the past, present and future. *SPE-106978 presented at the Production and Operations Symposium, Oklahoma City, Oklahoma, USA, 30 March–3 April*.

Maure, A., F. Dietrich, U. Gómez, J. Vallesi, and M. Irusta (2001). Waterflooding optimization using biotechnology: 2-year field test, La Ventana Field, Argentina. *SPE-69652 presented at Latin American and Caribbean Petroleum Engineering Conference, Buenos Aires, Argentina, 25–28 March*.

Maure, A., A. A. Saldana, and A. R. Juarez (2005). Biotechnology application to EOR in Talara off-shore oil fields, northwest Peru. *SPE-94934 presented at Latin American and Caribbean Petroleum Engineering Conference, Rio de Janeiro, Brazil, 20–23 June*.

McCabe, W. L., J. C. Smith, and P. Harriot (Eds.) (2005). *Unit Operations of Chemical Engineering* (Seventh ed.). McGraw-Hill, New York.

McInerney, M. J., K. Duncan, N. Youssef, T. Fincher, S. K. Maudgalya, M. J. Folmsbee, R. Knapp, R. R. Simpson, N. Ravi, and D. Nagle (2005). Development of microorganisms with improved transport and biosurfactant activity for enhanced oil recovery. Technical report, Department of Botany and Microbiology, and Department of Petroleum Engineering, University of Oklahoma, USA.

Mei, S., L. Wei, L. Guangzhi, H. Peihui, H. Zhaowei, C. Xinghong, and W. Ying (2003). Laboratory study on MEOR after polymer flooding. *SPE-84865 presented at the IOR Conference in Asia Pacific, Kuala Lumpur, Malaysia, 20–21 October*.

Molz, F., M. Widdowson, and L. Benefield (1986). Simulation of microbial growth dynamics coupled to nutrient and oxygen transport in porous media. *Water Resour Res* 8, 1207–1216.

Murphy, E. and T. Ginn (2000). Modeling microbial processes in porous media. *Hydrogeol J* 8, 142–158.

Nagase, K., S. T. Zhang, H. Asami, N. Yazawa, K. Fujiwara, H. Enomoto, C. X. Hong, and C. X. Liang (2002). A successful field test of microbial eor process in Fuyu Oil-field, China. *SPE-75238 presented at the IOR Symposium, Tulsa, Oklahoma, USA, 13–17 April*.

Nazina, T., D. Sokolova, A. Grigor'yan, Y.-F. Xue, S. Belyaev, and M. Ivanov (2003). Production of oil-releasing compounds by microorganisms from the Daqing Oil Field,

China. *Hydrogeol J* 72, 206–211.

Nielsen, J., J. Villadsen, and G. Lidén (2003). *Bioreaction engineering principles* (First ed.). New York: Kluwer Academic/Plenum Publishers.

Nielsen, S. M., K. Jessen, A. A. Shapiro, M. L. Michelsen, and E. H. Stenby (2010). Microbial enhanced oil recovery: 3D simulation with gravity effects. *SPE-131048 presented at the EUROPEC/EAGE Conference and Exhibition, Barcelona, Spain, 14–17 June*.

Nielsen, S. M., A. A. Shapiro, M. L. Michelsen, and E. H. Stenby (2010). 1D simulations for microbial enhanced oil recovery with metabolite partitioning. *Transport Porous Med* 85, 785–802.

Orr, F. M. (2007). *Theory of gas injection processes*. TIE-LINE Publications.

Peihui, H., S. Fengrong, and S. Mei (2001). Petroleum hydrocarbon as a sole carbon source. *SPE-72128 presented in the Asia Pacific IOR Conference, Kuala Lumpur, Malaysia, 8–9 October*.

Portwood, J. T. (1995). A commercial microbial enhanced oil recovery technology: Evaluation of 322 projects. *SPE-29518 presented at the Production Operations Symposium, Oklahoma City, Oklahoma, USA, 2–4 April*.

Rafique, M. A. and U. Ali (2008). Microbial enhanced oil recovery (MEOR) with special emphasis to the "uneconomical reserves". *SPE-113272 presented at the Indian Oil and Gas Technical Conference and Exhibition, Mumbai, India, 4–6 March*.

Raiders, R., D. Freeman, G. Jenneman, R. Knapp, and M. McInerney (1985). The use of microorganisms to increase the recovery of oil from cores. *SPE-14336 presented at ATCE, Las Vegas, Nevada, USA, 22–25 September*.

Raiders, R., T. Maher, R. Knapp, and M. McInerney (1986). Selective plugging and oil displacement in crossflow core systems by microorganisms. *SPE-15600 presented at ATCE, New Orleans, Louisiana, USA, 5–6 October*.

Ravera, F., M. Ferrari, and L. Liggieri (2000). Adsorption and partitioning of surfactant in liquid-liquid systems. *Adv Colloid Interfac* 88, 129–177.

Rockhold, M. L., R. R. Yarwood, and J. S. Selker (2004). Coupled microbial and transport processes in soils. *Vadose Zone J* 3, 368–383.

Samir, M., M. A. El Ela, S. El Marsafy, S. El Tayeb, A. A. Waly, and M. H. Sayyouth (2010). New incubated *Pseudomonas aeruginosa* bacteria for increasing oil recovery under reservoir conditions. *SPE-126104 presented at the North Africa Technical Conference and Exhibition, Cairo, Egypt, 14–17 February*.

Sarkar, A., G. Georgiou, and M. Sharma (1994). Transport of bacteria in porous media: II. A model for convective transport and growth. *Biotechnol Bioeng* 44, 499–508.

Segovia, G. C., V. A. Huerta, and G. C. Gutierrez (2009). Improving MEOR performance by a selection methodology in mature oilfields. *SPE-123072 presented at Latin American and Caribbean Petroleum Engineering Conference, Cartagena, Colombia, 3 May –3 June*.

- Sen, R. (2008). Biotechnology in petroleum recovery: The microbial EOR. *Prog Energy Combust* 34(6), 714 – 724.
- Sen, T., D. Das, K. Khilar, and G. Suraishkumar (2005). Bacterial transport in porous media: New aspects of the mathematical model. *Colloids Surface A* 260, 53–62.
- Shafai, M. and K. Vafai (2009). Biofilm affected characteristics of porous structures. *Int J Heat Mass Tran* 52, 274–581.
- Sharma, M. and G. Georgiou (1993). Microbial Enhanced Oil Recovery Research – Final Report prepared for U.S. Department of Energy. Technical report, Department of Petroleum Engineering, University of Texas, Austin, USA.
- Shen, P., B. Zhu, X.-B. Li, and Y.-S. Wu (2006). The influence of interfacial tension on water/oil two-phase relative permeability. *SPE-95405 presented at the IOR Symposium, Tulsa, Oklahoma, USA, 22–26 April*.
- Soleimani, S., P. J. V. Geel, O. B. Isgor, and M. B. Mostafa (2009). Modeling of biological clogging in unsaturated porous media. *J Contamin Hydrol* 106, 39–50.
- Stevik, T. K., K. Aa, G. Ausland, and J. F. Hanssen (2004). Retention and removal of pathogenic bacteria in wastewater percolating through porous media: A review. *Water Res* 38, 1355 – 1367.
- Streeb, L. P. and F. G. Brown (1992). MEOR – Altamont/Bluebell Field project. *SPE-24334 presented at Rocky Mountain Regional Meeting, Casper, Wyoming, USA, 18–21 May*.
- Sugai, Y., H. Chengxie, T. Chida, and H. Enomoto (2007). Simulation studies on the mechanisms and performances of MEOR using polymer producing microorganism *Clostridium* sp. TU-15A. *SPE-110173 presented at Asia Pacific Oil and Gas Conference and Exhibition, Jakarta, Indonesia, 30 October–1 November*.
- Sugihardjo, E. H. L. and S. W. Pratomo (1999). Microbial core flooding experiments using indigenous microbes. *SPE-57306 presented at Asia Pacific IOR Conference, Kuala Lumpur, Malaysia, 25–26 October*.
- Sunde, E., J. Beeder, R. K. Nilsen, and T. Torsvik (1992). Aerobic microbial enhanced oil recovery for offshore use. *SPE-24204 presented at the IOR Symposium, Tulsa, Oklahoma, USA, 22–24 April*.
- Taber, J. (1969). Dynamic and static forces required to remove a discontinuous oil phase from porous media containing both oil and water. *SPE J* 9, 3–12.
- Tadmouri, R., C. Zedde, C. Routaboul, J.-C. Micheau, and V. Pimienta (2008). Partition and water/oil adsorption of some surfactants. *J Phys Chem B* 112, 12318–12325.
- Thiele, M. R. (1991). *Modeling multiphase flow in heterogeneous media using streamtubes*. Ph. D. thesis, Department of Petroleum Engineering, Stanford University, USA.
- Thullner, M. (2009). Comparison of bioclogging effects in saturated porous media within one- and twodimensional flow systems. *Ecol Eng* 36, 176–196.

- Tufenkji, N. (2007). Modeling microbial transport in porous media: Traditional approaches and recent developments. *Adv Water Resour* 30, 1455–1469.
- Updegraff, D. M. (1983). Plugging and penetration of petroleum reservoir rock by microorganisms. In E. C. Donaldson and J. B. Clark (Eds.), *Proceedings of the 1982 International Conference on Microbial Enhancement of Oil Recovery*.
- UTCHEM (2000). *Technical Documentation for UTCHEM 9.0 – A three dimensional chemical flood simulator*. Reservoir Engineering Research Program, Center for Petroleum and Geosystems Engineering at the University of Texas at Austin, USA.
- Vadie, A. A., J. O. Stephens, and L. R. Brown (1996). Utilization of indigenous microflora in permeability profile modification of oil bearing formations. *SPE-35448 presented at the IOR Symposium Tulsa, Oklahoma, USA, 21–24 April*.
- Valdés-Parada, F. J., M. L. Porter, K. Narayanaswamy, R. M. Ford, and B. D. Wood (2009). Upscaling microbial chemotaxis in porous media. *Adv Water Resour* 32, 1413 – 1428.
- Van Hamme, J., A. Singh, and O. Ward (2003). Recent advances in petroleum microbiology. *Microbiol Mol Bio R* 67, 503–549.
- Vandevivere, P., P. Baveye, D. S. de Lozada, and P. DeLeo (1995). Microbial clogging of saturated soils and aquifer materials: Evaluation of mathematical models. *Water Resour Res* 31, 2173–2180.
- Wang, F. and V. V. Tarabara (2009). Permeability of fiber-filled porous media: Kozeny-Carman-Ethier modeling approach. *Environ Eng Sci* 26, 1149–1155.
- Wo, S. (1997). *The mathematical modeling and numerical approaches for microbial permeability modification enhanced oil recovery processes*. Ph. D. thesis, Graduate School of The University of Wyoming, USA.
- Youssef, N., D. R. Simpson, K. E. Duncan, M. J. McInerney, M. Folmsbee, T. Fincher, and R. M. Knapp (2007). In situ biosurfactant production by *Bacillus* strains injected into a limestone petroleum reservoir. *Appl Environ Microbiol* 73, 1239–1247.
- Zekri, A. Y. and R. A. Almehaideb (1999). Project of increasing oil recovery from UAE reservoirs using bacteria flooding. *SPE-56827 presented at ATCE, Houston, Texas, USA, 3–6 October*.
- Zhang, X., R. Knapp, and M. McInerney (1992). A mathematical model for enhanced oil recovery process. *SPE-24202 presented at IOR Symposium, Tulsa, Oklahoma, USA, 22–24 April*.
- Zhaowei, H., H. Peihui, L. Jianjun, C. Jianfei, G. Menghua, and C. Xinghong (2008). The application of hydrocarbon-degrading bacteria in Daqing’s low permeability, high paraffin content oilfields. *SPE-114344 presented at the IOR Symposium, Tulsa, Oklahoma, USA, 19–23 April*.
- Zhou, D., F. J. Fayers, and F. M. Orr (1994). Scaling of multiphase flow in simple heterogeneous porous media. *SPE-27833 presented at the IOR Symposium, Tulsa, Oklahoma,*

USA, 17-20 April.

ZoBell, C. E. (1947). Bacterial release of oil from oil-bearing materials. *World Oil* 126, 36-47.

Center for Energy Resources Engineering
Department of Chemical and
Biochemical Engineering
Technical University of Denmark
Søltofts Plads, Building 229
DK-2800 Kgs. Lyngby
Denmark

Phone: +45 4525 2800
Fax: +45 4525 4588
Web: www.kt.dtu.dk

ISBN : 978-87-92481-31-3